STUDIA

UNIVERSITATIS BABEŞ-BOLYAI

PHYSICA

1

1986

CLUJ-NAPOCA

ANUL XXXI 1986

STUDIA

UNIVERSITATIS BABEŞ-BOLYAI

PHYSICA

1

Redacţia : 3400 CLUJ-NAPOCA, str. M. Kogălniceanu, 1 ● Telefon 1 61 01

SUMAR – CONTENTS

STUDIA UNIV BABEŞ—BOLYAI, PHYSICA, XXXI, 1, 1986

EPR SPIN IMAGING BY USING DIPOLAR FIELDS

Al. NICULA*, S. NICULA*, L. GIURGIU, and I. URSU*****

Received April 24, 1986; accepted August, 12, 1986

Abstract. — The paper proposes obtention of spatial paramagnetic resonance, or spin imaging, by using a dipolar magnetic field created by a permanent magnet (or coil) having a moment of value $m = 0{,}17\ Am^2$ The method is efficient for paramagnetic centers having narrow linewidth, and for samples of small dimensions. DPPH and Mo^{5+} in a glassy matrix were used The dipolar field may also be used in NMR, to obtain images of protons or other nuclear spins.

Introduction. A great progress was achieved in magnetic resonance of late, concerning the spatial resonance transitions in magnetic fields with constant gradients, along various uni-, bi-, and three-dimensional directions [1] This new research field has determined the development of spin imaging techniques, which, especially in NMR, are used as medical diagnosis method [2, 3].

Tha spatial transitions study in constant field gradients is very recent in Electron Paramagnetic Resonance. Thus, K. Ohno [4] studied various radicals in some frozen and irradiated acids, by using constant field gradients. S.S. Eaton and G R. Eaton [5] imagined simple experimental arrangements to demonstrate how EPR may be used to achieve spin imaging They used a Varian E—9 spectrometer, in χ hand, and as investigated substances DPPH samples were chosen.

The aim of this paper is to present the first spin imaging EPR measurements, carried out at ITIM and at the University of Cluj-Napoca These studies were performed by using the technique available at the two laboratories, where spatial fields were added to the constant one, in order to get spin imaging. This time, the additional spatial fields were not constant gradients, but they had a dipolar structure, and we were the first to consider this experimental possibility. Besides DPPH we used transitional ions, too, and most suitable, giving remarcable results, was Mo^{5+} in an amorphous B_2O_3—Na_2O type matrix.

Electron Paramagnetic Resonance with constant fieldt gradient. The basic principle of spin imaging, or of spatial transitions with constant gradients, consists in that the resonance frequency is a function of $\vec{r}$ having the form

$$\nu(\vec{r}) = \frac{g\beta}{h} B(\vec{r}) \tag{1}$$

where B(r) consiats of constant field B_0, and constant gradient $G = \frac{\partial B}{\partial r}$ chosen along an arbitrary direction, so as

$$B(\vec{r}) = B_0 + \vec{G} \cdot \vec{r} \tag{2}$$

* *University of Cluj-Napoca, Department of Physics, 340 Cluj-Napoca, Romania*
** *ITIM—Cluj-Napoca, 3400 Cluj-Napoca, Romania*
*** *University of Bucharest, Faculty of Physics, Romania*

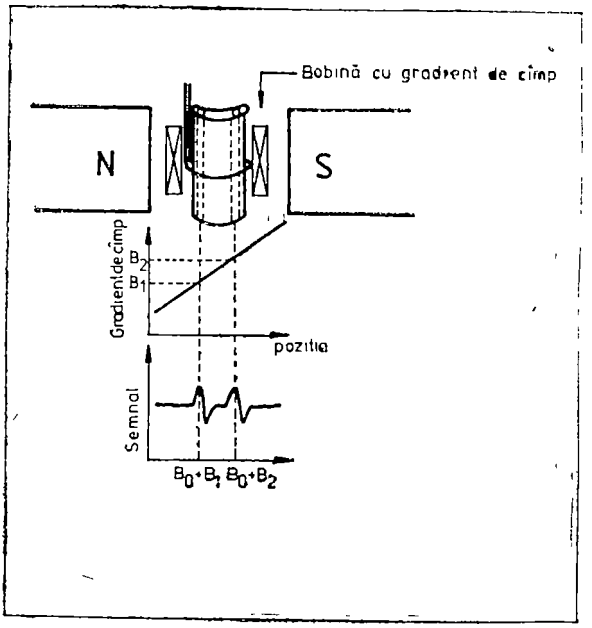

Fig 1 Experimental scheme for obtaining unidimentional spin imaging The two capillaries are oriented along the z axis, that is the field gradient direction. B_0 is the constant magnetic field, along the x axis, and B_1 and B_2 are the filed gradient contributions at the sites 1 and 2 where applied capillaries are placed

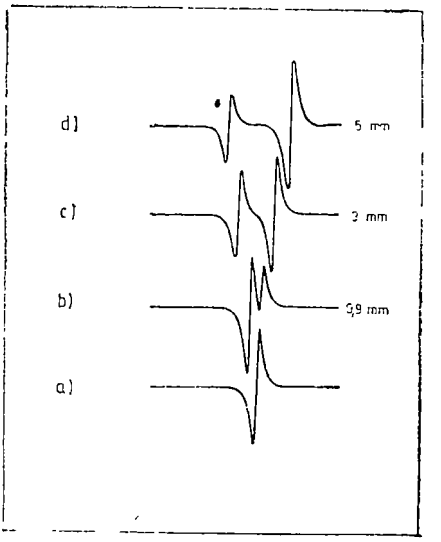

Fig 2 EPR spectrum for two DPPH samples (a) shows the lineshape without the field gradient application, (b), (c) and (d) show the lineshape for the DPPH samples at 0 9, 3 and 5 mm distances from each other The field gradient used was about 2 7 gauss/mm

The resonance spectrum obtained for this field configuration corresponds to a projection of the spin density of the substance, on the axis defined by field gradient vector G The experimental device is presented in Fig 1 [6].
A suggestive example concerning the spin imaging results is given in Fig. 2. Here, the ERP signals for two DPPH samples, disposed in capillaries at different at different distances of 0 9, 3 and 5 mm to each other, are shown In the field gradient absence the two spectra superimpose In presence of the field gradient the spectra progressively separate, as the distance between the samples rises [5]. This may be seen in Fig 2, too

Electron Paramagnetic Resonance in magnetic fields with dipolar structure. For realising, in our study, a spatial distribution of the resonace frequencies, or of the resonant fields, a dipolar field of a permanent magnet superimposed on the B_0 field was used Under such circumstances, the resonance condition may be written as

$$h\nu(\vec{r}) = g\beta\left[B_0 + \frac{\mu_0}{4\pi}\left(-\frac{|\vec{m}|}{r^3} + 3\frac{|(\vec{m}\cdot\vec{r})\ \vec{r}|}{r^5}\right)\right] \qquad (3)$$

where $\vec{r}$ is the distance from the permanent magnet center to the sample site, and $\vec{m}$ is magnetic dipole moment of the permanent magnet, having the value of 0.17 Am². The scheme of this experiment is presented in Fig. 3.

As it can be seen, the permanent magnet field lines superimposa the B_0 field lines (Fig 3 a) The intensity of the permanent magnetic field is expressed by the second term in the right side of relation (3) Its distance dependence may be observed in Fig 3. b for $\vec{r}$ varying along the dipolar axis In these conditions, the second term in the right side of equation (3) becomes

$$B_d = \frac{\mu_0}{4\pi} \frac{2m}{r^3} \qquad (4)$$

We obtained two sample holders for studying DPPH and Mo — compound in the magnetic field These teflon holders, are presented in Fig 4 The device used for the spin imaging study of DPPH contains four narrow channels having 0,5 mm in diameter, and disposed in the same plane, at equal distances of 2 mm from each other (Fig 4 a) The holder used for the Mo-glass is in such a way constructed that allows to stick two tiny glass samples in the same plane, at 3 mm distance from each other (Fig 4 b)

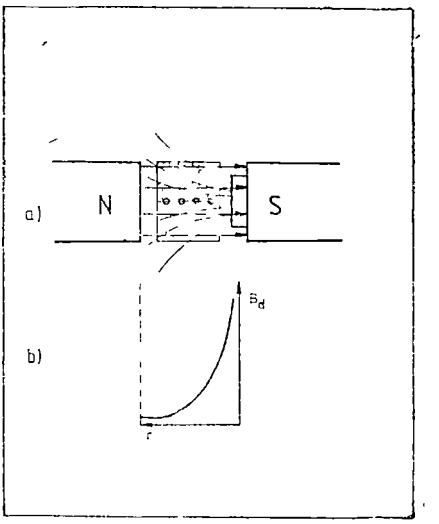

Fig 3 (a) Diagrams for obtaining the EPR spin imaging in a magnetic field having dipolar structure (b) Distance dependence of the magnetic field created by the permanent magnet.

For begining, we introduced these special shaped holders in the resonant cavity of the spectrometer, so as the samples containing plane be parallel to the constant field B_0 lines, as it may be seen in Fig 3 a The field at each sample site may be determined by using the law reprezented in Fig 3. b Then, the samples containing plane was orrienting to be perpendicular to the B_0 field lines in the resonant cavity, so as, this time, the law of the dipolar field variation at the sample sites is given by the second term on the right side of relation (3) In a more simple form, the mentioned term becomes

$$B_d = \frac{\mu_0}{4\pi} \frac{m}{r_i^3} (3\cos^2\theta_i - 1) \qquad (5)$$

where $i = 1, 2, 3, 4$ for DPPH and $i = 1, 2$ for Mo For a better understanding of the values entering in relation (5), Fig 5 must be observed

Beside the above described experiments, concerning the spin imaging in dipolar fields, other experiments were done when the field variation was approximately constant, but its direction was perpendicular to field B_0 Some bidimensional spin imaging were thus obtained This condition was achieved without a permanent magnet, by outward displacement of the resonant cavity from central region of the static magnetic field, where a pronounced field gradient exists. This may be considered constrant along a region of about 1 cm

Experimental results. By setting the DPPH in the cavity, with the samples containing plane parallel to the B_0 field lines, the resonance spectrum shows four lines, the distance between them varying according to relation (4)

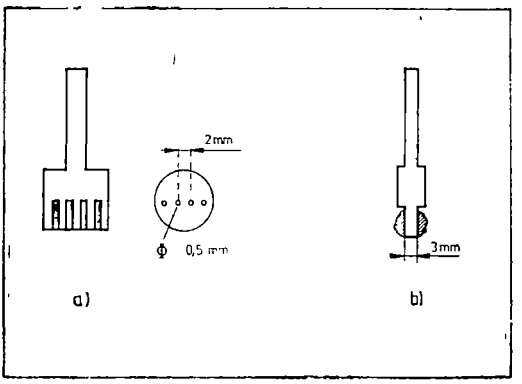

Fig. 4 .Teflon devices for obtaining the spin imaging: (a) for the DPPH samples; (b) for the MO^{5+}-glasses

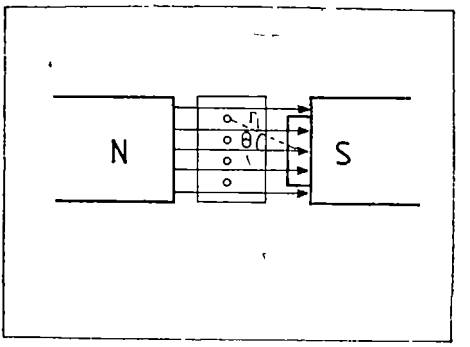

Fig 5. Diagram of the experiment of introducing the DPPH samples in a plane perpendicular to the B_0 magnetic field lines

If the plane of the four samples is now perpendicular to the B_0 field lines in the cavity, according to the relation giving the dipolar field, a single line is never obsrrved More lines will be obtained, two in the most fortunate case, when one succeeds to align the magnetic field axis exactly to the middle of the four orifices of the holder. In any case, the distance between the lines becomes smaller, then in the previous case and our performance is that of three lines, obtained closer together. The two situations are presented in figure 6.

We had less success in the dipolar spin imaging of Mo, because the $1/r^3$ dependence of the dipolar field, the weak magnet intensity, and the large linewidth, at the two samples site, insensible to their position, caused no separation of the two signals at field variation, but only a slight modification of the line-width. By passing from a position parallel to the B_0 field lines, to the perpendicular one, a 10 gauss variation of the Mo^{5+} linewidth was noticed. A greater succes was obtained for Mo, when the spatioal transitions were studied in an approximatively constant field gradient, for displacing the cavity out of the space between the poles of the electromagnet. This case was already mentioned and the field gradient varies perpendicular to B_0. In this case the resonance spectrum consists in two lines when the samples are in a plane perpendicular to B_0, and a single line when they are in a plane parallel to B_0 This situation is given in Fig. 7.

It can be easily seen that a great gradient makes the lines be splitted, though Mo^{5+} linewidth is about 50 gauss when the field gradient is missing. In that last case the fact that the field gradient is constant is confirmed by the spin imaging of DPPH On can see in Fig. 8 that for sitting the four DPPH samples device perpendicular to the B_0 filed lines, the signals are equally spaced, and for disposing the four samples plane parallel to B_0, a single line is obtained.

Conclusions. For both DPPH and Mo, spin imaging in dipolar field and constant gradients fields were obtained. For all we know, the spatial transitions in dipolar fields and their images were nowhere discussed, and these for

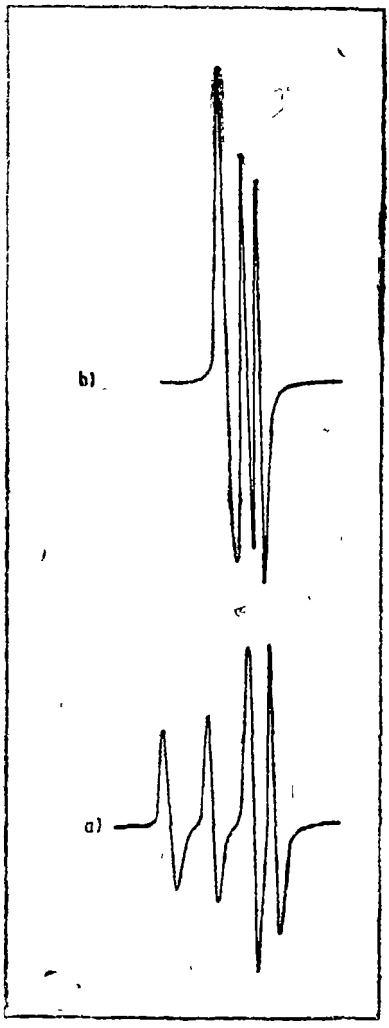

Fig. 6. Spectrum obtained after placing the DPPH samples in the cavity: (a) in a plane parallel to the B_0 filed lines; (b) perpendicular on B_0 lines

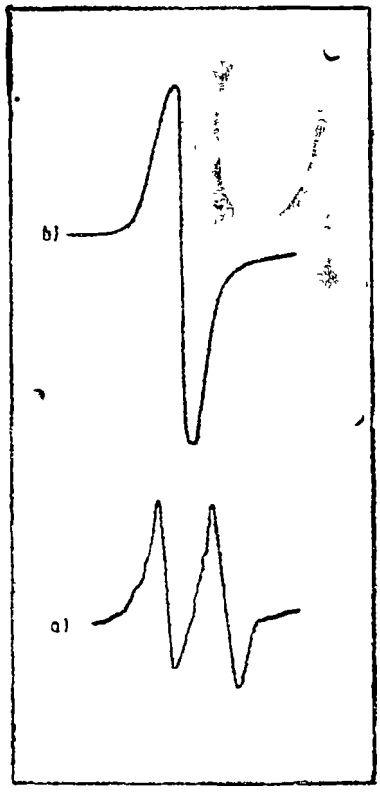

Fig 7 Spectra obtained for Mo^{5+}-glasses in an aprox constant filed gradient (a) the samples are disposed in a plane perpendicular to the B_0 field lines, (b) the samples are disposed in a plane parallel to B_0

DPPH in constnt gradient fields in our country were studied for the firs time by us in Cluj-Napoca, and the international literature on this problem contains only the paper of S. S Eaton and G. R. Eaton [5] The disadvantage of the proposed method lies in its limitation to very small spaces in

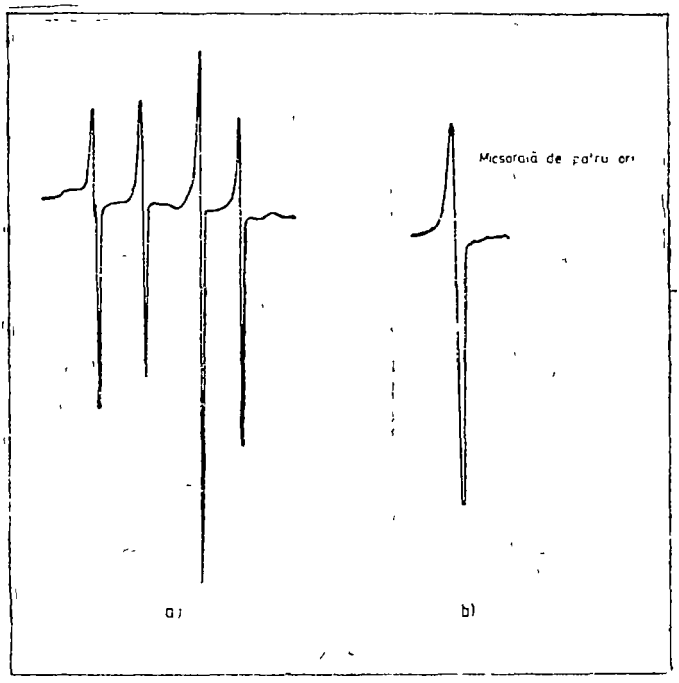

Fig. 8. Spectra obtained for DPPH in a constant field gradient · (a) the sample plane lies perpendicular to the B_0 fi eld lines. (b) the plane is parallel to the constant field lines.

the cavity, due to the microwave technique used. The same procedure may be applied, perphaps more efficiently, for obtaining the spin imaging by the dipolar spatial field method in the nuclear magnetic resonance.

REFERENCES

1. W V. House and P C Lauterbur, SPIE vol 173, „Application of Optical Instrumentation in Medicine" VII, p 356 (1979)
2. P Mansfield and P. G. Morris, „Advances in Magnetic Resonance" Supplement 2, „NMR Imaging in Biomedicine" Academic Press, New York/London (1982)
3. E. R. Andrew, *Conferința internațională Ampère*, București (1985)
4. K. Ohno, *Journal of Magnetic Resonance*, **50**, 145 (1982)
5. S. S. Eaton and G. R. Eaton, *Journal of Magnetic Resonance*, **59**, 474, (1984).
6. L. J Berliner and H. Fuji, SCIENCE, **227**, 517 (1985).

STUDIA UNIV BABEŞ—BOLYAI, PHYSICA, XXXI, 1, 1986

REGENERAREA ELECTROCHIMICĂ A CATALIZATORULUI DE Pd OTRĂVIT CU COMPUŞI DE SULF

FELICIA BOTA*, R. V. BUCUR**

Intra în redacţie la 22 martie 1985, acceptat la 12 august 1986

ABSTRACT. — Electrochemical Regeneration of Palladium Poisoned with Sulphur Compounds. Adsorption of tiourea (THU) on Pd electrode surface is presented using an anodic oxidation with a linear sweep voltametric technique The method is suitable to obtain the catalitic regeneration properties of palladium electrode surface

În ultimii ani, pe plan mondial se manifestă un interes crescînd pentru hidrurile metalice în probleme de stocare şi transformare a energiei [1] Problema cea mai importantă care se pune este durata de viaţă a unei hidruri metalice În general, menţinerea unui catalizator în stare perfectă de funcţionare este o chestiune foarte dificilă Se constată frecvent că catalizatorii utilizaţi în aceste scopuri prezintă, după un timp de funcţionare, un fenomen de îmbătrînire, care reduce mult activitatea lor catalitică În timpul operaţiei catalitice au loc o serie de procese fizice şi chimice care tind să anuleze centrii activi, sau să îngrădească accesibilitatea lor Reducerea activităţii catalitice poate avea loc fie printr-o reducere a centrilor activi prin fuzionarea particulelor fazei active, fie o reducere a lor datorită curentului de gaz care poate disloca părţi de pe suprafaţa catalizatorului, fie că faza activă de la suprafaţă interacţionează cu suportul său, scufundîndu-se de-a dreptul în el şi, în sfîrşit, se pot adsorbi la suprafaţa catalizatorului diverse componente, ajungîndu-se în final la excluderea unor evenimente catalitice viitoare

Dintre aceste procese de deteriorare, menţionate mai sus, numai ultimul din ele este definit ca otrăvire catalitică în sensul strict al cuvîntului. Într-o definiţie mai largă, otrăvirea include, de asemenea, depunerea de substanţă din exterior în mod direct pe suprafaţa activă din punct de vedere catalitic, sau, mai concret, la intrarea canalelor sau porilor suportului pe care faza catalitică este dispersată Aceste depozite opresc accesul la un întreg ansamblu de centri activi În ambele cazuri, rezultatul este acelaşi descreşterea activităţii catalitice, ca urmare a creşterii procesului de dezactivizare Otrăvirea este un aspect specific deosebit de important, cu consecinţe tehnologice şi chiar economice. Pe măsură ce tehnica a avansat, problema otrăvirii catalizatorilor s-a ameliorat, cantitatea de substanţă contaminată descrescînd cu ordine de mărime prin mărirea gradului de puritate al substanţelor utilizate [2]

Se ştie că hidrogenul obţinut prin procesul de electroliză conţine urme de sulf, prin aerosolii antrenaţi din soluţia de acid sulfuric Efectul prezenţei sulfului pe suprafaţa unui electrod din paladiu a fost ilustrat prin măsurători

* *Universitatea din Cluj-Napoca, Facultatea de fizică, 3400 Cluj-Napoca, România*
** *ITIM — Cluj-Napoca, România*

de desorbție galvanostatică a hidrogenului dintr-un electrod de paladiu neotrăvit și otrăvit cu sulf provenit din tiouree, cysteină, Na_2S și CS_2 [3]

Prezența compușilor cu sulf pe electrodul de paladiu afectează de asemenea și reacția Volmer anodică [4], modificîndu-se parametrii cinetici

Se trage concluzia că prezența urmelor de sulf impurifică suprafața electrodului de paladiu, ceea ce duce la descreșterea activității catalitice Se pune deci problema de a găsi mijloace adecvate pentru regenerarea catalizatorului

O metodă deosebit de eficientă este metoda voltametriei la tensiune liniar variabilă (VTLV) [5] Măsurătorile s-au efectuat cu un sistem electroanalitic, Electroscan TM 30 (Bekman), utilizînd o celulă termostatată, în care se află soluția 0,1 N H_2SO_4 și trei electrozi electrodul de lucru (Pd), electrodul de referință (e n h) și nu contraelectrod (Pt), în atmosferă de argon, la 25°C Otrăvirea electrodului s-a făcut în mod controlat, în soluții de tiouree de diverse concentrații, timp de 5 secunde. După otrăvire, electrodul este spălat cu apă dublu distilată, pentru a se înlătura urmele de soluție. Acest electrod, care are sulf adsorbit pe suprafața sa, este supus unui proces de oxidare anodică la o tensiune liniar variabilă, de la valoarea de echilibru, pînă la 1,6 V în regiunea anodică și apoi o revenire în sens invers pînă la 0,3 V în regiunea catodică. Curbele potențial-curent s-au înregistrat la o viteză de 20 mV/s. După acest ciclu aplicat, electrodul a fost scos din celulă, spălat cu apă dublu distilată și reintrodus în celulă, unde se așteaptă stabilirea unui nou echilibru, după care se reia un nou ciclu, descris mai sus, ș.a.m.d.

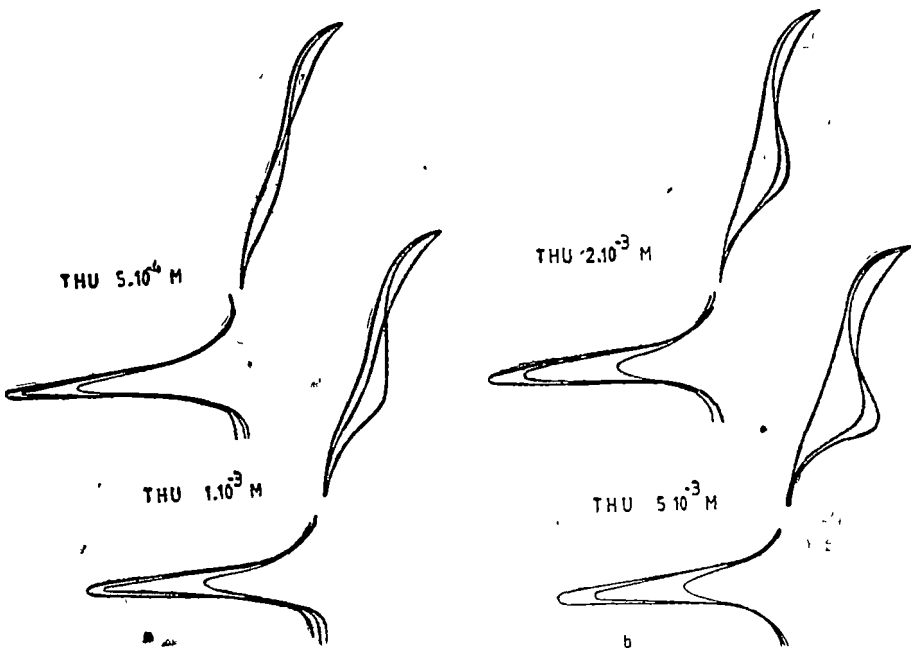

Fig 1.

După cîteva asemenea cicluri se constată că oricît s-ar repeta această operaţie, se obţine o aceeaşi curbă, procesul devenind absolut reproductibil. Aceasta indică faptul că substanţa adsorbită a fost complet înlăturată de pe suprafaţa electrodului, restabilidui-i-se acestuia caracteristicile pe care le-a avut înainte de a fi otrăvit. Prin însumarea ariilor obţinute în procesul anodic se poate calcula sarcina electrică consumată în procesul anodic, mărime care permite evaluarea cantităţii de substanţă adsorbită pe suprafaţa electrodului

În figură sînt prezentate curbele înregistrate pentru patru concentraţii diferite de tiouree (THU) După cele trei cicluri descrise, electrodul de paladiu este curat. Se observă că ariile în procesul anodic cresc cu mărimea concentraţiei soluţiei, fapt care arată o creştere a gradului de otrăvire a suprafaţei electrodului În felul acesta, metoda permite evaluarea cantităţii de substanţă adsorbită, determinîndu-se gradul de acoperire a suprafeţei, iar pe de altă parte, prin aplicarea unui număr de cicluri repetate VTLV, se obţine regenerarea suprafeţei electrodului, restabilindu-i-se toate caracteristicile iniţiale

BIBLIOGRAFIE

1 T B Flanagan, Hidrieds for Energy Storage, 135, Norway, 14—19 August 1977
2 H Wroblova, M Green, *Electrochimica* Acta, 8, 679, 1983
3 R V Bucur, F Bota, *Electrochimica* Acta, 29, 1283, 1984
4. R V Bucur, F Bota, *Electrochimica* Acta, 28, 1373, 1983
5 R V Bucur, P. Mărgineanu, *Electrochimica* Acta, 29, 1297, 1984

STUDIA UNIV BABEŞ—BOLYAI, PHYSICA, XXXI, 1, 1986

DETERMINAREA TITLULUI UNOR MONEDE ANTICE DIN ARGINT PRIN ACTIVARE CU NEUTRONI

C. COSMA*, T. FIAT*, V. ZNAMIROVSCHI*, V. MERCEA*, L. DĂRĂBAN**, V. MORARIU**, D. BOROS***, D. ALICU*** and R. ARDEVAN***

Intra în redacţie la 12 iulie 1986, acceptat la 12 august 1986

ABSTRACT. — **Title Determination of Ancient Coins by a Neutron Activation Method.** The silver concentration of 40 Roman and Greek coins (70—250 A C) was determined by using an Am—Be neutron source for activation analysis. The silver concentration shows a maximum arround the year 110 A C which corresponds to the flourishing period of the Roman Empire after the Dacian wars. Also, the measurement by gamma spectrometry may lead to singling out the forged coins.

Introducere. Studiul conţinutului în metale preţioase a unor relicve antice (monede, obiecte de podoabă, obiecte de cult, etc.) este util în cercetările de arheologie, putînd da informaţii despre perioadele de înflorire sau de decadenţă economică a unei epoci istorice date. Studiul întregului spectru al compoziţiei elementale şi mai ales determinarea impurităţilor poate aduce dovezi privind sursele de materii prime (fier, cupru, argint, aur etc.) utilizate de administraţia perioadei respective [1-6].

Din cauza valorii artistice şi istorice a monedelor, ele nu pot fi deteriorate sau distruse, ceea ce implică folosirea metodelor de analiză nedistructive. Folosirea analizei de suprafaţă nu este reprezentativă în toate cazurile deoarece în decursul timpului monedele pot suferi fenomene de coroziune electrochimică ceea ce duce la o îmbogăţire în metale nobile a suprafeţei (Au, Ag) în timp ce celelalte elemente îşi vor diminua concentraţia [6].

Determinarea compoziţiei elementale a cîtorva monede existente la Muzeul de Istorie al Transilvaniei a fost făcută şi anterior [7], folosindu-se metode chimice şi spectroscopice distructive.

În lucrarea de faţă a fost determinată concentraţia argintului (titlul) folosind metoda analizei prin activare cu neutroni termici pentru un set de 40 monede antice, romane şi greceşti, găsite pe teritoriul României şi emise înainte şi respectiv după cucerirea Daciei. S-a făcut şi un studiu calitativ al elementelor majoritare însoţitoare argintului prin spectrometrie de fluorescenţă în raze X [8].

Metoda experimentală. Determinarea titlului argintului s-a făcut determinînd cantitatea de argint din fiecare monedă şi împărţind această cantitate la masa monedei. În acest scop s-a folosit tehnica analizei prin activare cu neutroni cuplată cu o metodă gama-spectroscopică. Cele 40 de monede şi etalonul au fost iradiate în condiţii identice într-un flux de neutroni termici proveniţi de la o sursă de Am—Be [9]. Ca etalon s-a folosit o probă de Ag pur

* *Universitatea din Cluj-Napoca, Facultatea de fizică, 3400 Cluj-Napoca, România*
** *Institutul de Tehnologie Izotopică şi Moleculară, 3400 Cluj-Napoca, România*
*** *Muzeul de Istorie al Transilvaniei, 3400 Cluj-Napoca, România*

(m = 2,036 g) de formă și masă apropiate modelelor analizate Așezarea identică în flux a probelor s-a realizat cu ajutorul unui dispozitiv avînd posibilitatea de fixare a probelor (prin plasturizare) și a acestuia în canalul în care se face iradierea Cei doi izotopi stabili ai Ag au fost activați prin reacțiile:

$$^{107}_{47}Ag + ^{1}_{0}n \rightarrow ^{108}_{47}Ag \ (T = 2,4 \text{ min}); \ ^{108\,m}_{47}Ag \ (T = 5 \text{ ani}) \quad (1)$$

$$^{109}_{47}Ag + ^{1}_{0}n \rightarrow ^{110}_{47}Ag \ (T = 24 \text{ s}) . \ ^{110\,m}_{47}Ag \ (T = 253 \text{ zile}) \quad (2)$$

La dezintegrarea beta a ^{108}Ag și a ^{110}Ag pe lîngă particulele β sînt emise și mai multe energii gama obținîndu-se în final $^{108}_{46}Pd$, $^{108}_{48}Cd$ și respectiv $^{110}_{48}Cd$ în stări fundamentale Figura 1 reproduce spectrul gama obținut în cazul iradierii timp de 20 min a etalonului Spectrul s-a ridicat folosind un analizator cu 512 canale de tip NTA—512M cuplat cu un detector GeLi de tip Kovo R 327—1 avînd un volum util de 30 cm^3 și o rezoluție de 2,3 keV pentru picul de 662 keV al ^{137}Cs

După cum se observă din relațiile (1, 2) folosirea unor timpi de iradiere mai lungi este nejustificată, deoarece perioadele de înjumătățire a celor doi izotopi formați prin activare sînt de 2,4 min pentru ^{108}Ag și de 24 s pentru ^{110}Ag Etalonarea spectrului din Fig 1 s-a realizat folosind surse etalon de ^{241}Am, ^{137}Cs și ^{60}Co După cum se observă pe acest spectru cele mai reprezentative fotopicuri identificate sînt cele de 430 keV și 620 keV pentru ^{108}Ag și cel de 660 keV pentru ^{110}Ag, energii gama indicate și în literatură [10].

Încercarea de a determina concentrația argintului din monede folosind aceste fotopicuri precum și condițiile optime de iradiere, răcire și măsurare ne-a condus la concluzia că pentru a obține rezultate cu un grad de precizie sub 5% sînt necesare fluxuri de neutroni de 10—20 ori mai mari ca cel dat de sursa de Am—Be avută la dispoziție. Din această cauză, această cale a fost abandonată, însă rezultatele obținute precum și spectrul din Fig 1 ne-au oferit o ieșire din această situație După cum se observă pe acest spectru două din cele trei energii mai importante emise la activarea argintului apar destul de grupate în intervalul 600—680 keV Această grupare a sugerat folosirea

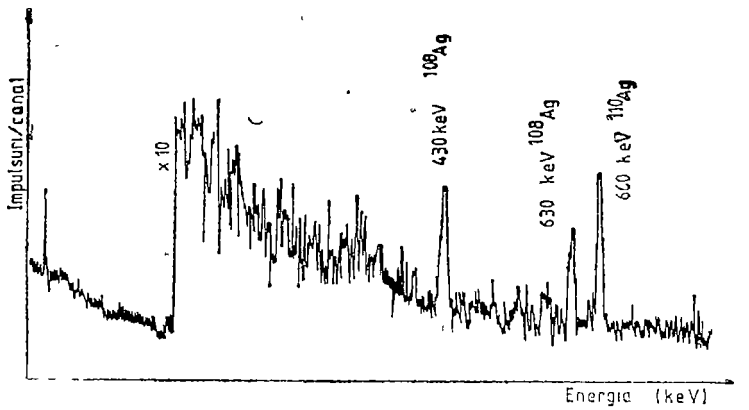

Fig 1 Spectrul etalonului obținut cu detector GeLi

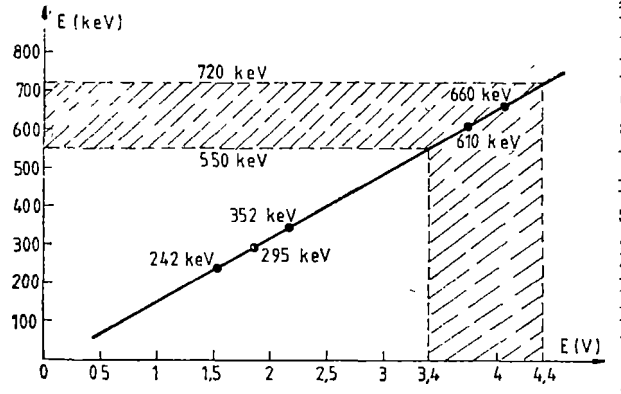

Fig. 2. Etalonarea spectrometrului monocanal RFT 20120

în locul detectorului Ge—Li a unui detector cu scintilaţie NaI(Tl) care are o eficacitate de 6—8 ori mai mare pentru aceste energii şi a măsurării vitezei de numărare sub ambele fotopicuri simultan. În acest scop s-a folosit un spectrometru gama monocanal de tipul RFT 20120 cuplat cu o sondă scintilatoare avînd un cristal de Na(Tl) de dimensiuni 45 × 40 mm. Spectrometrul a fost operat la o tensiune de 870 V pe fotomultiplicator şi în condiţii de amplificare optimă. Pentru etalonare s-a folosit energia de 662 keV a ^{137}Cs şi energiile de 295 keV, 352 keV şi 609 keV a pechblendei [11]. Pentru micşorarea fondului, măsurătorile au fost efectuate cu sonda scintilatoare şi proba închisă într-un turn de plumb Folosind aceste energii a fost ridicată dreapta de etalonare din Fig 2. Fixînd pragul analizatorului la valoarea 3,4 V şi operînd cu lărgimea ferestrei de 1V, corespunzătoare unui domeniu energetic de 170 keV se va acoperi după cum rezultă de pe figură domeniul energetic 550—720 keV, domeniu care include cele două picuri de 620 keV şi 660 keV ale argintului.

Pragul a fost fixat la valoarea minimă de 550 keV (3,4 V) şi pentru a evita pătrunderea picului cu energia de 511 keV a cuprului pe care l-am presupus ca posibil aliat al argintului în monede [8].

Măsurători şi rezultate. Cu ajutorul metodei descrise mai sus am determinat concentraţia argintului din cele 40 de monede în două serii de măsurători. Concentraţia, în procente de greutate, a fost determinată cu relaţia:

$$c(\%) = \frac{m_e}{m_m} \frac{A_m - F}{A_e - F} \cdot 100 \qquad (3)$$

unde:

m_e = masa etalonului (2,036 g);
m_m = masa monedei (1,7—4 g);
A_m = numărul de impulsuri înregistrate în prezenţa monedei în intervalul 550—720 keV;
A_e = numărul de impulsuri înregistrate în prezenţa etalonului în acelaşi interval şi acelaşi timp;
F = numărul de impulsuri datorat fondului în intervalul de mai sus.

Pentru a găsi titlul monedei concentraţia din relaţia de mai sus (3) se multiplică cu un factor de 10. Atît monedele cît şi etalonul în timpul măsurătorilor au fost lipite de fereastra de intrare a scintilatorului asigurînd astfel o geometrie de măsură cu eficienţă maximă ($\simeq 2\pi$). Cele două serii de măsurători s-au efectuat după următorul program:

Seria I: timp de iradiere, $t_{ir} = 8$ min; timp de răcire $t_r = 25$ s; timp de măsură $t_m = 4$ min.

Seria II: timp de iradiere, $t_{ir} = 2$ min, timp de răcire $t_r = 20$ s; timp de măsură, $t_m = 1$ min.

Măsurătorile din prima serie au urmărit să prindă cît mai multe impulsuri atît sub fotopicul de 660 keV, cît şi sub cel de 620 keV, dar din cauza fondului ridicat ($\simeq$ 300 imp/4 min) măsurătorile din această serie sînt afectate de erori mari ($\simeq$ 10%) Raportul dintre viteza de numărare a probei şi a fondului este în acest caz unitar. Seria a doua de măsurători a fost efectuată în scopul măririi raportului semnal-zgomot (activitatea probei/fond), redu cînd totodată şi timpul total necesar analizei unei monede, $t_{ir} + t_r + t_m$, la 3,5 min faţă de 12,5 min în cazul primei serii În această a doua serie s-a urmărit prinderea unui număr cît mai mare de impulsuri datorate picului de 660 keV cu timpul de înjumătăţire de 24 s. Acest lucru s-a realizat prin reducerea la limita posibilului (15—20 s) a timpului de răcire, timpi mai scurţi fiind accesibili numai în cazul folosirii unei poşte pneumatice. Raportul dintre activitatea monedei şi activitatea fondului s-a ridicat în acest caz la valoarea de 2,5 şi deci rezultatele din această serie sînt afectate de erori mai mici ($\simeq$5%). Numărul de impulsuri, A_m, din relaţia (3) este media a 3—5 măsurători iar pentru A_e şi F au fost efectuate cîte 10 măsurători. Stările metastabile ale argintului, ^{108m}Ag şi ^{110m}Ag au o contribuţie neînsemnată în spectru atît din cauza secţiunilor de activare mai mici [12] cît mai ales din cauza perioadelor de înjumătăţire mari (1, 2) Prin alegerea intervalului energetic considerat sînt excluse fotopicurile izotopilor ^{64}Cu şi ^{66}Cu, activate odată cu argintul. Eventuala contribuţie în acest interval, prin efect Compton, a energiilor ^{66}Cu mai mare de 720 keV este mică datorită secţiunii de activare cu un ordin de mărime mai mică decît a argintului, pe de-o parte, şi pe de altă parte din cauza factorilo de schemă foarte mici ai acestor radiaţii [12]. De asemenea izotopii fierului susceptibili de a se activa, ^{54}Fe şi ^{58}Fe pe lîngă secţiunile de activare mici au şi abundenţe izotopice mici şi de asemenea timpi de înjumătăţire mari

Izotopii plumbului, după cum se ştie se activează foarte greu. Energiile gama emise la activarea aurului, şi care se pretează şi el la determinări cantitative prin această metodă, fiind inferioare intervalului energetic considerat nu produc interferenţe la determinarea argintului O eventuală sursă de erori pe care o semnalăm aici se poate datora cantităţilor diferite de bor şi cadmiu din monezi şi etalon şi care din cauza secţiunilor de absorbţie foarte mari pot absorbi o parte din fluxul de neutroni destinat activării argintului

Contribuţia nesemnificativă a altor elemente activate avînd perioade de înjumătăţire de acelaşi ordin de mărime cu cele ale argintului, în intervalul energetic considerat, este exclusă după cum rezultă şi din Fig. 3.

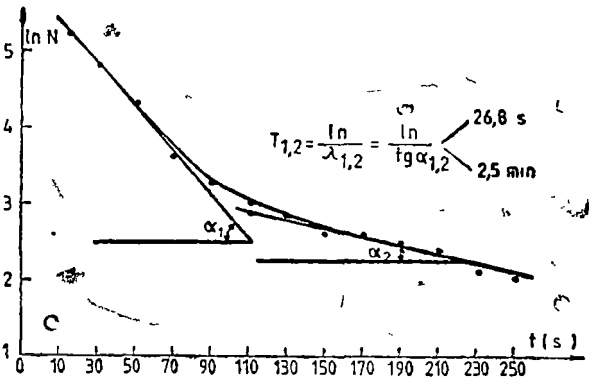

Fig. 3. Variaţia în timp a activităţii monedei nr. 1.

Această figură reproduce scăderea activităţii în timp pentru una din monedele analizate Perioadele de înjumătăţire determinate din această figură de 25 min şi respectiv 26,8 s corespund celor doi izotopi ai argintului.

Folosind relaţia (3) cu A_m A_e şi F măsurate în condiţiile descrise s-au obţinut pentru concentraţiile de argint din cele 40 monede analizate valorile din Tabelul 1

Tabel 1

Valorile concentraţiei argintului în procente de greutate din cele 40 monede

Nr crt	Moneda (proveniența)	Concentraţia (%) Seria I	Seria II	Nr crt	Moneda (proveniența)	Concentraţia (%)
1	Denar, Antoninus Pius (140—143 e n)	86	89,4	21	Denar, Severus Alexander (222—228 e n)	78
2	Denar, Caracallax (196—198 e n)	56	57,6	22	Denar, Caracalla (196—198 e n)	77
3	Denar, Lucius Verus (166 e n)	88	96	23.	Denar*, Elagabal (218—222 e n.)	45,5
4	Denar, Marcus Aurelius (168 e n)	80	79,9	24	Denar, Antonius Pius (140—143 e.n)	79,5
5	Denar, Geta (209 e n)	80,1	85,5	25	Denar, Srptimius Severus (196—197 e n)	91
6	Denar, Septimius Severus (198—200 e n)	77	79,4	26	Denar, Vespasianus (74 e n.)	90
7	Denar, Traianus (114—115 e n)	96,7	98,6	27	Denar, Domitianus Caesar (79 e.n)	3
8	Denar, Vespasianus (74 e n)x	82	86,8	28	Antoninian, Philippus II (244—246 e n)	74,5
9	Denar, Traianus (102 e n)	96,6	96,3	29	Denar, Severus Alexander (231—235 e n)	5
10	Drahmă, Dyrhachium (sf sec III î e n)	91,8	91,9	30	Denar, Caracalla (207 e.n)	79
11	Denar, Traianul 108—111 e n)	~100	~100	31	Denar, Septimius Severus (201 e n)	80
12	Denar, Caracalla (206—210 e n)	93	91	32	Denar, Traianus (114—117 e n)	12
13	Drahmă, Dyrrhachium (sf sec, III î e n)	84,3	83,3	33	Denar, Hadrianus (119—122 e n)	72
14.	Antoninian, Philippus II (244—247 e n)	51,8	44	34	Antoninian, Philippus I (248 e n.)	4
15.	Denar, Hadrianus (128—138 e n)	85	84,8	35	Denar, Lucilla (161—180 e n)	2
16.	Denar, Traianus (102 e n)	97	95,2	36	Denar, Hadrianus (125—128 e n)	92,5
17	Denar, Traianus	90,2	91,6	37	Denar, Severus Alexander (222 e n)	79
18	Denar, Caracalla (207 e.n)	68	66	38	Denar*, Iulia Paula (218—220 e n)	87
19	Denar, Severus Alexander (222—228 e n)	—	6ş	39	Antoninian, Hostilianus (251 e n)	49,5
20	Denar, subaerat, Antonius Pius (147—148 e n)	—	10	40	Denar, Severus Alexander (227 e n)	36

* Emise de monetăria din Antiochia [13] [15]

Discuţii. Monedele 1—20, adică cele din partea stîngă a Tabelului 1 au fost găsite în castrul roman de la Gherla. Acest grup include 16 denari, 2 drahme greceşti din sec. III î e.n, un antoninian şi un denar subaerat (mo-

nedă de cupru placată cu argint). Dacă comparăm cele două coloane, cuprinzînd concentrațiile determinate în cele două serii, se observă o concordanță bună între valorile obținute. Diferențele mai mari semnalate la monedele 3, 5, 8, 14 nu sînt semnificative fiind în limita erorilor statistice și avînd în vedere că rezultatele din prima serie au o precizie în jur de 8% iar cele din seria a doua de ≈5%.

Dacă nu luăm în discuție denarul subaerat acest grup de monede nu cuprinde nici un fals, lucru de înțeles dacă avem în vedere poziția armatei în imperiu și faptul că în castru majoritatea locuitorilor erau soldați O valoare mai slabă o prezintă monedele nr. 2 și 18 din timpul împăratului Caracalla în timpul căruia a fost adoptată și o reformă monetară prin introducerea unei monede noi „antoninianul" (1 antoninian = 2 denari). Toate monedele romane descoperite în castrul de la Gherla au fost emise de monetăria din Roma [13].

Monedele din partea dreaptă a tabelului 1 (21—40) au fost descoperite la Ulpia Traiana Sarmizegetusa și cuprind în prezentarea istorică inițială 17 denari și 3 antoninieni. Două din aceste monede (nr. 23 și 38) sînt emise în Siria, la Antiochia, iar restul la Roma În afară de moneda nr. 32 ($c_{Ag}=12\%$) emisă în timpul domniei lui Traian și care este recunoscută de istorici ca un fals antic apar în plus și unele neconcordanțe care vor trebui elucidate în viitor de către istorici în legătură cu monedele nr 23, 27, 29, 34 și 35. Astfel moneda nr 23 care este un denar emis la Antiochia are o concentrație de argint mică, sub 50% și s-ar părea că pune într-o anumită lumină relația dintre monetăria din Roma și cea din Antiochia. Monedele nr. 27, 29 și 35 sînt în mod sigur fie falsuri, fie confuzii istorice. Același lucru se poate spune și despre moneda nr. 34 care este un antoninian Ceilalți doi antoninieni (28 și 39) la fel ca și antoninianul din prima serie (nr. 14) au valori ale concentrației argintului mai mici decît denarii. O concentrație mică a argintului, și

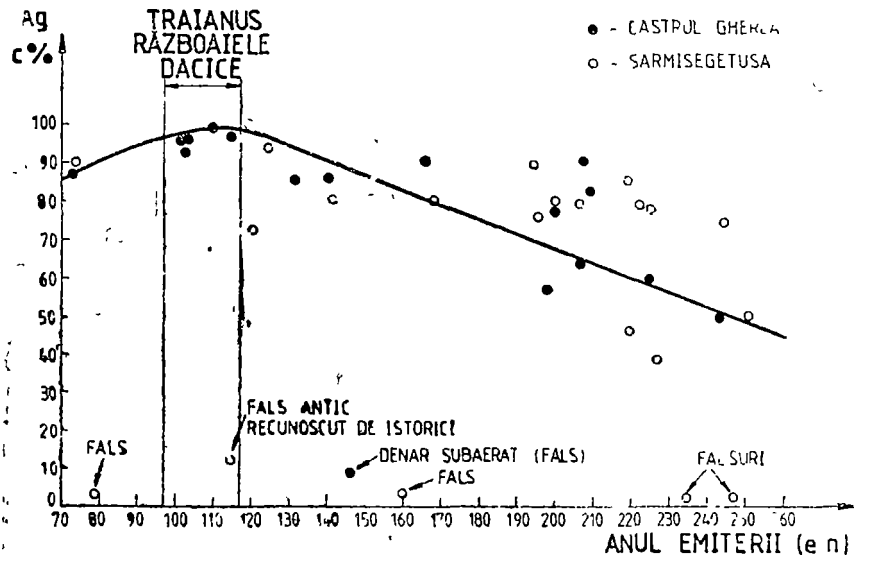

Fig. 4. Evoluția în timp a concentrației argintului din monedele antice

care face o notă discordantă faţă de alte monede emise în aceeaşi perioadă şi sub acelaşi împărat, o prezintă moneda nr 46 (36% Ag)

Comparînd monedele din castrul de la Gherla cu cele de la Ulpia Traiana Sarmizegetusa se observă că în cazul Ulpiei Traiana apar mai multe situaţii Astfel se constată că în cazul monedelor de la Ulpia Traiana apar falsuri şi încă într-o proporţie destul de mare De asemenea există o gamă mai largă de variaţie a concentraţiei argintului la monedele din capitala provinciei. Dacă avem în vedere că centrul administrativ al provinciei era şi un important centru comercial, varietatea mai mare a monedelor de aici este într-un fel justificată. Reprezentînd concentraţia argintului în funcţie de anul emiterii pentru cele 38 de monede romane se observă o curbă cu un maxim în jurul anului 110 e n. (Fig 4) maxim ce coincide cu perioada de maximă dezvoltare a Imperiului Roman din timpul domniei lui Traian

Acest maxim, după cum se observă pe figură este imediat următor cuceririi Daciei de către Traian, cînd după cum se ştie aurul şi argintul Daciei au luat drumul Romei [14]. Vom semnala, de asemenea, valoarea slabă a două din cele patru monede analizate şi care au fost emise în partea a doua a domniei lui Severus Alexander, perioadă în care se semnalează de altfel şi începutul declinului Imperiului Roman

BIBLIOGRAFIE

1. J. N. Barrandon, *J Radioanal. Chem*, **55**, 317 (1980)
2. A A Garous, *Archaeometry*, **10**, 78 (1967)
3 R W Thiele, U Aunghin, U Kyaw, *Archaeometry*, **14**, 199 (1972)
4 Ch Calouhi, E Hourani, R Loos, S Melki, *Nucl Instr Methods*, **200**, 553 (1982)
5. C Cosma, T Fiat, V Znamirovschi, L Dărăban, V Morariu, D. Boroş, D Alicu, „The first Balkanian, Sympossium of the Activation Analysis", Varna, Bulgaria, 1985
6. C Beşliu, V Cojocaru, M Constantinescu, V Grecu, M Ivaşcu, V. Mateiciuc, S Spiridon, P. Stancu, C Stirbu, Pieprint Univ Bucureşti (1982)
7. E. Stoicovici, Florica Stoicovici, *Acta MN* **XI**, 19 (1974)
8. T. Fiat, C Cosma, L Dărăban, V Morariu, *A şasea sesiune anuală de comunicări* „Progrese în fizică", Sibiu, 1984, p 640
9. T. Fiat, L Dărăban, *Studia Univ Babeş-Bolyai, ser Phys*, **21**, 74 (1976)
10. S. A. Lis, Ph K Hopke, J L Fasching, *J Radioanal Chem*, **25**, 303, (1975)
11. C Cosma, I. Mastan, V Znamirovschi, *Stud. Cerc Fiz*, **33**, 351 (1981)
12 D. T. Goldman, „Chart of the nuclides", U S Atomic Energy Comission, 1965
13. H. Matingly, E Sydenhamm, „Roman Imperial Coinage", London, 1923
14. J. Carcopino, „L'or des Daces at les Finances de Rome sous Trajan Dacia", I, 1924
15. H. Ceka, „Questions de numismaqtique Illyrienne", Tirana, Albania, 1973

STUDIA UNIV BABEŞ—BOLYAI, PHYSICA, XXXI, 1, 1986

AXIALLY SYMMETRIC WHISTLER MODE IN A BOUNDED WARM RELATIVISTIC ELECTRON BEAM-PLASMA SYSTEM

J. KARACSONY*, S. COLDEA* and C. BĂLEANU*

Received: October 17, 1985; accepted August 12, 1986

ABSTRACT. — The present work investigates excitation of the small amplitude axially symmetric whistler mode in a bounded warm relativistic electron beam-plasma system with cylindrical geometry, in an external magnetic field Oscillation frequency and growth rates have been found for whistler, in a cylindrical plasma waveguide with a low density beam moving near the axis. It is found that the whistler mode can be excited only by cyclotron resonance under anomalous Doppler effect condition. A temperature correction in the growth rate was obtained.

Introduction. As previously shown, the passage of an electron beam through plasma, in the absence or presence of an external magnetic field, gives rise to instabilities [1 — 4]. It is known that, at $\omega_p \gg \omega_e \gg \omega$, in an infinite plasma a branch of oscillations usually called whistler can be excited [1]. A similar branch of oscillations may be found for a bounded plasma [5—6].

The dispersion relation for the whistler modes, excited in a bounded system of a cold magnetized plasma penetrated by a cold nonrelativistic electron beam could be obtain using the general dispersion relation describing the bulk waves [5—6]; by solving this dispersion equation expressions for frequencies and growth rates of the whistler waves in the bounded system were determined [5—6]. These instabilities can appear in a cylindrical cold nonrelativistic electron beam-cold plasma system only under cyclotronic resonance ($\omega_w = k_z \quad v_0 - \omega_e$), in the condition of anomalous Doppler effect. Because experimentally it is very difficult to obtain a monoenergetic beam and even an initially cold beam turns into a warm beam as a consequence of its quasilinear relaxation, the aim of the present paper is to investigate the possibility for excitation of axially symmetric whistler waves in a cylindrical geometry, considering a warm relativistic electron beam and a cold magnetized plasma.

Derivation of the Dispersion Relation. The cylindrical configuration considered will consist of a perfectly conducting guide of radius R filled with cold plasma, with a coaxial warm relativistic electron beam of radius $r(R > r)$, and an external magnetic field applied along the axis of the guide. The density of the beam is assumed to be small compared to plasma density, thus $\varepsilon = n_b/n_p \ll \ll 1$.

The important steps for derivation of the dynamic dispersion relation for bounded geometry have been presented by Kitsenko *et al* [5] for cold nonrela-

* *University of Cluj-Napoca, Department of Physics, 3400 Cluj-Napoca, Romania*

tivistic electron beam-plasma system. It has been found useful to write the expression for the dielectric tensor ε_{ij} in an invariant form

$$\varepsilon_{ij} = \left(a - b\frac{k_\perp^2}{k_z^2}\right)\delta_{ij} + \frac{b}{k_z^2}k_i k_j + \left(c_1 + c_2\frac{k_\perp^2}{k_z^2}\right)h_i h_j + i\left(d + f\frac{k_\perp^2}{k_z^2}\right)\cdot$$
$$\cdot\,\varepsilon_{ijl}\,h_l + i\frac{f}{k_z^2}\,[k_i(\vec{k}\times\vec{h})_j - k_j(\vec{k}\times\vec{h})_i] + \frac{b}{k_z^2}\,(\vec{k}\times\vec{h})_i(\vec{k}\times\vec{h})_j \qquad (1)$$

where $\vec{h}$ is the unit vector directed along external magnetic field $\vec{B}_0$, $k_z = \vec{k}\cdot\vec{h}$, $k_\perp^2 = k^2 - k_z^2$, δ_{ij} is the Kronecker symbol, and ε_{ijl} is a complete antisymmetric tensor of the third order The expression for coefficients a, b, c_1, c_2, d and f are given in [5] Supposing $\omega_p \gg \omega_e \gg \omega$ it has been found from general dispersion equation the following dispersion relation for whistler mode

$$\frac{1}{T_w^{\mathrm{I}}}\cdot\frac{J_1(T_w^{\mathrm{I}}r)}{J_2(T_w^{\mathrm{I}}r)} = \frac{1}{T_w^{\mathrm{II}}}\cdot\frac{J_1(T_w^{\mathrm{II}}r)\,Y_1(T_w^{\mathrm{II}}R) - J_1(T_w^{\mathrm{II}}R)\;\;Y_1(T_w^{\mathrm{II}}r)}{J_0(T_w^{\mathrm{II}}r)\,Y_1(T_w^{\mathrm{II}}R) - J_1(T_w^{\mathrm{II}}R)\;\;Y_0(T_w^{\mathrm{II}}r)} \qquad (2)$$

where

$$T_w^2 = \frac{\omega^2}{c^2}\cdot\frac{(a - N_z^2)^2 - d^2}{a - N_z^2} \qquad (3)$$

$N_z = k_z c/\omega$ and J_n and Y_n are the Bessel and Neumann functions of order n, respectively. Superscript I and II denote quantities related to region I (plasma + beam of thickness $2r$) and to region II (adjacent annular region filled with plasma and bounded by a perfectly conducting cylinder of radius R)

Since the previously derived solution is heavily based on the hermitian properties of tensor ε_{ij} given in equation (1) for cold beam-plasma system, and on the fact that $\varepsilon_{11} = \varepsilon_{22}$, hence the dielectric tensor which can be derived for the finit temperature relativistic electron-beam-cold plasma system should possess these properties It can easly be proved that by expanding the dielectric tensor for warm relativistic electron beam-plasma system, deduced in [7], with respect to small values of $k_\perp \bar{v}_\perp\;\gamma_0/\omega_e$, and neglecting terms of order $k_\perp^2\bar{v}_\perp^2\gamma_0^2/\omega_e^2$ and higher, identifying to equation (1), all the previously derived results hold if we substitute the six dielectric constants a, b, c_1, c_2, d and f, respectively, by a', b', c_1', c_2', d' and f', where

$$a' = 1 - \frac{\omega_p^2}{\omega^2 - \omega_e^2} + \frac{\varepsilon}{2\gamma_0}\;\frac{\omega_p^2}{\omega^2}\left\{\left[s_0 + s_1\left(\frac{T_\perp}{T_\parallel} - 1\right)\right]\;Z(s_1) + \right.$$
$$\left. + \left[s_0 + s_{-1}\left(\frac{T_\perp}{T_\parallel} - 1\right)\right]\cdot Z(s_{-1}) + 2\left(\frac{T_\perp}{T_\parallel} - 1\right)\right\} \qquad (4)$$

$$b' = -\frac{\varepsilon}{\gamma_0}\;\frac{\omega_p^2}{2\omega^2}\left\{\frac{\omega + \omega_e/\gamma_0}{\omega_e/\gamma_0}\;\left[s_0 + s_{-1}\left(\frac{T_\perp}{T_\parallel} - 1\right)\right]\;Z(s_{-1}) - \right.$$
$$\left. - \frac{\omega - \omega_e/\gamma_0}{\omega_e/\gamma_0}\cdot\left[s_0 + s_1\left(\frac{T_\perp}{T_\parallel} - 1\right)\right]\cdot Z(s_1) + 2\left(\frac{T_\perp}{T_\parallel} - 1\right)\right\} \qquad (5)$$

$$c_1' = -\frac{\omega_p^2}{\omega^2} + \frac{\omega_p^2}{\omega^2 - \omega_e^2} + \frac{\varepsilon}{\gamma_0^3} \cdot \frac{\omega_p^2}{k_z^2 \bar{v}_{||}^2} (1 + s_0 \quad Z(s_0)) + c \quad \frac{\omega_p^2}{\omega^2} \cdot$$

$$\left\{ \frac{\omega}{\omega_e} \quad \left[s_0 + s_{-1} \left(\frac{T_\perp}{T_{||}} - 1 \right) \right] \quad Z(s_{-1}) - \frac{\omega}{\omega_e} \quad \left[s_0 + s_1 \left(\frac{T_\perp}{T_{||}} - 1 \right) \cdot Z(s_1) \right] \right. \tag{6}$$

$$c_2' = \frac{\varepsilon \quad \omega_p^2 \gamma_0}{2\omega_e^2} \quad \left\{ -2 \frac{T_\perp}{T_{||}} s_0 Z(s_0) + \frac{\omega + \omega_e/\gamma_0}{\omega} \left[s_0 + s_{-1} \left(\frac{T_\perp}{T_{||}} - 1 \right) \right] \cdot Z(s_{-1}) + \right.$$

$$\left. + \frac{\omega - \omega_e/\gamma_0}{\omega} \left[s_0 + s_1 \left(\frac{T_\perp}{T_{||}} - 1 \right) \right] \quad Z(s_1) \right\} \tag{7}$$

$$d' = -\frac{\omega_p^2}{\omega \omega_e} - \frac{\varepsilon}{2\gamma_0} \quad \frac{\omega_p^2}{\omega^2} \left\{ \left[s_0 + s_1 \left(\frac{T_\perp}{T_{||}} - 1 \right) \right] \quad Z(s_1) - \right.$$

$$\left. - \left[s_0 + s_{-1} \left(\frac{T_\perp}{T_{||}} - 1 \right) \right] \quad Z(s_1) \right\} \tag{8}$$

and

$$f' = \frac{\varepsilon \cdot \omega_p^2}{2\omega\omega_e} \left\{ 2 \frac{T_\perp}{T_{||}} s_0 Z(s_0) - \frac{\omega - \omega_e/\gamma_0}{\omega} \left[s_0 + s_{-1} \left(\frac{T_\perp}{T_{||}} - 1 \right) \right] \cdot Z(s_{-1}) - \right.$$

$$\left. - \frac{\omega + \omega_e/\gamma_0}{\omega} \left[s_0 + s_1 \left(\frac{T_\perp}{T_{||}} - 1 \right) \right] \cdot Z(s_1) \right\} \tag{9}$$

where

$$s_n = \frac{\omega - k_z v_0 - n\omega_e/\gamma_0}{k_z \bar{v}_{||}} \quad (n = 0, \pm 1) \tag{10}$$

$$\bar{v}_{||} = \sqrt{\frac{T_{||}}{m \quad \gamma_0^3}} \tag{11}$$

and $\gamma_0 = (1 - v_\theta^2/c^2) \cdot Z(s_n)$ is the plasma dispersion function

$$Z(s_n) = -e^{-s_n^2/2} \left[\int_0^{s_n} exp\,(\xi^2/2) d\xi - 1 \left(\frac{\pi}{2} \right)^{1/2} \right] \tag{12}$$

Parameters $T_w^{I,II}$ are not to be confused with temperature $T_{\perp,||}$

Whistler mode excitation. The density of the beam passing in region I is assumed to be small compared to plasma density ($\varepsilon \ll 1$) In first approximation, one may neglect the beam contribution to the dielectric tensor Thus, from equation (2) it is obtained

$$J_1(T_{w0} \quad R) = 0 \tag{13}$$

whereas from expression (3), in the absence of the beam and due to condition $\omega_p \gg \omega_e \gg \omega$, T_{w0} is defined by

$$T_{w0}^2 = -k_z^2\left(1 - \frac{\omega_p^4}{N_z^4\omega^2\omega_e^2}\right) \tag{14}$$

For the wave frequency from relation (13) there results

$$\omega_w = \frac{|\omega_e \cos\theta_w|}{K} \tag{15}$$

where

$$K = \frac{\omega_p^2 R^2}{(k_z^2 R^2 + x_{1\nu}^2)c^2}, \quad \cos\theta_w = \frac{k_z R}{\sqrt{k_z^2 R^2 + x_{1\nu}^2}} \tag{16}$$

where $x_{1\nu}$ are the roots of the Bessel function of the first order.

To calculate the growth rate we write the dispersion relation (2) for whistler wave under the from:

$$D(\omega, k_z, \varepsilon) = \frac{1}{T_w^{\mathrm{I}}} \cdot \frac{J_1(T_w^{\mathrm{I}} r)}{J_0(T_w^{\mathrm{II}} r)} - \frac{1}{T_w^{\mathrm{II}}} \cdot \frac{J_1(T_w^{\mathrm{II}} r) Y_1(T_w^{\mathrm{II}} R) - J_1(T_w^{\mathrm{II}} R) Y_1(T_w^{\mathrm{II}} r)}{J_0(T_w^{\mathrm{II}} r) Y_1(T_w^{\mathrm{II}} R) - J_1(T_w^{\mathrm{II}} R) Y_0(T_w^{\mathrm{II}} r)} \tag{17}$$

considering that for T_w^{I} at a low beam density, the following expression is valid

$$T_w^{\mathrm{I}^2} = T_w^{\mathrm{II}^2} \cdot \left\{1 + \frac{\varepsilon}{4\gamma_0} \cdot \frac{\omega_p^2 k_0^2}{\omega^2 T_w^{\mathrm{II}^2}} \left\{\left[s_0 + s_1\left(\frac{T_\perp}{T_\parallel} - 1\right)\right] \cdot Z(s_1) \cdot \right.\right.$$
$$\cdot \left(\frac{1 + \cos\theta_w}{\cos\theta_w}\right)^2 + \left[s_0 + s_{-1}\left(\frac{T_\perp}{T_\parallel} - 1\right)\right] \cdot Z(s_{-1}) \cdot \left(\frac{1 - \cos\theta_w}{\cos\theta_w}\right)^2 +$$
$$\left.\left. + 2\left(\frac{T_\perp}{T_\parallel} - 1\right)(T_w^{\mathrm{II}^2} + 2k_0^2 N_z^2)\right\}\right\} \tag{18}$$

This expression has been obtained from (3) neglecting the terms of the second and higher orders with respect to ε.

Now, expanding (17) with respect to ε one can write the dispersion relation for whistler mode under the form

$$D_0(\omega, k_z) + \varepsilon \cdot \frac{\omega_p^2}{4\gamma_0 c^2 T_{w0}^2} \left\{\left[s_0 + s_1\left(\frac{T_\perp}{T_\parallel} - 1\right)\right] \cdot Z(s_1)\left(\frac{1 + \cos\theta_w}{\cos\theta_w}\right)^2 + \right.$$
$$+ \left[s_0 + s_{-1}\left(\frac{T_\perp}{T_\parallel} - 1\right)\right] \cdot Z(s_{-1})\left(\frac{1 - \cos\theta_w}{\cos\theta_w}\right)^2 + 2\left(\frac{T_\perp}{T_\parallel} - 1\right) \cdot$$
$$\left. \cdot \left[T_{w0}^2 + 2\frac{\omega^2}{c^2}N_z^2\right]\right\} T_{w0}^2 \cdot r \frac{J_1^2(T_{w0} r) + J_0^2(T_{w0} r) - 2J_0(T_{w0} r) J_1(T_{w0} r)}{J_0^2(T_{w0} r)} = 0 \tag{19}$$

where $D_0(\omega, k_z)$ is only the plasma contribution to the dispersion relation.

At a first approximation, the frequency of whistler mode found from equation $D_C(\omega, k_z) = 0$ and is given by relation (15)

To obtain the growth rate we will expand (19) about ω_w. Neglecting the terms of the second and higher orders with respect to ω_i, and ε, we get, under cyclotron resonance condition $\omega_w = k_z v_0 - \omega_c/\gamma_0$ (anomalous Doppler effect), the following expression

$$\omega_i = -\sqrt{\frac{\pi}{2}} \cdot \frac{\varepsilon}{4\gamma_0} \eta_{lw} \quad \omega_w \quad \left[s_0 + s_{-1} \left(\frac{T_\perp}{T_\parallel} - 1 \right) \cdot \left(\frac{1 - \cos \theta_w}{\cos \theta_w} \right)^2 exp \left(- \frac{s_{-1}^2}{2} \right) \right] \quad (20)$$

where

$$\eta_{lw} = \frac{r^2}{R^2} \cdot \frac{J_1^2\left(\varkappa_{1\nu} \frac{r}{R}\right) + J_0^2\left(\varkappa_{1\nu} \frac{r}{R}\right) - \frac{2R}{\varkappa_{1\nu} r} J_1\left(\varkappa_{1\nu} \frac{r}{R}\right) J_0\left(\varkappa_{1\nu} \frac{r}{R}\right)}{J_0^2(\varkappa_{1\nu})} \quad (21)$$

Because at cyclotron resonance under the condition of anomalous Doppler effect s_0 is negative, relation (20) indicates instability since $|s_0| \gg |s_{-1}|$

Conclusion. The present work deals with the problem of exciting whistler wave in a plasma wave guide with an axial low density warm relativistic electron beam running through it The excited wave frequency coincides with that obtained for cold beam-plasma system It is found that the whistler mode can be excited only by cyclotron resonance under anomalous Doppler effect condition. In the calculated growth rate appears a geometry factor depending on the relation between plasma and beam radii The expression of this factor coincides with that obtained for cold beam-plasma system

A temperature correction to the result previously done for the cold relativistic beam-plasma system in the expresion of the growth rate was obtained. If we put $\gamma_0 = 1$ in this growth rate expression one obtained the growth rate for warm nonrelativistic electron beam-plasma system calculated in [8].

REFERENCES

1. A. I. Akhiezer, „Elektrodinamika plazmy", Moskva, Nauka, 1974
2. A. I. Akhiezer, Ya B Fainberg, *Dokl Akad Nauk*, **69**, 555 (1949), *Zh Exp. Teor Fiz.*, **21**, 1262 (1951)
3. D Bohm, E Gross, Phys Rev, **75**, 1851, 1864 (1949)
4. K. N Stepanov, A B Kitsenko, *Zh. Teckn Fiz*, **31**, 167 (1961)
5. A. B. Kitsenko, M M Shoucri, *Plasma Phys*, **10**, 23 (1968)
6. M. M Shoucri, A B Kitsenko, *Plasma Phys*, **10**, 699 (1968)
7. J Karácsony, V Selinger, *Bull Math Soc Sci Math R S R*, **24** (72), 363 (1980).
8. M. M. Shoucri, *Plasma Phys*, **11**, 429 (1969)

STUDIA UNIV. BABEŞ—BOLYAI, PHYSICA, XXXI, 1, 1986

STRUCTURE OF A SEMICRYSTALLINE CERAMIC BODY COMPRISING FERROELECTRIC COMPOUNDS

AL. NICULA*, LIANA SANDRU and LUCREŢIA BUNEA*****

Received: November 15, 1985, accepted August 12, 1986

ABSTRACT. The paper presents two vitroceramics bodies These bodies haven been made by molding and shaping a batch to form a body comprising finely divided ferroelectric crystalline compounds having the desired electric properties, such as $BaTiO_3$ and sintering the body without melting or otherwise altering its ferroelectric crystalline components These vitroceramics were studied by means of X-ray, Differential Thermal Analysis or D.T.A

Introduction. Bodies from crystalline materials have usually been made by molding and shaping a batch to form a body comprising finely divided ferroelectric crystalline compounds having the desired dielectric properties such as $BaTiO_3$ with very small amounts of siliceous or ergillaceous bonding materials, and sintering the body without melting or otherwise altering its ferroelectric crystalline components. Such compounds were studied by Guy E Rindone [1].

The *Differential Thermal Analysis* of a glass composition consisting essentially of BaO, TiO_2, SiO_2 and Al_2O_3 was performed by Andrew Herezog and Stanely D. Stookey [2].

By sintering $BaTiO_3$ and sole niobates or in mixture with other titanates, zirconates and stannates with small quantities of liants, semicrystalline products with ferroelectric phase are obtained having important dielectric properties, The products were burned at a temperature ranging between 1100—1300°C. temperatures at which resists only the platinum and palladium electrodes For the cheaper electrodes made of silver or copper, which do not resist at these temperatures, semicrystalline masses having a large dielectric constant can be worked out.

The vitroceramics made up of a multitude of crystals, in a greater proportion, homogeneously disperssed in vitreous matrix have null porosity and ferroelectric crystalline phases of very small dimensions.

The ferroelectric components of vitroceram can exist under the from of barium, strontium [2], cadmium titanates, sodium, potassium, lithium, cadmium, lead barium niobates, lead, cadmium zirconates, sodium or cadmium tantalates, wolfram trioxide, lead or lanthanum ferrate, iron germanate included in a vitreous matrix of SiO_2, Al_2L_3, B_2O_3 or P_2O_5.

The dielectric properties of one group of ferroelectric ceramic bodies containing $BaTiO_3$ was investigated by Nicula Al. and all [3].

* *University of Cluj-Napoca, Department of Physics, 3400 Cluj-Napoca, Romania*
** *IPG — Ploieşti, Romania*
*** *C.E.R.O — Cluj-Napoca, Romania*

Partially crystallized glasses from the $x(SrO \cdot TiO_2) \cdot (1 - x)3SiO_2$ Na_2O system were investigated by differential thermal analysis [4]

The present paper reffer to semicrystalline ceramic bodies containing $BaTiO_3$ which were studied by means of X-ray and thermodifferential analysis

Experimental. In order to obtain the melt we used barium carbonate, TiO_2, Uricani quartz, calcinated aluminium oxide, CaF_2, MgO, ZnO, boric and limestone The dosed raw materials were introduced in a glass tank at a temperature of 1400°C, being maintained for 4 to 8 hours in an atmosphere of oxidants After melting the glass was quenched in cold water, a part of it was manually dragged in thin sheets The firt was crushed and then subject to thermal treatment in view of crystallization.

The thermodifferential analysis was achieved with a M O M Budapest derivative record (slope recorder), with a heating speed of 10°C/min and a sensibility D T A. of 1/10 The X-ray diffraction spectra were obtained at a DROM-3 (USSR) diffractometer at room temperature The dilatation tests were performed with a Leith-type dilatometer.

The dielectric constant and loss angle measurements were made at room temperature by the „Automatic C bridge, type E 315 A" (Polish made) that measures simoultaneously the capacity and loss angle values with and without sample

Results and Discussions. Two samples were experimented sample 1, belonging to system $x(BaO \; TiO_2) \; (1 - x) \cdot (4SiO_2 - Al_2O_3$ and sample 2, belonging to system $x(BaO \cdot TiO_2) \; 1 - x) \cdot (2B_2O_3 - CaO)$.

The two investigated samples had the following composition (weight percent):

Sample 1 65% $BaTiO_3$; 21,3% BaO, 7,5% SiO_2, 3,4% Al_2O_3, 0.4% MgO; 2,4% ZnO

Sample 2. 70% $BaTiO_3$; 11,7% BaO, 12,7% B_2O_3, 5,6% CaO

The first system was heat treated at 770°C for 3 hours, whereas the second system at 1000°C for 2 5 hours By means of the thermal differential analysis we had in view the optimal temperature of thermal treatment

Figure 1 shows the thermodifferential analysis (T D.A) curves for both sample 1 and 2

The structural transformation as evidenced by the endothermal curve begins at values (tg) of 520°C for the first sample and 670°C for the second one.

The first minimum of the endothermal curve represents the softening point (t_{soft}) of the glass at values of 565°C, respectively 710°C for the two investigated samples.

By further heating of the sample an exothermal reaction occurs, according to X-ray diffraction data the peak of the curve indicates crystallization of the ferroelectric component as a first crystallization phase The following peaks represents other phases.

For the first sample the crystallization temperature is 665°C and for the second one 890°C. Further, endothermal reactions occur again representing the melting of the respective crystalline phases.

The temperature field for the thermal treatment ranges between the temperature of the thermodifferential analysis (T D A) first peak (520°C, 670°C,

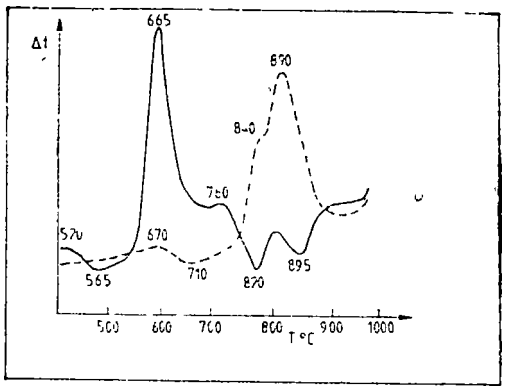

Fig. 1 The DTA curves for the two samples: sample 1 — full curve, sample 2 — dashed curve

respectively) and a temperature with 50°C lesser that the rising point of the first melting curve (of the ferroelectric phases) which is 840°C for the first sample, for the second sample no determination could be done because the limit of 1000°C, (the limit of possible work with the derivative recorder), was overpassed. We applied a thermal treatment for 3 hours at 770°C and 1 min at 800°C for sampel 1, and for 2.5 hours at 1000°C, and 1 min. at 1020°C for sample 2

The glass as a frit subject to X-ray diffraction indicates vitreous phase only (Figure 2) and for the thermal treated one, it indicates the ferroelectric phase

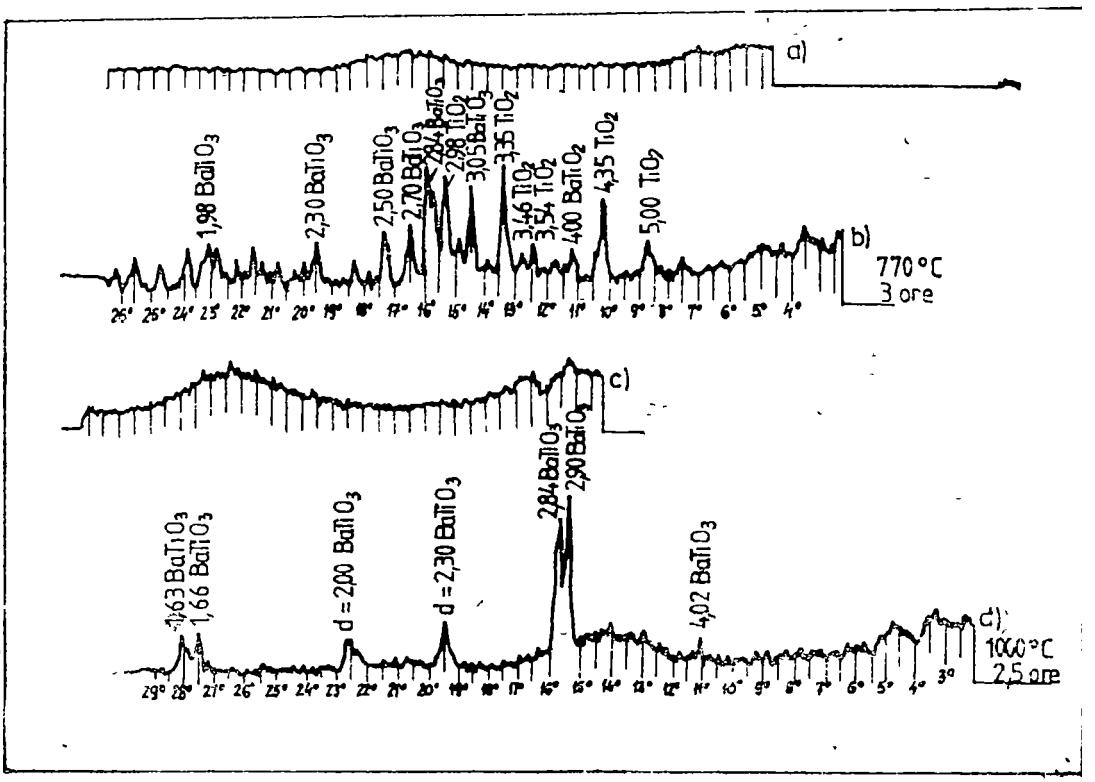

Fig. 2 X-rays spectral for the studied samples before (a, c) and after (b, d) thermal treatment.

The dilatation curves, having a anomalous behaviour due to the para- to ferroelectric phase transition, at 100°C for the first sample, and 120°C for the second one, are represented in Figure 3. These temperature values are the Curie points for the two samples.

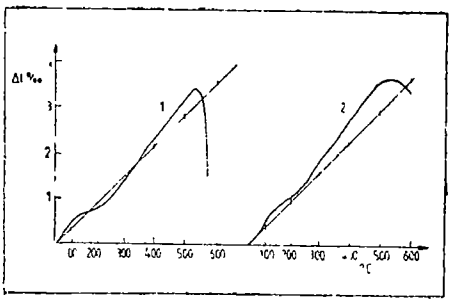

Fig 3 Dilatation curves for the two studied samples

We chose the two samples with SiO_2, Al_2O_3 and B_2O_3, which have the role to promoting formation of the glass In the first sample we also introduced an small quantity of CaF_2 (1%) in order to improve the dielectric properties and the melting characteristics of the glass, favoring crystallization To prevent forming of other composites, as barium titanosilicates, an exces of BaO *versus* the stoichiometric equivalent of $BaTiO_3$ is desirable.

An exces of SiO_2 or a Al_2O_3 deficiency diminishes the value of the dielectric constant and leads to undesired formation of silicates [2]. As the viscosity of the melt is very law, the presente of clearing agents is not necessary. It is preferable to introduce BaO in the form of $BaCO_3$ because it developes CO_2. To avoid spontaneous crystallization the samples were quenched in water rapidly The introduction of small quantities of ZnO, Mg O, also contributed to the rising of the dielectric constant [1] The effect of the simultaneous introduction of CaF_2 with ZnO and MgO was observed as lowering of the Curie point as it is seen in Figure 3. The thermal treatment the fglass is subjected to, for crystallization, is achieved at a temperature proportional in value to the content in ferroelectric phase [2].

Conclusions. Two varieties of semicrystalline ceramics bodies, that is: $x(BaO \cdot TiO_2)(1 - x)(4SiO_2 - Al_2O_3)$ and $x(BaO \cdot TiO_2)(1 - x) \cdot (2B_2O_3 - CaO)$ were prepared, and analised by means of X-rays diffraction and Differential Thermal Analysis, before and after thermal treatment. The treatment was performed in two stages, the first one for nucleation, the second for sample crystallisation.

According to X-rays diffraction spectrum the samples are vitreous matrices before thermal treatment and policrystalls after thermal treatment. Crystalline $BaTiO_3$ was evidenced.

The effect of small metal-oxides as additions in the sample was the Curie point lowering, as evidenced by means of T.D.A. curves.

REFERENCES

1. Guy E. Rindone, *High Dielectric Constant Glass*, United States Patent Office, 3, 107, 178, Patented Oct, 15, 1963.
2. Andrew Herezog and Stanley D Stookey, *Glass and Methods of Divitrifying same and Making a Capacitar therefrom*, United States Patent Office, 3, 195, 030, Patented July 13, 1965.

3 Al Nicula, L Sandru, L Bunea, „Semicrystalline ceramic bodies comprising ferroelectric crystalline compounds such as $BaTiO_3$, CONSILOX", 1984, Cluj-Napoca
4 I Ardelean, V Simon, S Simon, E Tătaru, „Structure and some physical properties of partially crystallized glasses from the $x(SrO\ TiO_2)(1-x)\ 3SiO_2\ Na_2O$ system", *National Symposium on Physics of Amorphous Materials*, May, 1981
5 Al Nicula, D Stamires and J Turkewich, *St berc Fiz*, Tom **17** (7), 755, (1964).
6 Al Nicula, L Cociu, I Nicula — *Sesiunea Universitătii*, Cluj-Napoca, 1977

STUDIA UNIV BABEŞ—BOLYAI, PHYSICA, XXXI, 1, 1986

ELECTRICAL CONDUCTIVITY STUDIES ON $N_2H_6SO_4$ SINGLE CRYSTALS

IOAN BARBUR*

Received, january 24, 1986; accepted August 12, 1986

ABSTRACT. – Electrical conductivity measurements over a range of temperature on $N_2H_6SO_4$ single crystals are raported The d-c conductivity was found to be anisotropic The activation energy in intrinsec region is found to be 0 47 eV in agreement with appropriate values for proton conduction in other hydrogen-bonded compounds The results are discussed on the basis of a "one-dimensional conductor" model of similar crystals

Introduction. A number of hydrogen — bonded crystals have peculiar electrical properties Ammonium hydrogen sulphate NH_4HSO_4, and ammonium sulphate $(NH_4)_2SO_4$ show ferroelectric transition phenomena [1,' 2]. Lithium hydrazinium sulphate $LiN_2H_5SO_4$, and its isomorphous hydrazinium sulphate $N_2H_6SO_4$ are also hydrogen-bonded crystals. Pepinsky *et al* [3] observed that the conductivity of $LiN_2H_5SO_4$ interfered with ferroelectric hysteresis, and Blinc [4] has studied the influence of γ-irradiation on the electrical properties of this compound From extensive dielectric measurements the protonic conduction in this compound was established and it was concluded that it is not ferroelectric [5]. The appearent hysteresis loops are explained as resulting from saturation of the a.c conduction

From conductivity studies the activation energies were obtained in extrinsic and intrinsic region. The variation of the energies with temperature is explained on the basis of a "one— dimensional" model of this compound, in which local defects have pronounced effects on the carrier mobility, unlike in izotropic dielectrics [6].

Earlier it was reported that hydrazinium sulphate $N_2H_6SO_4$ has a ferroelectric phase transition at —50°C [3] In our earlier report [7] an electron spin resonance study was made on the defects produced by γ-irradiation on hydrazinium sulphate No ferroelectric effects were observed on ESR spectra. Our recent dielectric measurements [8] also indicate that $N_2H_6SO_4$ is not ferroelectric, in good agreement with similar conclusions on isomorphous lithium hidrazinium sulphate

The purpose of this work is to determine the characteristics of the electrical conductivity in $N_2H_6SO_4$ in order to observe any possible anisotrophy and to conclude on proton conduction as noticed by Schmidt *et al.* [5].

Experimental. Hydrazinium sulphate exists in two forms. monoclinic and orthorombic In the present measurements orthorombic crystals several milimeters in size were used The unit cell of hydrazinium sulphate contains four formula units, the space group being $D_4^2 - 2_12_12_1$ The parameters of the unit cell are: $a_0 = 8\,251$ Å, $b_0 = 9.159$ Å, $c_0 = 5\,532$ Å [7]

* *University of Cluj-Napoca, Department of Physics, 3400 Cluj-Napoca, Romania*

Hydrazinium sulphate was purified by recrystalization in bidistilled water. Uncolored single crystals of about 3 to 4 mm were obtained by slow evaporation at room temperature from corresponding saturated solution.

The d.c. conductivity measurements were carried out along the a and c axes, using a cell which was fabricated in our laboratory and a teraohmmeter of type RT — 2201. Electrical conductivity measurements were performed from 298 K to 453 K. The temperature was measured by a copper-constantan thermocouple wich was placed close to the crystal A ceramic tube with heater coil was used to ansure uniform heating in the vicinity of the crystal.

Results and Discussion. The electrical conductivity of $N_2H_6SO_4$ was found to be anisotropic. The absolute values of the conductivity in the directions of the a and c crystalographic axes at room temperature were determined to be as follows:

a axis: $\sigma = (9.6 \pm 0,1) \times 10^{-12}$ ohm^{-1}cm^{-1}

c axis: $\sigma = (1.4 \pm 0.1) \times 10^{-10}$ ohm^{-1}cm^{-1}.

The anisotropic character of the electrical conductivity in $N_2H_6SO_4$ is less pronounced than in $Li(N_2H_5)SO_4$ [5].

The easiest conduction along the c axis in $N_2H_6SO_4$ could be explained on the basis of a „one-dimensional conductor" model of the isomorph $Li(N_2H_5)SO_4$. According to Schmidt *et al.* [5] the infinite chains of hydrogen bonds run through the crystal in the direction of the c — axis and conduction is proved to be protonic [9].

The activation energy of the carriers along the c crystallographic axis, was determined by measuring the conductivity over the temperature range from 25°C to 180°C In Fig. 1. the conductivity along the a and c axis is ploted against the inverse absolute temperature.

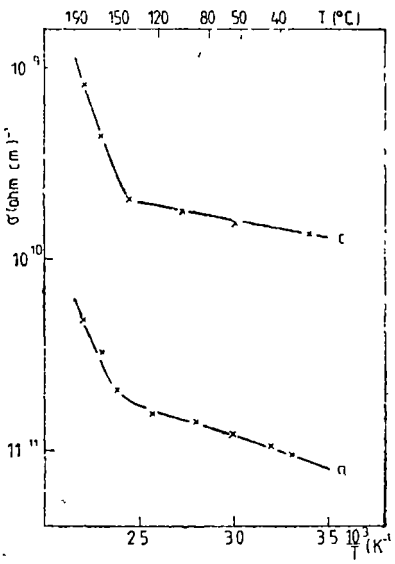

Fig. 1. A plot of the d-c conductivity σ along the *a* and *c* axis versus 1/T.

The conductivity plot obtained can be divided in two regions: extrinsic and intrinsic one The activation energies obtained for both regions, along the c axis are given in Table 1 for $N_2H_6SO_4$ together with those of other compounds available in the literature. It is well known that the extrinsic part is determined by impurities and in our case the low activation energy in this region is due to inter-channel diffusion, resulting from low barrier between channels near certain defects.

At high temperature, in the intrinsic region, the activation energy of 0.47 eV is in good agreement with the values obtained for proton conduction in potassium dihydrogen phosphate [10] and in ice [11].

The electrical conductivity in $N_2H_6SO_4$ by proton transfer is a sequence of hydrogen bonds linking the hydrazinium groups in the

Table 1

Activation energies (in eV) for different compounds

Compound	E (eV)		Reference
	intrinsic	extrinsic	
$Li(N_2H_5)SO_4$ VO'	0 83	0 65	[6]
$Li(N_2H_5)SO_4$ pure	0 85	-	[9]
KH_2PO_4	0 55	-	[10]
ice	0 53	-	[11]
$N_2H_6SO_4$	0 47	009	present work

crystal structure The existence of ...N–H...N–H...N–H...N–H...N–H... chains permits the transfer of protons along the hydrogen bond from a nitrogen to the next one and thus occurs a large electrical conductivity along the c axis as in $Li(N_2H_5SO_4)$ [9].

REFERENCES

1. Pepinsky R., Vedam K, Hoshino S, and Osaka Y., *Phys Rev*, **111**, 1508 (1958)
2. Mathias B *T*, and Remeika J. P, *Phys. Rev*, **103**, 262 (1956)
3 Pepinsky R, Vedam K, Okaya Y, and Hoshino S, *Phys Rev* **111**, 1467 (1958)
4. Blinc R, Schara M, and Poberaj S, *J Phys Chem. Solids*, **24**, 559 (1963)
5. Schmidt V. H, Drumheller J E, and Howell F L., *Phys. Rev.* **B4**, 4582 (1971)
6 Reddy A. D, Rao S M. D, and Sastry G S, Phys. Stat Sol. (a) **70**, 269 (1982)
7 Barbur I, *Phys Stat sol* **34**, 711 (1969)
8. Barbur I, and Babos L, *Studia Univ Babeş-Bolyai, Physica* **29**, 43 (1984)
9 Vanderkooy J, Cuthbert J D., and Petch H E., *Can. J Phys* **42**, 1871 (1964)
10 Mason W. P, *Piezoelectric crystals and their application to ultrasonics*, D. Van Nostrand Company, Inc., New York, 1950, p. 142
11. Bradley R. S., *Trans Faraday Soc* **53**, 687 (1957).

STUDIA UNIV BABEŞ—BOLYAI, PHYSICA, XXXI, 1, 1986

MAGNETIC SUSCEPTIBILITY AND KNIGHT SHIFT OF THE INTERMETALLIC COMPOUND Dy_2Al_{17}

IULUI POP*, NATALIA DIHOIU** and LILIANA POP*

Received February 12, 1986; accepted August 12, 1986

ABSTRACT. — A new intermetallic compound Dy_2Al_{17} was synthesized, which crystalizes in a hexagonal structure, with lattice parameters a = 11 788 Å and c = 11.322 Å, isostructural with intermetallic compound Gd_2Al_{17} Temperature dependence of the magnetic susceptibility fits a Curie-Weiss law $\chi = \frac{C}{T + \theta_p} + \chi_0$, $\theta_p = -64$ K, and $\mu_{ef/Dy^{3+}} = 10\,59\mu_B$ From the linear dependence of the Knight shift *vs* temperature $K = K_0\left[1 + \frac{J_{sf}(g_f - 1)\chi_f(T)}{2g_f\mu_B}\right]$, the experimental value was determined for the phenomenological exchange constant, $J_{sf} = -1\,41 \times 10^{-3}$ eV, and by extrapolation $K_0 = 0.191\%$.

Introduction. The intermetallic compound Dy_2Al_{17} is a new compound, isostructural with the intermetallic compound Gd_2Al_{17} reported in a previous papaer [1], and presents the similar magnetic behaviour pointed out by the temperature dependence of the reciprocal magnetic susceptibility, and by the temperature dependence of the Knight shift.

Experimental. The intermetallic compound Dy_2Al_{17} was prepared by melting stoichiometric amounts of the elements in a high purity argon atmosphere. The purity of the starting elements was 99,9% for Dy, and 99,99% for Al. The magnetic susceptibility was measured using a Faraday type of magnetic balance, having a 10^{-8} e m u. sensityvity, in the temperature range 120 K — 1.120 K

The NMR spectra of ^{27}Al nuclei were taken by a JNM—3 spectrometer at 9.212 MHz, improved by a broadline attachment JNM—BH—2 at several temperatures in the range from 120 K to 460 K in a specially designgned dewar. The Knight shift was determined with reference to the ^{27}Al resonance in $AlCl_3$ solution The X-ray measurements were obtained using a TUR—M—62 spectrometer

Results and discussion. X-ray investigation showed a hexagonal crystal structure for Dy_2Al_1 intermetallic compound with lattice parameters a = = 11 788 Å and c = 11.322 Å.

* *University of Cluj-Napoca, Department of Physics, 3400 Cluj-Napoca, Romania*
** *University of Braşov, Department of Physics, Romania*

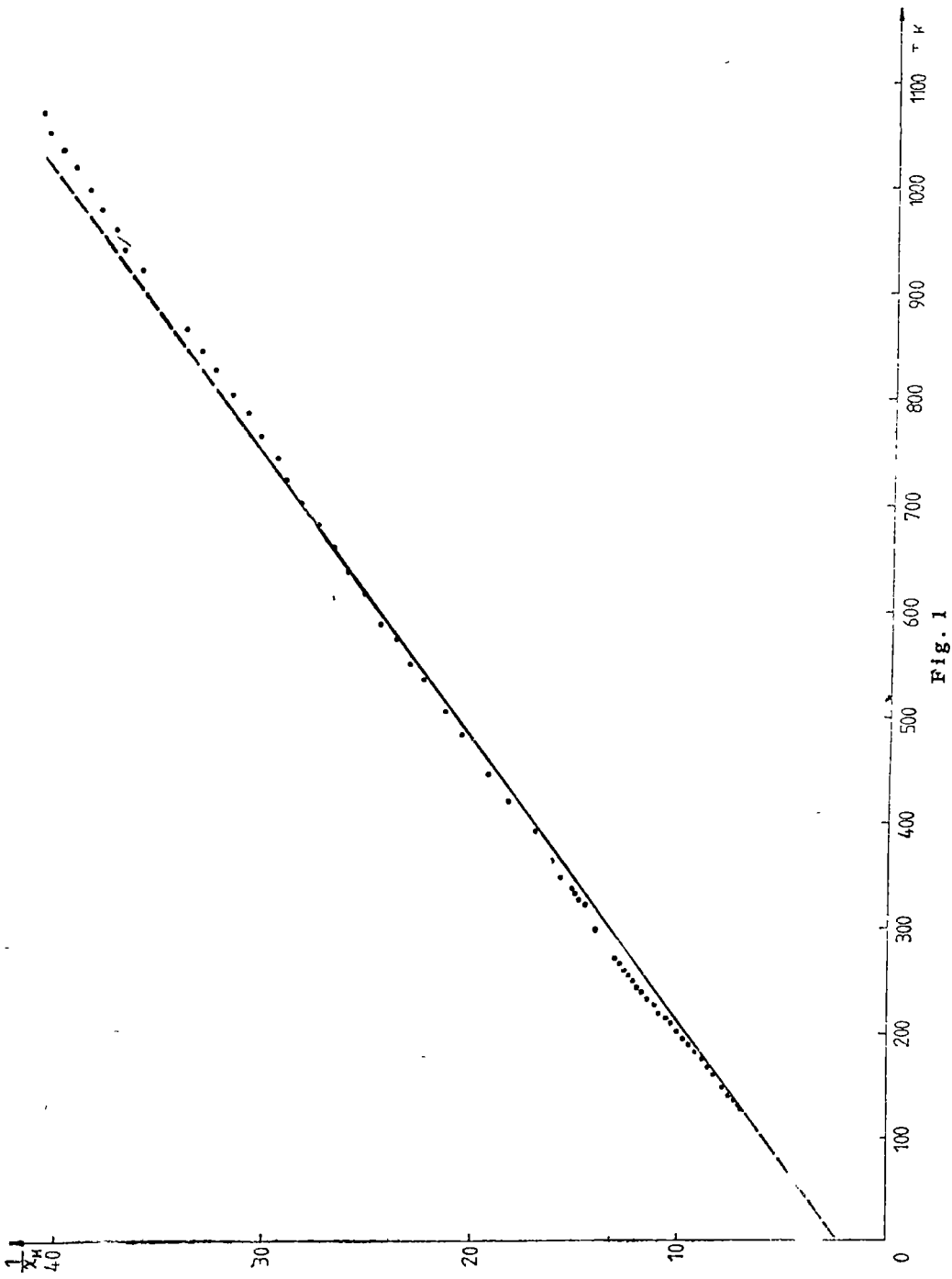
$\frac{1}{\chi_M}$
40
30
20
10
0
100
200
300
400
500
600
700
800
900
1000
1100
T K

Fig. 1

The temperature dependence of the molar reciprocal magnetic susceptibility shown in Fig 1, fits a Curie—Weiss law with an additional temperature independent term i e

$$\chi = \frac{C}{T + \theta_p} + \chi_0. \quad (1)$$

with $\theta_p = -64$ K

From the slope of the linear part of the temperature dependence $\frac{1}{\chi}$ (T) was determined the Curie constant value C = 27 65 The effectiv magnetic moment value determined per unit formula from this value is 14 933 μ_B, the corresponding value per Dy^{3+} ion is 10 59 μ_B, very close to 10 6 μ_B obtained from the Van Vleck theory From the linear representation $\chi\left(\frac{1}{T + \theta_p}\right)$ was obtained the numerical value for the independent part of magnetic susceptibility $\chi_0 = 1\,5 \times 10^{-3}$ emu/mol , wich correspond to Pauli magnetic susceptibility arising from the conduction electrons contribution in the intermetallic compound The negativ value of the paramagnetic Curie temperature, θ_p, suggests a possible antiferromagnetic ordering at low temperatures of the Dy^{3+} magnetic moments

The thermal variation of the Knight shift increases monotonically as the temperature increases and is positive in the investigated temperature range, as one can see in the Figure 2.

If we represent the Knight shif versus molar magnetic susceptibility, χ_M, (Fig. 3) of the Dy_2Al_{17} intermetallic compound, having the temperature as parameter, a linear dependence is obtained with positive slope dK/dT, similar to that obtained before [2] for Gd_2Al_{17} intermetallic compound

The obtained linear dependence is in agreement with the well known Eq. (1) [3, 4], derived in the case of a uniform polarization of the conduction electrons by the 4f spins,

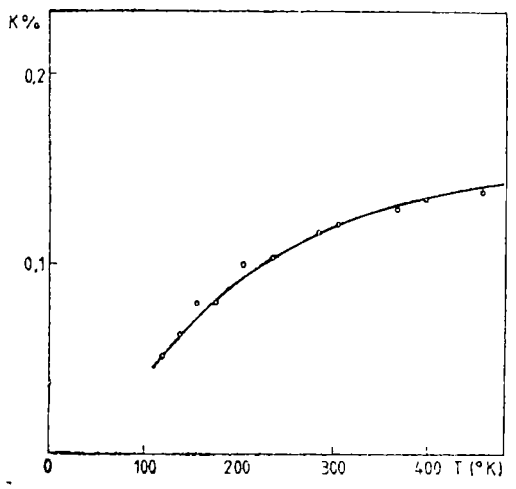

Fig 2

$$K = K_0\left[1 + \frac{J_{sf}(g_f - 1)\,\chi_f(T)}{2g_f\mu_B}\right], \quad (2)$$

where J_{sf} is the phenomenological exchange constant, g_f is the 4f-electron g value, and K_0 is the Knight shift due to the Pauli paramagnetism. The experimental value for $K_0 = 0.191\%$ is exactly the same as for Gd_2Al_{17}, as it was to be expected, because the compounds are isostructural The experimental value for $J_{sf} = -1.41 \times 10^{-3}$ eV

Conclusions. A new intermetallic compound Dy_2Al_{17} was obtained, wich crystallizes in a hexagonal structure, isostructural with Gd_2Al_{17}. This inter-

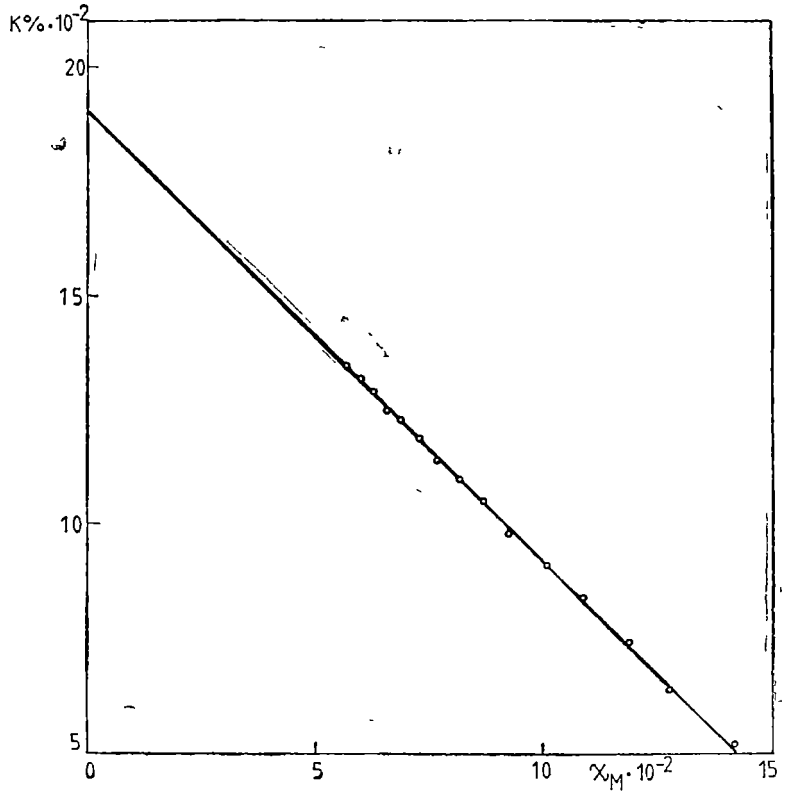

Fig. 3

metallic compound shows paramagnetic behaviour with localized magnetic moments of the Dy^{+3} ions and fits a Curie—Weiss law affected by a temperature independent term. The effective magnetic moment per Dy^{3+} ion $\mu_{ef} = 10\,59\ \mu_B$, very close to the theoretical value $\mu_{ef} = 10.6\,\mu_B$ derived from the Van Vleck's theory.

The Knight shift of the ^{27}Al nuclei in the Dy_2Al_{17} intermetallic compound was determined with reference to the ^{27}Al resonance in $AlCl_3$ solution, and was found temperature dependent and positive. From the linear dependence of the Knight shift versus bulk molar magnetic susceptibility the phenomenological constant was derived to be $J_{sf} = -1.41 \times 10^{-3}$ eV

REFERENCES

1. Iuliu Pop, Natalia Dihoiu and Marin Coldea, *J Phys. Chem. Solids*, vol 43, No. 2, pp. 125—128, 1982.
2. Marin Coldea, Natalia Dihoiu, and Iuliu Pop, *J Phys Chem Solids*, 42, 563—565, 1981.
3. V. Jaccarino, B. T. Matthias, M. Peter, H. Suhl, and J. H Wernick, *Phys. Rev. Lett*, 5, 251, 1960.
4 V. Jaccarino, *J. Appl. Suppl.* 32, 102, 1961.

STUDIA UNIV BABEŞ—BOLYAI, PHYSICA, XXXI, 1, 1986

EFFECT OF A GRAVITATIONAL FIELD DUE TO A ROTATING BODY ON THE POLARISATION OF THE DIRAC PARTICLE BEAM

Z. GÁBOS*

Received: February 25, 1986, accepted August 12, 1986

ABSTRACT. — The paper presents the modification of the Dirac particles polarisation in the case of their scattering in the gravitational field generated by a rotating, rigid, homogeneous spherical body with very small dimensions. As the effect is small, we shall assume the first approximation The results follow our previous work on the case of the non-rotating spherical body [5].

1°. The following convention is assumed $x^1 = x$, $x^2 = y$, $x^3 = z$, $x^4 = ict$. We write the components of the metric tensor in the form . $g_{\mu\nu} = \delta_{\mu\nu} + h_{\mu\nu}$. For the non-vanishing components $h_{\mu\nu}$, when $A/r \ll 1$, we use the wellknown expressions [1] .

$$h_{11} = h_{22} = h_{33} = -h_{44} = \frac{2r_0}{r},$$
$$h_{j4} = h_{4j} = g_j = \mathrm{i}\frac{4r_0A^2}{5cr^3}(\vec{\Omega} \times \vec{x})_j, \tag{1}$$

where A is the sphere radius , $\vec{x}$ and r are the position vector and the distance from the sphere centre, respectively , $r_0 = kM/c^2$ and $\vec{\Omega}$ are the gravitational radius and the angular velocity af the body, respectively (k is the gravitational constant and M is the mass of the body)

Using (1), for the Dirac matrices, which satisfy the conditions

$$\{\gamma_\mu, \gamma_\nu\} = 2g_{\mu\nu}, \quad \{\gamma^\mu, \gamma^\nu\} = 2g^{\mu\nu} \tag{2}$$

we obtain, within the first approximation

$$\gamma_j = \left(1 + \frac{r_0}{r}\right)\overset{\circ}{\gamma}_j, \quad \gamma_4 = \left(1 - \frac{r_0}{r}\right)\overset{\circ}{\gamma}_4 + (\vec{g}, \vec{\overset{\circ}{\gamma}}), \tag{3}$$

$$\gamma^j = \left(1 - \frac{r_0}{r}\right)\overset{\circ}{\gamma}_j - g_j\overset{\circ}{\gamma}_4, \quad \gamma^4 = \left(1 + \frac{r_0}{r}\right)\overset{\circ}{\gamma}_4 \tag{4}$$

We denote by $\overset{\circ}{\gamma}_j$, the Dirac matrices, used in the Minkowski space .

$$\overset{\circ}{\gamma}_j = \begin{pmatrix} 0 & -\mathrm{i}\sigma_j \\ \mathrm{i}\sigma_j & 0 \end{pmatrix}, \quad \overset{\circ}{\gamma}_4 = \begin{pmatrix} 1 & 0 \\ 0 & -1 \end{pmatrix}. \tag{5}$$

* *University of Cluj-Napoca, Department of Physics, 3400 Cluj-Napoca, Romania*

2°. To describe the interaction of the gravitational field with the Dirac particle we apply the second quantization method To this end we need the density of the interaction Hamiltonian This we obtain from the Dirac equation [3] of the particle of rest mass m_0

$$\gamma^\mu \frac{\partial \Psi}{\partial x^\mu} + \left[\frac{1}{4} \gamma^\mu \gamma^\nu \left(\frac{\partial \gamma_\nu}{\partial x^\mu} - \Gamma^\sigma_{\nu\mu} \gamma_\sigma \right) + \frac{m_0 c}{\lambda} \right] \Psi = 0, \tag{6}$$

which we rewrite in the form

$$i\hbar \frac{\partial \Psi}{\partial t} = \hat{H} \Psi \tag{7}$$

Using (3), (4) and (6) and keeping only the terms which are linear in r_0, we are lead to

$$\hat{H} = -ic\hbar \overset{\circ}{\alpha}_j \frac{\partial}{\partial x^j} + m_0 c^2 \overset{\circ}{\gamma}_4 + ic\hbar \frac{r_0}{r} \left(\overset{\circ}{\alpha}_j \frac{\partial}{\partial x^j} - 1 \frac{\partial}{\partial x^4} + \frac{1}{4} \overset{0}{\alpha}_j x_j + \right.$$

$$\left. + 1 g_j \frac{\partial}{\partial x^j} \right) - 1 \frac{c\hbar}{4} \left(\operatorname{rot} \vec{g}, \vec{\overset{\circ}{\Sigma}} \right), \tag{8}$$

where

$$\overset{\circ}{\alpha}_j = \begin{pmatrix} 0 & \sigma_j \\ \sigma_j & 0 \end{pmatrix}, \quad \overset{\circ}{\Sigma}_j = \begin{pmatrix} \sigma_j & 0 \\ 0 & \sigma_j \end{pmatrix} \tag{9}$$

We interpret operator (8) as an operator in the Minkowski space The first two terms give the well-known $\hat{H}_0$ operator of the free Dirac particle. The remaining terms give the operator for the field-particle interaction

In the second step, the desired quantity is obtained from operator (8) Thus, using (7) and (8) the following expression may be written

$$\frac{i\hbar}{2} \left(\Psi^+ \frac{\partial \Psi}{\partial t} - \frac{\partial \Psi^+}{\partial t} \Psi \right) \tag{10}$$

from which we can obtain both the Hamiltonian density of the free Dirac field and the interaction Hamiltonian density

$$H_{int} = -\frac{ic}{4} h_{\mu\nu} \left| \overline{\Psi} \overset{\circ}{\gamma}_\mu \frac{\partial \Psi}{\partial x^\nu} - \frac{\partial \overline{\Psi}}{\partial x^\mu} \overset{\circ}{\gamma}_\nu \Psi \right) - i \frac{ic}{4} \left(\operatorname{rot} \vec{g}, \Psi^+ \vec{\overset{\circ}{\Sigma}} \Psi \right). \tag{11}$$

The first part of expression (11) was proposed by S. Gupta [2]

3°. We shall describe the scattering of the Dirac particles having the initially well-defined linear momentum $\vec{p}_0$, in a reference system with the origin in the centre of the sphere and the third axis in the direction of $\vec{p}_0$ We can write in this case the following components for the initial and final linear momenta:

$$\vec{p}_0(0,\ 0,\ p_0),\ \vec{p}(p_0 \sin \vartheta \cos \varphi,\ p_0 \sin \vartheta \sin \varphi,\ p_0 \cos \vartheta) \tag{12}$$

We shall denote the initial and final helicityes of the Dirac particle by λ_0 and λ.

By passing from H_{int} to the $\hat{H}_{int}$ operator and by building up with its aid the $\hat{S}$ operator, we can obtain the following expression for the differential cross section, by appling the usual methods for the $\lambda_0 \to \lambda$ transition:

$$d\sigma = \frac{m_0^2 r_0^2}{16\, p_0^2 \sin^4 \frac{\vartheta}{2}} \mid u_\lambda^+(\vec{p}) M u_{\lambda_0}(\vec{p}_0) \mid^2 d\omega \tag{13}$$

For very smal linear dimensions of the body, the matrix M is given by:

$$M = 2E_0 + c(\vec{\alpha}, \vec{P}) + \frac{2A^2}{5\hbar}(\vec{\Omega}, \vec{Q})(\vec{\Sigma}, \vec{Q}) + i\frac{8A^2}{5\hbar}(\vec{\Omega}, \vec{R}), \tag{14}$$

where E_0 is the energy of the particle and

$$\vec{P} = \vec{p} + \vec{p}_0, \quad \vec{Q} = \vec{p} - \vec{p}_0, \quad \vec{R} = (\vec{p} \times \vec{p}_0). \tag{15}$$

To evaluate the effect of the gravitational field on the Dirac particle polarisation, let us consider the particular case of an initial state with longitudinal polarisation equal to 1, when the particles have positive helicity By simple calculus, one is thus lead to the following expression for the longitudinal polarisation.

$$P_l = \frac{\cos\vartheta + (2\beta^2 + \beta^4)\cos^2\frac{\vartheta}{2} + L_1}{1 + (2\beta^2 + \beta^4)\cos^2\frac{\vartheta}{2} + L_2}, \tag{16}$$

where

$$L_1 = 2D(\vec{n}, \vec{e}_Q)\sin^3\frac{\vartheta}{2} + D^2\left[(\vec{n}, \vec{e}_R)^2 \sin^2\vartheta\cos\vartheta - (\vec{n}, \vec{e}_Q)^2 \sin^4\frac{\vartheta}{2}\right], \tag{17}$$

$$L_2 = -2D(\vec{n}, \vec{e}_Q)\sin^3\frac{\vartheta}{2} + D^2\left[(\vec{n}, \vec{e}_R)^2 \sin^2\vartheta + (\vec{n}, \vec{e}_Q)^2 \sin^4\frac{\vartheta}{2}\right], \tag{18}$$

with

$$\beta = \frac{v_0}{c} = \frac{p_0}{m(v_0)c}, \quad \vec{n} = \frac{\vec{\Omega}}{|\vec{\Omega}|}, \quad \vec{e}_Q = \frac{\vec{Q}}{|\vec{Q}|}, \quad \vec{e}_R = \frac{\vec{R}}{|\vec{R}|}, \tag{19}$$

$$D = \frac{4A^2\Omega p_0^2}{5\hbar E_0} = 2\frac{|\vec{J}|}{\hbar}\frac{m}{M}\beta^2. \tag{20}$$

In (20), $\vec{J}$ denotes the angular momentum of the body.

4° Before commenting on expression (16), two observations are apropriate. The first one concerns the scattering angle ϑ, for which the following expression is available within the classical approximation:

$$\operatorname{tg}\frac{\vartheta}{2} = \frac{r_0}{b\beta^2} \tag{21}$$

(b is the shock-parameter).

Although relationship (21) belongs to the zero order approximation, it can however be used for an orientative evaluation of the effect.

The second observation relates to the fact that we have considered states of helicity for both the initial and final states The value of cos ϑ from P_l, in this case, is a consequence of the calculus method employed, rather than being a true effect Thus one has to substract cos ϑ from the value given by (16) in order to obtain the desired effect

It follows from (16) that P_l depends on the particle velocity, the gravitational radius of the central body, its angular momentum and mass, the schock parameter and the angles between the vectors $\vec{n}$, $\vec{e}_Q$ and $\vec{n}$, $\vec{e}_R$ The result is valid for small b/A and A However under these conditions the effect is very small, unmeasurable

One can expect that the effect becomes measurable in the case of larger central body dimensions Howevers, serious problems arise in this case in writing down matrix M which occurs in expression (13)

REFERENCES

1 L D Landau, E M Lifşit, *Teoria polia*, Moskva, 1960, p 363—367
2 S Gupta, *Proc Phys Soc*, **A 65** (1952), 608
3 E Schmutzer, *Ann Physik*, **29** (1973), 75
4 V B Berestetţki, E M Lifşit, L P Pitaevski, *Relativistskaia kvantovaia teoria* vol I, Moskva, 1968, p 373
5 Z Gábos, A Pászkán, Studia Univ Babeş-Bolyai, ser Physica, **29** (1984), 52

STUDIA UNIV BABEŞ—BOLYAI, PHYSICA, XXXI, 1, 1986

THE METALLOGRAPHIC INVESTIGATION OF TI-AL ALLOYS USING A SCANNING ELECTRON MICROSCOPE

TRAIAN PETRIŞOR, NICOLAE FARBAŞ***, ALIN GIURGIU**** and IULIU POP***

Received: May 10, 1986, accepted August 12, 1986

ABSTRACT. — The metallographic investigations were made on a series of Ti—Al solide solution, using a scanning electron microscope. This pointed out a dendritic structure past the melting of the alloys After heat treatment at 1,100°C for 100 h, and a new annealing at 700°C for 20 h the alloy consists from the homogeneous crystallites of the α — solid solutions.

Introduction. Titanium has two allotropic modifications [1] α-titanium up to 1,155K, which crystallizes into a hexagonal close-paked lattice with the parameters a = 2.9503 and c = 4 8631 Å (c/a = 1 5873); and β-titanium at higher temperatures The latter has a body-centered cubic lattice with lattice parameter a = 3.3132 Å at 1,173 K The density of α-titatium is 4.505 g/cm^3, and that of β-titanium is 4.32 g/cm^3 at 1,173 K.

Recently [2] the experimental results on α-titanium indicate the existence of an anomaly in the temperature dependence of magnetic suceptibility, of electrical resistivity and of specific heat. The similitude between temperature dependence of the magnetic susceptibility of α-titanium and that of pure chromium suggests that α-titanium is an itinerant electron antiferromagnet with the Néel temperature of 276 ± 4 K.

In order to study the influecne of non-magnetic impurities on the electron itinerant antiferromagnetism of α-titanium we investigated [3] the magnetic properties of Ti-Al alloys. The samples were annealed at 1,100°C for 100 h and 20 h at 100°C with the aim of obtaining the α-phase. After this, the samples were metallographic examined in order to prove the formation of α-phase In this paper the results of metallographic investigations are presented using a scanning electron microscope.

Experimental. The equilibrium phase diagram [1] of Ti—Al alloys indicates a limited solubility of aluminium in titanium. The α-solid solution (solid solution of aluminium in α-titanium) is stable in the concentration interval from 0 to 30 at % Al. For this reason we prepared alloys whith the concentration up to 20 at % Al, only. The alloys were prepared from 99.99% pure titanium and 99.999% pure aluminium, in an argon arc furnace on a water cooled cooper hearth. The arc melted buttons were turned and remelted more than four times to insure homogeneity To prevent oxidation of the melts, the furnace chamber was evacuated and pruged with argon several times before melting.

* *University of Cluj-Napoca, Department of Physics, 3400 Cluj-Napoca Romania*
** *Institute of Metrology, 3400 Cluj-Napoca, Romania*
*** *Institute of Welding, 1900 Timişoara, Romania*
*** *Polytechnical Institute, 3400 Cluj-Napoca, Romania*

Fig 1 Section before annealing through $Ti_{97}Al_3$ allooy (magnification 500 X)

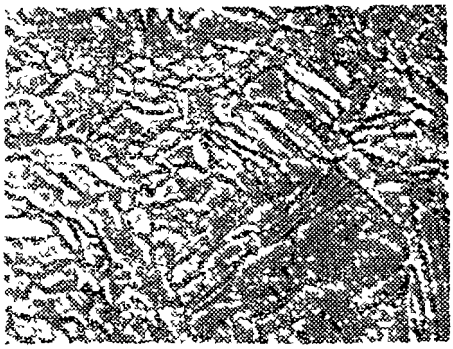

Fig 2 Section before annealing through $Ti_{83}Al_{17}$ alloy (magnification 500 x)

The samples were annealed at 1,100 °C for 100 h in an argon atmosphere. After this the samples were annealed at 700 °C for 20 h to ensure the formation of α-phase

In order to point out the effect of heat-treatment the samples have been metallographic investigated, before and after heat treatment, using a scanning electron microscope In Figs 1—4 the scanning electron micrographs are show before and after heat treatment for the samples containing 3 and 17 at. % Al. The micrographs have been obtained with the same magnification.

As it can be seen from Figs. 1 and 2, before annealing the samples have a dendritic structure specific for the dendritic segregation Solid solution crystall of the dendritic type are usually formed when the sample is rapidly cooled from the liquid phase (in our case the samples were rapidly cooled out in the water cooled copper hearth). As a result of nonequilibrium crystallization the chemical composition of crystals of α-solid solution is variable over a cross section of the crystals The greater difference in temperature between the solidus and liquidus lines, the greater difference is in composition between the liquid and solid phases, and the grater degree of dendritic segregation in the solid

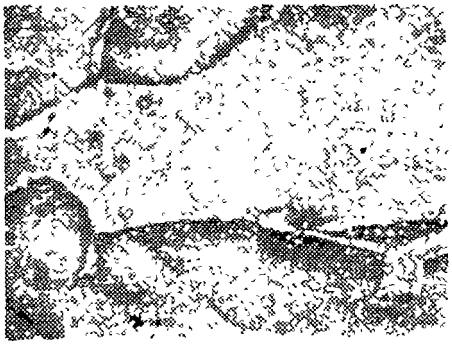

Fig. 3. Section after annealing through $Ti_{97}Al_3$ alloy (magnification 500 x).

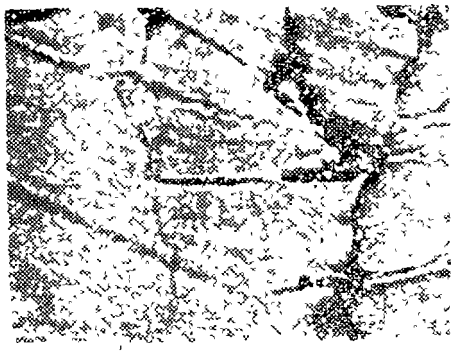

Fig 4 Section after annealing through $Ti_{83}Al_{17}$ alloy (magnification 500 x).

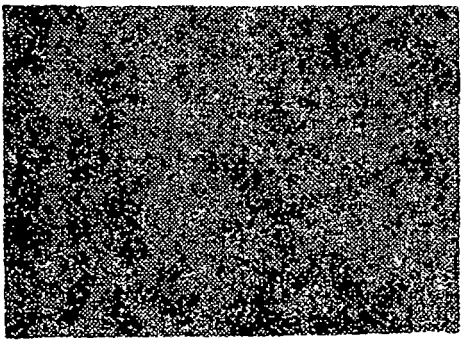

Fig 5 Image formed using the aluminium K_α radiation for the $Ti_{93}Al_3$ alloy before annealing

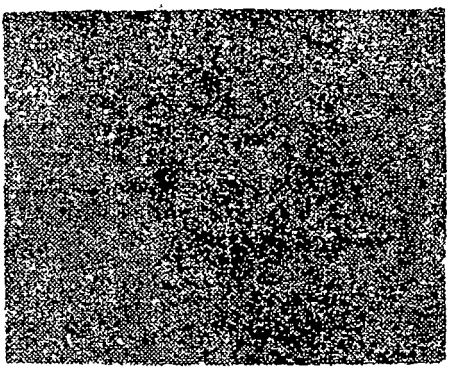

Fig 6 Image formed using the aluminium K_α radiation for the $Ti_{83}Al_{17}$ alloy before annealing

alloy. Owing to the different etching patterns obtained for portions of the solid solution having different compositions, the inhomogeneity within each crystallite can be readily revealed in microanalysis (Figs 1 and 2)

In order to eliminate the effect of dendritic segregation, the samples were annealed at 700 °C (somewhat below the solidus line) for 20h After such treatment, called diffusion annealing or homogenizing the dendritic structure of the alloy is no longer evident, and the alloy consists of homogeneous crystals of solid solution (Fig 3 and 4)

The distribution of aluminium atoms in alloy was determined by adding an X-ray detector the scanning electron microscope for the detection of the characteristic spectrum of X-rays emitted by aluminium atoms In Figs 5—8 the images obtained with K_α radiation of aluminium are shown for the samples containing 3 and 17 at % Al, before and after anneal From the comparison of this figures one can see that the distribution of aluminium atoms is more uniform after anneal. This fact was also confirmed by the metallographic analysis

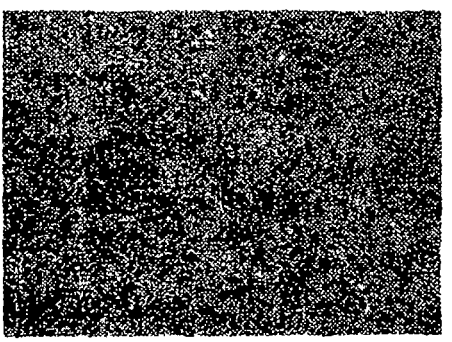

Fig 7 Image formed using the aluminium K_α radiation for Ti_3Al_3 alloy after annealing

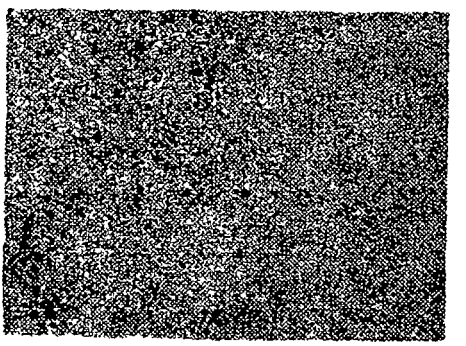

Fig 8 Image formed using the aluminium K_α radiation for $Ti_{83}Al_{17}$ alloy after annealing

Conclusions. In this paper the results of metallographic investigation of Ti-Al alloys are presented using a scanning electron microscope This investigations point out that after preparation in the argon-arc furnace the samples have a dendritic structure The dendritic segregation appears because the samples were rapidly cooled on the water cooled copper hearth As a result of nonequilibrium crystallization the chemical composition of crystals of α-solid solution is variable over a transvers section of the crystals

In order to eliminate the effect of dendritic segregation the samples were annealed at 700°C for 20 h The metallographic investigations point out that such a treatment eliminates the dendritic structure In conclusion the sample consists of homogeneous crystallites of the α-solid solution This fact is also confirmed by the distribution of aluminium atoms in sample

REFERENCES

1 M Hansen and K Anderko, „Constitution of Binary Alloys", Mc Grow-Hill Book Company, New York (1958)
2 I Pop, T Petrişor, A Giurgiu and A Néda, *J Phys Chem Solids*, **46**, 1077 (1985)
3 T Petrişor, I Pop, A Giurgiu, N Farbaş, *J Mag and Magn Materials* (in press)

STUDIA UNIV BABEŞ—BOLYAI, PHYSICA, XXXI, 1, 1986

DETERMINATION OF THE ALUMINIUM CONTENT IN GLASSES AND VITROCERAMICS BY FAST NEUTRON ACTIVATION

L. DĂRĂBAN*, T. FIAT*, C. COSMA*, M. SĂLĂGEAN***, A. PANTELICĂ***, I. CHEREJI**, O. COZAR*, V. ZNAMIROVSCHI* and L. MÎNZATU*

Received April 29, 1986, accepted August 12, 1986

ABSTRACT. — The results obtained by neutron activation analysis on two samples of vitroceramic and Vycor glass are reported. A new method of analysis by neutron activation that can by applied even in the case of small concentrations of Al in the silicon matrix is also presented

Introduction. The neution activation is a useful analysis method for industrial and reserch laboratories because of its undestroyer character, rapidity and high precision. In last times it was very much implemented in industry and the use of isotopic neutron sources make it abbordable in almost any laboratory.

We attempt to improve a method of neutron activation for glass and ceramics industry, using the nuclear reactor and an Am—Be isotopic source of neutrons in order to determine the aluminium content. The knowledge of Al and Si content has a great importance because it is necessary for rapid control of the ratio between Al_2O_3 and SiO_2. This problem was treated before by some others authors [1—3], but it is very difficult to apply this to very small concentrations of Al in the silicon matrix because the appearance of some interference nuclear reactions. In the present work we report a new method of analysis by neutron activation, which can by applied even in the case of small concentrations of Al in the silicon compounds.

Determination of Al and Si by neutron activation. According to literature data [4], it results that Al and Si can be determined by three and respectively four nuclear reactions (Table 1). Other possible reaction channels are practically difficult to achive and have been omitted.

From Table 1 it results that interference reactions appear in the detection of ^{27}Mg and ^{28}Al radioisotopes when the studied samples contain a mixture of Si and Al oxides. The ^{28}Al occurs from reactions of the ^{27}Al with slow neutrons and from ^{28}Si with fast neutrons.

We noticed that the radioisotopes given in the fourth column of Table 1 can also occur from the other accompaning elements which are present in the samples. The identification characteristic data and nuclear reactions which lead to the occurence of the isotopes used in the neution activation analyses of the Al and Si are given in Tables 2 and 4.

* *University of Cluj-Napoca, Department of Physics, 3100 Cluj-Napoca, Romania*
** *Institute of Isotopic and Molecular Technology, 3100 Cluj-Napoca, Romania*
*** *I F I N — Bucharest, Romania*

Table 1

Nuclear reactions which can by used for determination of Al and Si

Analysed element	Target isotope	Nucleear reaction	Formed radioisotope	T1/2
Al	^{27}Al	$^{27}Al(n, \alpha)\ ^{24}Na$	^{24}Na	15 h
	^{27}Al	$^{27}Al(n, p)\ ^{27}Mg$	^{27}Mg	9 5 m
	^{27}Al	$^{27}Al(n, \gamma)\ ^{28}Al$	^{28}Al	2 3 m
Si	^{30}Si	$^{30}Si(n, \alpha)\ ^{27}Mg$	^{28}Mg	9 5 m
	^{28}Si	$^{28}Si(n, p)\ ^{28}Al$	^{28}Al	2 3 m
	^{29}Si	$^{29}Si(n, p)\ ^{29}Al$	^{29}Al	6 6 m
	^{30}Si	$^{30}Si(n, \gamma)\ ^{31}Si$	^{31}Si	2 6 h

The following conclusions result from these data

I. Aluminium can by analysed by irradiation with fast neutrons (channel 3) measuring the radioactivity of ^{24}Na if the samples have not considerable amounts of Mg. Reaction (1) is neglijable in the case of small concentration of Na where the neutrons are fast.

II If the samples do not have comparable amounts of P, the silicon can by analysed using the ^{28}Al radioisotope from reaction (8) which occurs with fast neutrons The interference reaction (7) with ^{27}Al is neglijable in the presence of fast neutrons This possibility has been used previously to determine the Si and Al content [1—3] in the following way before silicon was measured by fast neutrons using reaction (8) which vanishes at the slowness of the neutrons and when reaction (7) occurs, this being used at the determination of Al. Because of the slowness of the neutrons an unthermalized component appears together with the slow neutrons the big errors take place

III Reaction (6) is a tempted for the determination of Al using fast neutrons, but it cannot be used because of silicon presence in the sample which leads to interference reaction (5) on the ^{27}Mg

IV At great beams of slow neutrons (nuclear reactors) reaction (11) can be also used for the silicon determination However our measurements have given great errors at 99% SiO_2 content

V. In the case of two different nuclear reactions with fast neutrons and which lead to the same radioactive nucleus (5 and 6) it would be possible to discriminate them with help of the different value of the cross sections at a given energy of the neutron beam In this idea reactions (6) and (8) have been previously used [5—8] at a neutron energy of 14 MeV

VI. The influence of the accompaning elements (as Na) is negligible if their concentrations are small

The III—VI criterions are not usefull in the case of our samples, for which the aluminium content in a concentration of 1% must be determined in the presence of a great silicon content. From the previous considerations it is clear that for determination of Al it is necessary to use an independent channel, different from that of Si. This is the channel labelled by (3) in the Table 2.

Table 2

Nuclear data of analysed isotopes

Analysed radioisotope	$T_{1/2}$	Characteristic energy [KeV]	Relativ intensity [%]	Nuclear reaction	Target isotope	Label of identification
		3850	0.09	$^{23}Na(n, \gamma)\,^{24}Na$	^{23}Na	(1)
^{4}Na	15 h	2754	100	$^{24}Mg(n, p)\,^{24}Na$	^{24}Mg	(2)
		1368	100	$^{27}Al(n, \alpha)\,^{24}Na$	^{27}Al	(3)
		1014	43	$^{26}Mg(n, \gamma)^{27}Mg$	^{27}Mg	(4)
^{27}Mg	9 5 m	844	100	$^{30}Si(n, \alpha)\,^{27}Mg$	^{30}Si	(5)
		170	1	$^{27}Al(n, p)\,^{27}Mg$	^{27}Al	(6)
		1779	100	$^{27}Al(n, \gamma)\,^{28}Al$	^{27}Al	(7)
^{28}Al	2 3 m			$^{28}Si(n, p)\,^{28}Al$	^{28}Si	(8)
				$^{31}P(n, \alpha)\,^{28}Al$	^{31}P	(9)
^{9}Al	6.6 m	2426	18	$^{29}Si(n, p)\,^{29}Al$	^{29}Si	(10)
		1273	100			
^{31}Si	2 6 h	1266	100	$^{30}Si(n, \gamma)\,^{31}Si$	^{30}Si	(11)
				$^{31}P(n, p)\,^{31}Si$	^{31}P	(12)
				$^{34}S(n, \alpha)\,^{31}Si$	^{34}S	(13)

Experimental results. The determination of the aluminium content silicon matrix has been performed using an ^{241}Am—^{9}Be isotopic neutron source with a flux of $1\,1 \times 10^{7}$ n/s The analysis of the major elements in the samples was made at the nuclear reactor of VVR—S type from Măgurele — Bucharest. The results obtained by irradiation at the nuclear reactor of two samples of vitroceramic and Vycor glass are given in Table 3.

Table 3

The analysis of impurities by thermal neutron activation

Element*	Vitroceramic [p p.m]	Vycor glass [p p.m]
Fe	210 ± 15	60 ± 8
Ca	165 ± 17	274 ± 15
K	25 ± 7	26 ± 8
Na	23.1 ± 0.3	20 ± 0.2
Ba	25 ± 4	13 ± 4
Cr	$3\,7 \pm 0\,4$	$1.5 \pm 0\,2$
Ce	3.2 ± 0.2	2.1 ± 0.1
Nd	3 ± 1	2 ± 1
Te	1.8 ± 0.3	—
La	1.5 ± 0.1	0.9 ± 0.1

* The following elements As, Au, Eu, Hf, Lu, Sb, Sc, Sm, Th, U, Yb are in the concentrations smaller than 0.4 ppm and they do not given in table 3.

The irradiations with $^{241}Am—^{9}Be$ neutron source have been made by introducing the source in a channel of irradiation capsule (specially projected) which has been fixed at one meter distance from any protection wall so that thermal neutrons would be not obtained by scattering This irradiation geommetry was established by the fast neution activation of the metallic aluminium with different values of the thermal component according to reaction channels 3,6 and 7 in Table 2 Gamma spectra of the irradiated samples have been recorded with a Ge—Li detector of KOVO type coupled at NTA—512—M multichannel analyser The isotopic source with a constant beam of fast neutrons (4 5 MeV) can lead to good results only by long and cyclic irradiations The used samples had the weights from 25 g to 250 g and irradiation times between 2 and 4 days The cooling time was 5 minutes and the gamma spectrum of the ^{24}Na isotope (Fig 1) has been accumulated for 4000 seconds

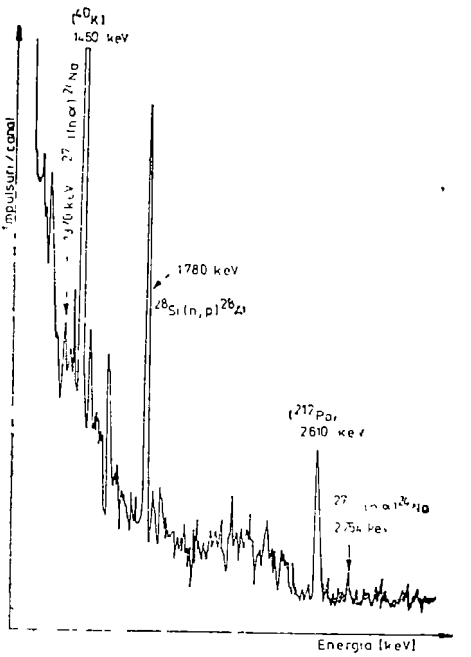

Fig 1 Characteristic gamma spectrum.

Table 4

Concentration of Al_2O_3[%]

Sample	Weight [g]	The energy analysed peak[keV] 1368 6	2754 1
vitroceramic	250	0 6± 0 16	1 0± 0 43
Vycor glass	25	1 7± 0.45	1 65± 0 62

The determination of Al content has been made with the help of peaks of 1368.6 KeV and 2754 1 KeV, using the Covell method The aluminium concentrations thus determined are situated in the range of 0.6—1 7% (Table 4).

As we have noticed before, our endeavours for silicon analysis by neutron irradiation with the nuclear reactor and the isotopic Am—Be source have been affected by great errors Because of the self-shielding effect in the sample and of the standard deviation of the method, the exact determination of a 99% SiO_2 content still remains difficult

REFERENCES

1. I. N Plaksin, E V Anchevskii, M A. Belyakov, *Dokl. Akad Nauk SSSR.* **163,** 1202 (1965)

2 M A. Belyokov, E V Anchevskii, E. P. Terent'ev, *Zavod Lab.*, **37,** 567 (1971)

3 S. Apostolescu, V. Avrigeanu, F. Georgescu, I. Ivan, „A 7-a sesiune anuală — Progrese în Fizică", ICEFIZ, Iași, 3–5 oct., p. 104 (1985)
4 S. A. Lis, Ph. K. Hopke, J. L. Fasching, *J. Rad. Chem.*, **24**, 125 (1975)
5 D. Grumpton, P. E. Francois, S. E. Hunt, *Nucl. Instr. Meth.*, **92**, 533 (1971)
6 D. E. Wood, *Nucl. Instr. Meth.*, **92**, 511 (1971)
7 J. Janczyszyn, S. Kwiecinski, L. Losks, W. Pohorecki, S. Taczanowski, *J. Rad. Chem.*, **31**, 259 (1976)
8 S. Gangadharan, S. Yegnasubramania, S. C. Misra, V. C. Gupta, *J. Rad. Chem.*, **24**, 57 (1975)
9 G. Peto, I. Jozsa, J. Csikai, G. M. Shuriet, Wiss. Z. *Techn. Univ. Dresden*, **21**, 4, 701 (1972)
10 R. Vanska, R. Rieppo, *Int. J. Appl. Radiat. Isotop.*, **30**, 513 (1979)

STUDIA UNIV BABEŞ—BOLYAI, PHYSICA, XXXI, 1, 1986

LINEAR SWEEP VOLTAMMETRY ON PALLADIUM ELECTRODE
I. The influence of thiourea upon hydrogen adsorption

FELICIA BOTA*

Received. April 18, 1986, accepted. August 12, 1986

ABSTRACT. — The influence of sulphur compounds upon the adsorption of hydrogen on palladium electrode is presented, by linear sweep voltammetry The presence of the two peaks for a clean electrode is reduced to a single one, when the electrode is poisoned in a saturated thiourea solution, because the hydrogen adsorption process is totally inhibited. The poisoning effect can be eliminated by some succesive oxidation-reduction cycles

Introduction. The behaviour of (Pd—H) electrode is strongly influenced by the properties of the interface region. These properties can be modified either by changing the physical structure of the surface layer [1, 2], or by chemisorption of some surface active substances.

The adsorption of thiourea THU on the surface of different electrodes presents an important interest in the electrode processes. Maoka and Enyo [3] have reported on the effect of THU upon the hydrogen entrance into palladium during the cathodic reaction. Recently, there has been reported on the strong effect that the adsorption of some sulphur compounds (especially THU) had upon the galvanostatic desorption of hydrogen dissolved in Pd electrodes [4].

The aim of this paper is to establish the influence of THU on the adsorption of hydrogen on palladium by means of linear sweep voltammetric technique

Experimental. The measurements were carried out with an Electroscan TM 30 Electroanalytical System (Beckman) using a three-electrode type cell provided with a thermostated jacket. The working electrode was a platinum disk (Ø = 2,2 cm) on which palladium was deposed by a current of 17,5 mA, for 30 s, exposed with both faces to the solution. The solution was 0,1 M H_2SO_4 of analytical grade deoxigenated with high purity argon.

The measurements were performed by applying the technique of linear sweep voltammetry, starting from different initial potential values, at which the electrode was kept for two minutes (the time necessary to establish the equilibrium) The typical current-potential recorded curves are shown in Fig 1

The eight curves correspond to different initial potential values E_0 70 mV (a), 90 mV (b), 100 mV (c), 110 mV (d), 120 mV (e), 130 mV (f), 140 mV (g), 150 mV (h).

We notice two peaks: one of them, appearing at about 120 mV corresponds to the absorbed hydrogen, the other one, at about 270 mV, corresponds to the adsorbed one. One can see that while the initial potential values are decreasing,

* *University of Cluj-Napoca, Department of Physics, 3400 Cluj-Napoca, Romania*

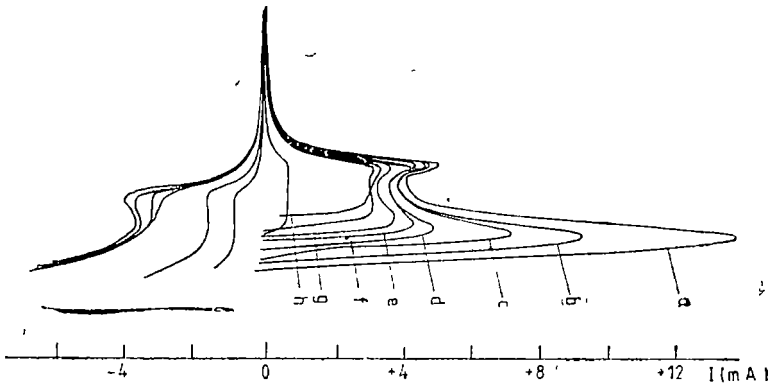

Fig. 1.

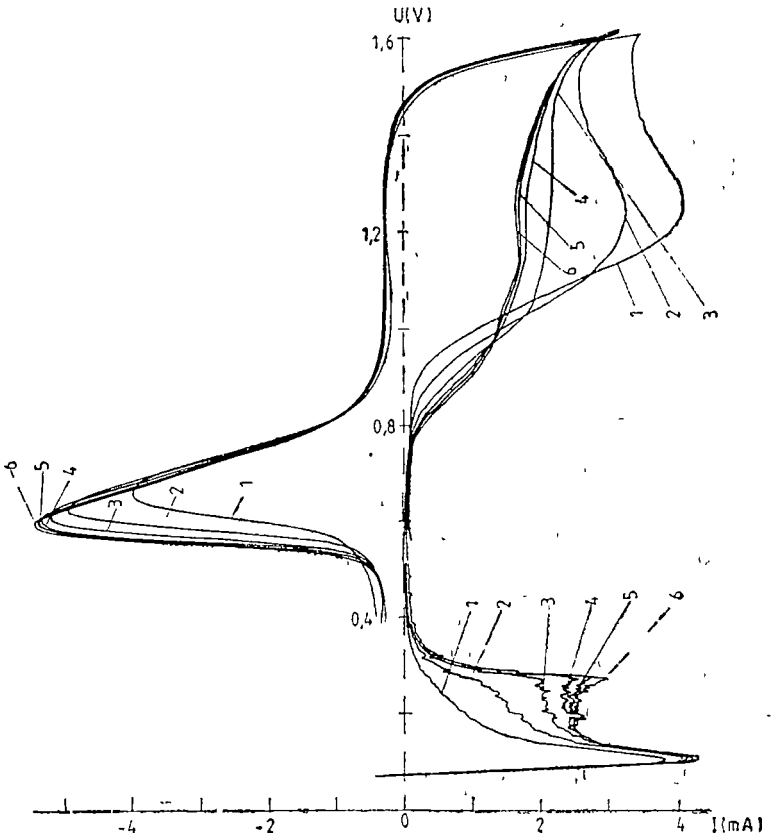

Fig. 2.

the height of the two peaks increases (the one of absorption increases much more than the other one, which tends to saturation value)

If the electrode surface is poisoned with sulphur, by keeping it in a thiourea saturated solution, we obtain only the peak of absorption, while the peak of adsorption does not exist (Fig. 2, curves 1).

Curves 2—5 take shape from the succesiv cycles of oxidation-reduction applied to the electrode in order to clean its surface (to move away the adsorbed poisonous substance). The initial potential for the six curves was the same, $E_0 = 70$ mV. We notice that the adsorption peak is appearing higher and higher when the number of cycles which are going up to 1,6 V increases, until the surface becomes clean, and its height remains constant. At the same time, the cathodic peak, which is connected with the real electrode surface increases too, and after 5—6 cycles it becomes constant (the surface in clean)

Conclusions. The main conclusions of this investigation are the following,

— Sulphur has a strong blocking effect upon the adsorption of hydrogen

— Sulphur compound preadsorbed is electrochemically stable in the adsorption/desorption range of hydrogen, but if the potential value goes up to 1,6 V, the desorption of sulphur occurs, and after a few cycles, the electrode surface becomes clean.

REFERENCES

1. R. V. Bucur and Felicia Bota, *Electrochimica Acta*, **27**, 521 (1982)
2. R. V. Bucur and Felicia Bota, *Electrochimica Acta*, **29**, 103 (1984)
3. T. Maoka and M. Enyo, *Surf. Technol.*, **9**, 147 (1979)
4. R. V. Bucur and Felicia Bota, *Electrochimica Acta*, **29**, 1283 (1984)

STUDIA UNIV BABEŞ—BOLYAI, PHYSICA, XXXI, 1, 1986

PARAMETRIC INSTABILITIES IN AN INHOMOGENEOUS PLASMA

C. BĂLEANU*, S. COLDEA* and J. KARACSONY*

Received. May 21, 1986, accepted August 12, 1986

ABSTRACT. — Parametric effects of a circularly polarized electric field on an inhomogeneous plasma in a constant magnetic field are studied by taking into account density gradients The spatial variation of the external electric field is neglected (dipole approximation) and only the weak inhomogeneity condition is considered It is obtained the threshold condition for parametric excitation of the circularly polarized response modes and of the ion-acoustic and Langmuir waves

Excitation of waves in an infinite homogeneous plasma, when the energy source for excitation is an externally applied oscilating electric field was intensively studied (2—4), (6), (8—9)

The purpose of our paper is to study the effects of inhomogeneity of the magnetized plasma on parametric instabilities excited by an electric pump field A previously introduced method (5) is extended to the case of an inhomogeneous plasma, when the applied field is a right-handed circularly polarized electric field propagating in the direction of the magnetic field $\vec{H}_{ext}$ The form of the electric and magnetic field is

$$\vec{E}_{ext} = Re\{E_0(\hat{e}_2 + \hat{e}_3)exp\,[i(k_0x - \nu t]\} \tag{1a}$$

$$\vec{H}_{ext} = H_0 \cdot \hat{e}_1 \tag{1b}$$

where $(\hat{e}_1, \hat{e}_2, \hat{e}_3)$ are versors of the coordinate axes

The perturbation metod used for the system of kinetic equation with relaxation collision term and Maxwell's equations (5) is applied to the case of an inhomogeneous plasma considering a developpment technique commonly used in the theory of parametric oscillations First the laboratory frame of reference is used and in the second part a transition is made to a frame which moves with the drift velocity of electrons, caused by the electric pump field Following these methods we could obtain and solve the dispersion relation for the considered system, with the aim to arrive to expressions of threshold conditions upon onset of the instabilities, the frequencies and growth rates of excited parametric oscillations

When the frequency of the left-handed response mode $\omega = \Omega - \omega_0'$ where $\Omega = eH_0/mc$ (2)

and $$\omega_0^2 = 4\pi N_0 e^2/m \tag{3}$$

* *University of Cluj-Napoca, Department of Physics, 3400 Cluj-Napoca, Romania*

with the plasma density beeing of the form

$$n_0 = N_0\Big\{1 + \eta_y(y - y_c) - \eta_y\Big[\frac{v_y(0)}{\Omega}\sin\Omega t + \frac{v_z(0)}{\Omega}\cos\Omega t + \\ + \frac{eE_0}{m(\Omega - \nu)}\Big(-\frac{\cos\nu t}{\nu} + \frac{\cos\Omega t}{\Omega}\Big)\Big] - \eta_z\Big[\frac{v_z(0)}{\Omega}\sin\Omega t - \\ - \frac{v_y(0)}{\Omega}\cos\Omega t + \frac{eE_0}{m(\Omega - \nu)}\Big(-\frac{\sin\nu t}{\nu} + \frac{\sin\Omega t}{\Omega}\Big)\Big] + \eta_y(y - y_0)\Big\} \tag{4}$$

where e and m are the electron charge and mass, $\vec{\eta}$ is defined by.

$$\vec{\eta} = N_0^{-1}\vec{\nabla}n_c|_{r=r_0} \tag{5}$$

the threshold condition is obtained as

$$\Lambda_0^2 > \frac{8}{3}\frac{mc^2}{n_0e^2T_e}\frac{\omega_0'^2(\Omega - \nu)^2}{\Omega}\Big(\frac{\nu_c}{\omega_0'} + f(\omega_0')\Big)\Big(\frac{\nu_c}{\omega_0'} + \frac{\omega_0'^2}{T_e}\frac{1}{k^2}f(\omega_0')\Big) \tag{6}$$

where $\Lambda_0^2 = E_0^2/8\pi N_0T_e$ is the external electric field energy density and the thermal energy density ratio, k is wave number of the response field, directed along the OX-axes, T_e is the electron temperature defined by $v_{T_e} = \sqrt{T_e/m_e}$, ν_c is the electron collision frequency, c is the light speed and

$$f(p) = \frac{\pi_p^{1/2}}{k(2T_e)^{1/2}}\exp\Big(-\frac{p^2}{2kT_e}\Big) \tag{7}$$

We have neglected the terms $\eta_y(y - y_0)$, $\eta_z(z - z_0)$, $\frac{ekE_0\eta_y}{2m\nu(\Omega - \nu)}$ and $\frac{ekE_0\eta_z}{2m\nu(\Omega - \nu)}$ in the considered approximation On the other hand the condition of weak spatial homogeneity ($k_0 \ll k$) is the dipole approximation

$$\Big|\frac{(\Omega - \omega_0')^2}{\nu^2} - \frac{(\Omega - \omega_0')\omega_0'}{\nu^2} - \frac{\omega_0'^2}{\nu^2}\cdot\frac{(\Omega - \omega_0')}{\nu^2}\Big(\frac{\nu_c}{\omega_0'} + f(\omega_0')\Big) + \\ + 2\Big(\frac{ekE}{2m\nu(\Omega - \nu)}\Big)^2 - i\Big(\frac{\nu_c}{\omega_0'} + f(\omega_0')^{-1}\Big| \geqslant 1 - \frac{\omega_0^2}{\nu(\Omega + \nu)}\Big) \tag{8}$$

with

$$\omega_0^2 = \frac{4\pi n_0e^2}{m} \tag{8'}$$

There is an other possibility for the onset of an instability in the case of a left-handed polarized response, with frequency $\omega = \nu - \omega_0'$, with the corresponding threshold condition

$$\Lambda_0^2 > \frac{8}{3}\frac{mc^2}{n_0e^2v_{T_e}^2}\frac{\omega_0'^2(\Omega - \nu)^2}{\nu(\nu - \omega_0' - \Omega) - \omega_0'(\nu - \Omega)}\Big(\frac{\nu_c}{\nu - \omega_0' - \Omega} + \\ + f(\nu - \omega_0' - \Omega)\Big)\Big(\frac{\nu_c}{\nu} + \frac{\omega_0'^2}{k^2v_{T_e}^2}f(\omega_0')\Big) \tag{9}$$

and the spatial homogeneity condition:

$$\left|\frac{(\nu-\omega_0')^2}{\nu^2}-\frac{(\nu-\omega_0')\omega_0'^2}{\nu^2(\nu-\omega_0'-\Omega)}+i\omega_0'^2\frac{(\nu-\omega_0')}{\nu^2(\nu-\omega_0'-\Omega)}\cdot\right.$$

$$\left(\frac{\nu_c}{\nu-\omega_0'-\Omega}+f(\nu-\omega_0'-\Omega)\right)+2i\left(\frac{ekE_0}{2m\nu(\Omega-\nu)}\right)^2\cdot$$

$$\left.\cdot\left(\frac{\nu_c}{\omega_0'}+f(\omega_0')\right)^{-1}\right|\geqslant 1-\frac{\omega_0^2}{\nu(\nu+\Omega)} \tag{10}$$

The threshold conditions (6) and (9) are identical with those previously obtained in (5) for the case of an homogeneous plasma. The expressions of growth rates of the instabilities are identical with corresponding expessions for the homogeneous case and we do not give here these expressions.

If we take instead of a linear polarized electric pump field (1), a right-handed circularly polarized pump field, which lies in the XOY-plane, and using density gradients $\vec{\eta}(-\eta, 0, 0)$, after some algebrical calculations we can arrive to the following dispersion relation for the case of four-plasmons coupling (with frequencies ω, $\omega\pm\nu$ and ν):

$$\frac{1}{\chi_e(\omega)}+\frac{1}{\chi_i(\omega)}=-\frac{\mu}{2}\left(\frac{\mu}{2}+J\cdot exp\ (i\beta)\right)\cdot$$

$$\frac{1}{1+\chi_e(\omega+\nu')}-\frac{\mu}{2}\left(\frac{\mu}{2}-J\cdot exp(-i\beta)\right)\cdot\frac{1}{1+\chi_e(\omega-\nu)} \tag{11}$$

To obtain the above dispersion relation we considered the pump field at high frequency (as $\nu\sim\omega_0$ or $\nu_0\sim 2\omega_0'/1/$), so it is assumed that the ions can not follow the high frequency field, i.e. $\mu_i=0$ and $\mu_e=\mu$.

χ_σ are the well known linear susceptibilities ($\sigma=e,\ i$)

$$\chi_\sigma(\omega)=\frac{1}{(k\lambda_{D\sigma})^2}\cdot\frac{1+(\omega+i\nu_\sigma+\omega_{*\sigma})\,L}{1+i\nu_\sigma\cdot L} \tag{14a}$$

where

$$L=\sum_{1=-\infty}^{\infty}I_1(b_\sigma)\,exp\,(-b_\sigma)\cdot Z(\xi_\sigma)/k_z\cdot v_{T\sigma} \tag{14b}$$

$$b_\sigma=k^2v_{T\sigma}^2/2\Omega_\sigma^2\ \ (14c);\quad \xi_\sigma=\frac{\omega+i\nu_\sigma-1\cdot\Omega_\sigma}{k_z\,v_{T\sigma}} \tag{14d}$$

$$\omega_{*\sigma}=\frac{\eta k_y\,T_\sigma}{m_\sigma\,\Omega_\sigma}\ \ (15a);\quad \lambda_{D\sigma}=\left(\frac{T_\sigma}{4\pi N_0 e^2}\right)^{1/2} \tag{15b}$$

I_1 beeing the modified Bessel function and T_σ — the temperature, When we neglect the ions motion, the dispersion relation for excitation of a single mode via density gradient coupling is·

$$1 + \chi_e(\omega) = J^2 \chi_e'(\omega) \frac{\chi_e'(\omega - \nu)}{1 + \chi_e(\omega - \nu)} + \frac{\chi_e'(\omega + \nu)}{1 + \chi_e(\omega + \nu)} \tag{16a}$$

with

$$\chi_e'(\omega) = \frac{1 + (\omega + i\nu_e) L}{1 + i\nu_e L} \cdot \frac{1}{k^2 \lambda_{De}^2} \tag{16b}$$

Considering that the magnetic field cancels in Eq (12), after the analysis of the parametric excitation of ion-acoustic and Langmuir waves, when $\nu = \omega_0 + \Lambda_0$, $\Lambda_0 \ll \omega_0$, we have obtained the following threshold condition:

$$\Lambda_0^2 = \frac{32\sqrt{3}\gamma_H^2 \gamma_L}{9(k_y c_s)^2 \omega_0} \tag{17a}$$

with

$$\gamma_H = -\frac{\nu_e}{2} \text{ (17b)}, \quad \gamma_L = -\frac{\nu_i}{2} \text{ (17c)}, \quad c_s = \left(\frac{T_e}{m_i}\right)^{1/2} \tag{17d}$$

Threshold expression (17) differs from the corresponding expression previously obtained for a linear polarized pump field (1) by factor k_y, which appear instead of k, for the case of a right-handed electric field.

On the other hand the calculated frequency of excited wave is

$$\omega_r = \pm \omega_s + \frac{\eta}{k_y} \cdot \frac{\sqrt{3}}{3} \cdot \gamma_L \tag{18}$$

where

$$k_r = (k_y \cdot c_s)^2 \quad \omega_0 \cdot \frac{\Lambda_0^2}{2} \tag{19a}$$

and

$$\omega_s^2 = (k_y \cdot c_s)^2 + \frac{K_r \Lambda_0}{\gamma_H^2 + \Lambda_0^2}$$

To obtain expressions (17) and (18) it was assumed that

$$k_y \gg \eta \tag{20}$$

and

$$\nu_i \ll kc_s \ll \nu_c \ll kv_{T_e} \tag{21}$$

From Eq (16) we can conclude that, for the pump field frequency $\nu = 2\omega_0' + \Lambda_0$, the threshold for excitation of the Langmuir wave and the instability range are the same as in the case of a linear polarized electric field.

Similarly, for $\nu = 2\omega_H + \Lambda_0$, $|\Lambda_0| \ll \omega_H$, where $\omega_H^2 = \omega_0'^2 + \Omega^2$ is the upper hybrid frequency, the range instability Λ_0 is obtained from Eq (16) and

has the same form as that obtained for a linear polarized pump field, for the case of a right-handed polarized pump field we have obtained another expression for threshold

$$\eta \cdot E_{0c} = 4 \frac{m}{e} \nu_c |\Omega| \cdot \frac{(1 + A)\left[\sqrt{2}(1 + A)^{1/2} - 1\right]}{A} \tag{22}$$

where $A = \omega_0'^2/\Omega^2$, ν_c is the collision frequency of electrons

Using the values $\Omega = 10^9\ s^{-1}$, $\nu_c = 10^6\ s^{-1}$ and $\eta = 1\ V/cm$, after calculations we obtain the threshold value as having the order of units of V/cm in the case in the right-handed polarized field, instead of order of tens units of V/cm previously obtained (1)

As a main result of our investigations we have found that the inhomogeneity of the plasma affect the parametric instabilities of the considered system, by exciting some new oscillation modes that do not appear in the homogeneous case, under the same conditions. We can conclude that a right-handed circularly polarized pump field can excite more efficiently the upper hybrid mode than a linear polarized electric field applied to an inhomogeneous plasma.

REFERENCES

1 J Amano, M Okamoto, J Phys Japan, **26**, 259 (1969)
2 M Porkolab, Physica 82 C, 86 (1976)
3. M Porkolab, R P H. Chany, *Rev. Modern Physics*, **50**, 745 (1978)
4 M. Porkolab, *Nuclear Fusion* 18, 367 (1978)
5. R Prasad, Phys Fluids 13, 1310 (1970)
6 V P Silin, „Parametriceskoie Vozdeistvye izlucenija bolishoi moscinosti na plazmu", Nauka, Moskva, 1973
7. V. P Silin, *J de Physique*, **38**, C6, 153 (1977)
8. K H Spatschek, *Fortschritte der Physik*, **24**, 687 (1976)
9. G. Wallis, D Sunder, *Beitr Plasma Physik*, **12**, 373 (1972).

STUDIA UNIV BABEŞ—BOLYAI, PHYSICA, XXXI, 1, 1986

ALGORITHMS FOR FOURIER TRANSFORM AND ITS APPLICATION IN THE EXAFS SPECTROSCOPY

N. ALDEA*, E. INDREA*, G. BORODI* and S. ASTILEAN**

Received: September 9, 1986, accepted September 25, 1986

ABSTRACT. — This paper describes algorithms for the Fourier trasform (FT) used in Extended X-ray Absorption Fine Structure (EXAFS) spectroscopy The main properties of the FT are revised and a comparison of the computational time has been carried out between classical, Filon and Cooley-Tukey algorithmus An extensive description of the EXAFS analysis of a Ni sample will be given

1 **Introduction.** The Fourier transform is one of the most common transformation occuring in nature Certain features associated with this transform are found, used by man in a variety of occupations and applications For example the FT-s are used in X-ray diffraction, X-ray spectroscopy, radar, network design, nuclear magnetic resonance, infrared spectroscopy, random process, probability, quantum physics boundary-value problems and encephalography This paper describes classical, Filon and Cooley-Tukey algorithms for Fourier transform

2. **Fourier Transform and its Properties.** The Fourier integral is defined by the expression (1)

$$H(f) = \int_{-\infty}^{\infty} h(t) \quad \exp(-2\pi i f t)\ dt \tag{1}$$

If the integral exists for every value of the parameter f then Eq (1) defines $H(f)$, the FT of $h(t)$. In general the FT is a complex quantity

$$H(f) = R(f) + iI(f) = |H(f)| \quad \exp(i\theta(f)) \tag{2}$$

where $R(f)$, $I(f)$ are real and imaginary part, respectively, $H(f)$ is the amplitude or Fourier spectrum of $h(t)$ and $\theta(f)$ is the phase angle

The inverse Fourier transform (IFT) is defined as

$$h(t) = \int_{-\infty}^{\infty} H(f) \quad \exp(2\pi i t f)\, df \tag{3}$$

* *Institute of Isotopic and Molecular Technology, P O Box 700, 3400 Cluj-Napoca, Romania*
** *University of Cluj-Napoca, Department physics, 3400 Cluj-Napoca, Romania*

In dealing with the FT there are a few basic properties·

— linearity. the FT of the sum is equal to the sum of the FT

$$\int_{-\infty}^{+\infty} [\alpha h_1(f) + \beta h_2(f)] \exp(-2\pi\imath ft)\, dt = \alpha H_1(f) + \beta H_2(f) \tag{4}$$

— time scaling: if the FT of $h(t)$ is $H(f)$, then the FT of h(kt) is

$$\int_{-\infty}^{\infty} h(kt) \exp(-2\pi\imath ft) dt = \int_{-\infty}^{\infty} h(t') \exp(2\pi\imath ft'/k) dt'/k = 1/k \cdot H(f/k) \tag{5}$$

where $k > 0$ is a real constant

— frequency scaling· if the IFT of the $H(f)$ is $h(t)$, the IFT of $H(kf)$ is given by $1/k \cdot h(t/k)$

— time shifting· if $h(t)$ is shifted by a constant, to then by substituting $s = t - t_c$, the FT becomes

$$\int_{-\infty}^{\infty} h(t - t_0) \cdot \exp(2\pi\imath ft)\, \mathrm{d}t = \exp(-2\pi\imath ft_c) \cdot H(f) \tag{6}$$

— frequency shifting: if $H(f)$ is shifted by a constant f_c, its IFT is multiplied by $\exp(2\pi\imath f_0)$

— differentiation· the n-th derivative of the function is proportional to the FT of the product of its FT and the n-th power of the independent variable

— convolution: the FT of the two functions in product is equal to the area under the curves of the FT of the multiplicand with the folded form of the FT of the multiplier as a function of the shifting distance between their origins.

$$\int_{-\infty}^{\infty} g(t) \cdot h(t) \cdot \exp(-2\pi\imath ft)\, dt = \int_{-\infty}^{\infty} G(f') \cdot H(f - f') df' \tag{7}$$

and

$$\int_{-\infty}^{\infty} G(f) \cdot H(f) \cdot \exp(2\pi\imath ft)\, df = \int_{-\infty}^{\infty} g(t') \cdot h(t - t')\, dt'$$

2. **The Discrete Fourier Transform.** Taking into account the properties of the Dirac distribution we can express a discrete series h_n such that:

$$h_n = \sum_{n=0}^{N=1} h(n\Delta t)\, \delta(t - n\Delta t) \tag{8}$$

where N is the number of the dirscrete points and Δ the increment of the t variable, with this assumption $\Delta f = 1/N\Delta t$

The FT of h_n may be simply stated by substituing (8) into (1) and interchanging the integration and the summation.

$$H(k\Delta f) = \sum_{n=0}^{N-1} h_n \quad \exp(-2\pi ikn\Delta t\Delta f) \tag{9}$$

An analogous argument will produce for the IFT.

$$h_n = 1/N \quad \sum_{n=0}^{N-1} H_k \quad \exp(2\pi ikn/N) \tag{10}$$

3 The Cooley-Tukey Algorithm. The classical metod of computing the discrete FT has been replaced for most purposes by the Cooley-Tukey algorithm (2) Let us consider a time series X_k consisting of N complex points. We first divide these series into two subseries Y_k and Z_k consisting of the odd and even points

$$\begin{aligned} Y_k &= X_0, X_2, \quad X_{2k} \\ Z_k &= X_1, X_3, \ldots X_{2k+1} \end{aligned} \qquad k = 0, 1, 2, \quad , N/2-1 \tag{11}$$

Now both Y_k and Z_k have discrete FT according to Eq. (9) and we shall call them B_r and C_r

$$\begin{aligned} B_r &= \sum_{k=0}^{N/2-1} Y_k \quad \exp(-4\pi irk/N) \\ C_r &= \sum_{k=0}^{N/2-1} Z_k \cdot \exp[-2\pi ir(2k+1)/N] \end{aligned} \qquad r = 0, 1, 2, \ldots, (N-1)/2 \tag{12}$$

Now let us rewrite the transform A_r in terms of its odd and even numbered points and relate them to B_r and C_r

$$A_r = B_r + \exp(-2\pi ir/N) \quad C_r \quad \text{for } 0 < r < N/2 \tag{13}$$

For values of r above $(N/2) - 1$, we find that B_r and C_r repeat periodically and.

$$A_r + N/2 = B_r - \exp(-2\pi ir/N) \quad C_r \text{ for } 0 < r < N/2 \tag{14}$$

We can continue this halving process by dividing Y_k into T_k and V_k series, having transforms D_r and E_r and Z_k into V_k and W_k series, each having transforms F_r and G_r, and so forth, until we have divided each array down into one point arrays

The easiest way to regard the point shufflings and recombinations necessary to realize the simplifications of the Cooley-Tukey method is to view the transform as a series of ln N steps ($N = 2^n$, n integer) which are performed on all data points. The necessary steps are shown schematically in a signal flow graph in Fig. 1. This graph shows the array X_k at the left side and the array A_r at the right side. Thus each new data points is calculated by relation (13) and (14). Examining Fig. 1, we find that while the arrays X_k on the left side start in their usual order, the array, A_r on the right side end up in a scrambled order

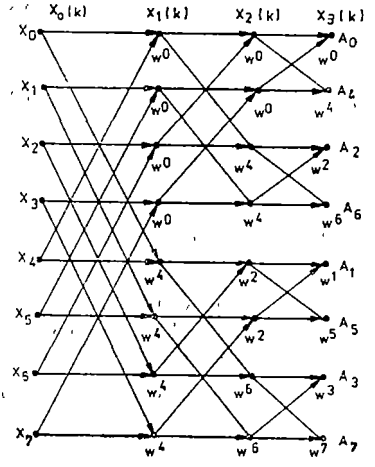

Fig 1. The signal flow graph the FT calculated with the Cooley-Tukey algorithm

A_0, A_4, A_2, A_6, A_1, A_5, A_3, A_7 The generality of this order may not be readily apparent but it can be best described by looking at the subscripts as binary numbers

$$0{-}000,\ 4{-}100,\ 2{-}010,\ 6{-}110,\ 1{-}001,$$
$$5{-}101,\ 3{-}011,\ 7{-}111$$

If those subscripts are bit-reversed in binary, we will have the natural order Thus the Cooley-Tukey algorithm produces a transform whose points are shuffed in binary bit inversion

4 **The Filon Algorithm.** We consider the limits of the interval of the Eq. (1), the finites numbers a and b, $(b = a + 2nk)$ The integration range (a, b) is divided into a number of $2n$ intervals equal to t, and therefore it is necessary to have an odd number of equally spaced values of the function $h(t)$ The imaginary part of integral is evaluated using Filon's quadrature formula (4)

$$H(f) = k[\alpha(fk)[h(a)\cos(fa) - h(b)\cos(fa)] + \beta(ft)S_{2n} + \gamma(ft)S_{2n-1}\} \quad (15)$$

where

$$S_{2n} = \sum_{i=0}^{n} h(t_{2i}) \cdot \sin(ft_{2i}) - 1/2h(a) \cdot \sin(fa) - 1/2 \cdot h(b)\sin\ (fb)$$

$$S_{2n-1} = \sum_{i=1}^{n} h(t_{2i-1}) \cdot \sin(f \cdot t_{2i-1}), \quad t_i = a + ik$$

$$\alpha(\theta) = 1/\theta + \frac{\sin 2\theta}{2\theta^2} - \frac{2\sin^2\theta}{\theta^3}$$

$$\beta(\theta) = 2\left(\frac{1 + \cos^2\theta}{\theta^2} - \frac{\sin 2\theta}{\theta^3}\right)$$

$$\gamma(\theta) = 4\left(\frac{\sin\theta}{\theta^3} - \frac{\cos\theta}{\theta^2}\right)$$

For small values of $\theta(\theta < 1)$ the values of α, β and γ are evaluated by developing in powers of θ up to the 10th, 12th and and 13th term respectively. The real part of the Fourier transform Filon's quadrature formula is:

$$H(f) = k\{\alpha(fk)[h(a) \cdot \sin(fa) - h(b) \cdot \sin(fb)] + \quad (16)$$
$$+ \beta(ft)C_{2n} + \gamma(ft)C_{2n-1}\}$$

where

$$C_{2n} = \sum_{i=0}^{n} h(t_{2i}) \cdot \cos(ft_{2i}) - 1/2h(a) \quad \cos(fa) - 1/2h(b) \cdot \cos(fb)$$

$$C_{2n-1} = \sum_{i=1}^{n} h(t_{2i-1}) \cdot \sin(f \quad t_{2i-1})$$

5 **Computational Time for Classical. Filon and Cooley-Tukey Algorithms.** Let us to consider the number of computations required if we use the conventional classical method We shall neglect the time required to compute the sine and cosine functions Then, for each $H(f)$ we must do N multiplications for real and imaginary part, hence 2N multiplications We must do N additions for the cosine transform and the same number for the sine transform, hence 4N operations are required for each f function If we wish to compute $H(f)$ for N/2 arguments, $2N^2$ operations are required for the conventional classical method

For the Cooley-Tukey algorithm as applied to this presentation, N must be an integer power of 2, $N = 2^n$ From relations (13) and (14) and from Fig. 1 we can see that the total number of operations is 3NlnN. Based on our computer program, we can esimate the computational time required for a FT, utilising the methods presented on § 3 and § 4, for the analitical function h(t)

$$h(t) = \begin{cases} \beta e^{-\alpha t} & t > 0 \\ 0 & t \leqslant 0 \end{cases} \tag{17}$$

From eq. (1) we obtained

$$H(f) = \frac{\beta}{\alpha^2 + (2\pi f)^2} \quad \exp\{i[\text{arctg}\ (2\pi f/\alpha)]\} \tag{18}$$

and phase function $\theta(f) = \text{arctg}(-2\pi f/\alpha)$

Each of these functions (real, imaginary part and phase function) are plotted in Fig 2 to illustrate the various forms of Fourier transform

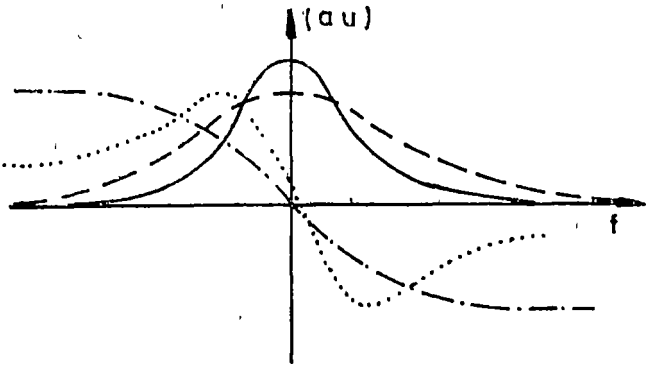

Fig 2. The various forms of the FT for the analitical function $h(t)$; (—) the magnitude function $H(f)$, ( ) the imaginary part of the FT, $I(f)$, (— —) the real part of the FT, $R(f)$; (—.—) the phase function, $\theta(f)$

The computational time of FT using classical, Filon and Cooley-Tukey algorithms for trial function (17) is presented in Table 1. The computer program for the Fourier transform was compiled for FELIX C—256 computer in FØR-TRAN language.

6. **Applications of the Fourier Transform in EXAFS.** EXAFS is a specific element of the scattering technique in which a core electron ejected by an X-ray photon probes the local environment of the absorbing atom. The ejected photoelectron is backscattered by the neighboring atoms around the absorbing atom and interferes constructively with the outgoing electron wave, depending on the energy of the photoelectron. The energy of the photoelectron is equal to the difference between the X-ray photon energy and a threshold energy associated with the ejection of the electron In the EXAFS experiment the photoelectron energy is varied by varying the energy of the incident X-ray beam. The interference between the outgoing and backscattered electron waves has the effect of modulating of the X-ray absorption coefficient. The absorption spectra determined experimentally exhibit oscillations in the absorption coefficient on the high energy sides of absorption edges. The electron wave k is related to the kinetic energy E and to the wavelength λ_1 by the relation:

$$k = (2mE)^{1/2}/\hbar = 2\pi/\lambda_1 \tag{19}$$

where m is mass of the electron and $\hbar = h/2\pi$.

The EXAFS function $\chi(k)$ is defined in terms of atomic absorption coefficients by:

$$\chi(k) = (\mu - \mu_0)/\mu_0 \tag{20}$$

where μ refers to the absorption by an atom from the material of interest and μ_0 refers to the atom in the free state

Theories of the EXAFS based on the scattering of the ejected photoelectron by atoms in the immediate vecinity of the absorbing atom gives an expression for $\chi(k)$ of the form (6)·

$$\chi(k) = \sum_j A_j(k) \cdot \sin[2kr_j + \delta_j(k)] \tag{21}$$

where the summation extends over j coordination shells, r_j is the radial distance from the j-th shell and $\delta_j(k)$ is the phase shift. The amplitude function $A_j(k)$ is given by:

$$A_j(k) = (N_j/kr_j^2) \cdot \exp(-2r_j/\lambda) \cdot \exp(-2k^2\sigma_j^2) \tag{22}$$

In this expression N_j is the number of atoms in the j-th shell, σ_j is the rms deviation of distance about r_j, $F(k)$ is the backscattering amplitude and λ is the mean free path for inelastic scattering. The backscattering factor depends on the kind of atom responsibile for the scattering. The analysis of EXAFS data for obtaining structural informations (N, r, σ, λ) generally proceeds by the use the Fourier transform and non-linear least square techniques. From $\chi(k)$, a radial structure function $|\Phi(r)|$ can be derived. The single shell signal may be isolated by Fourier transform (7):

$$\Phi(r) = (1/2\pi)^{1/2} \cdot \int_{k_{min}}^{k_{max}} k^n \chi(k) \cdot \exp(-2ikr) \cdot WF(k)dk \tag{23}$$

In this expression $WF(k)$ is a „window function" and the integral is extended over the available k range

The EXAFS spectra of Ni sample have been collected using a conventional X-ray spectrometer (TUR M-61 type) with a suitable device for introducing the sample into and off the X-ray beam

The experimental data $\mu(k)$ and the smooth form of $\mu_0(k)$, $\mu_s(k)$, are shown in Fig. 3. The EXAFS function $\chi(k)$ and the radial structure function $\Phi(r)$, determinated using the algorithms for the Fourier transform described above, are shown in Fig 4 and Fig 5, respectively.

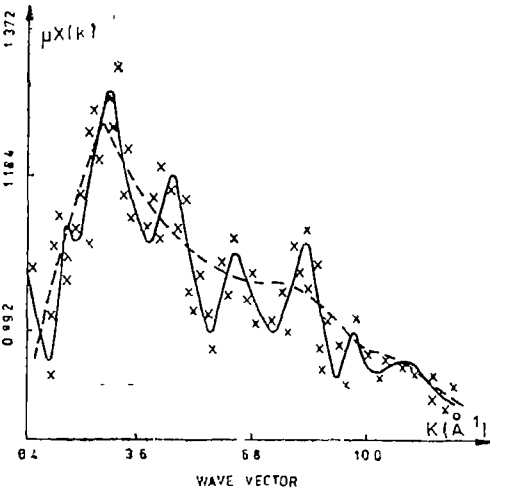

Fig 3. The EXAFS function of $\mu \cdot \chi(k)$ for the Ni sample; (xxx) the experimental $\mu(k)$ function, (—) the smoothed function $\mu(k)$, (— —) the $\mu_0(k)$ function

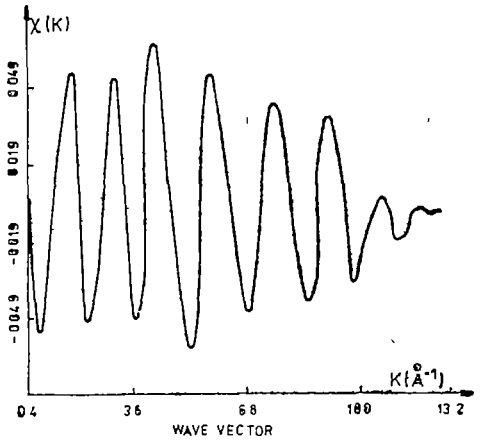

Fig. 4. The EXAFS function $\chi_1(k)$ for the first coordination shell of the Ni sample

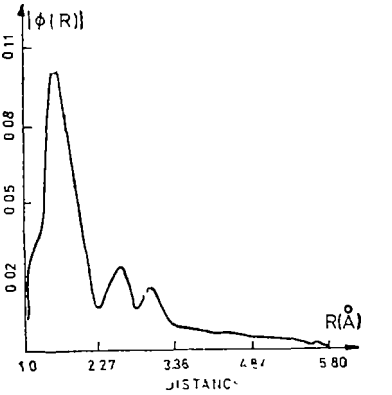

Fig. 5. The radial structure function $\Phi(R)$ for the Ni sample

Based on the computer program described in (8), we have obtained the phase shift function for the Ni sample, $\delta(k) = 0\,043\ k^2 - 1.718\ k - 2\,38$ Improvements in the data evaluation by means of the algorithms of the Fourier transform technique have raised the accuracies for the bound lenght determinations from EXAFS data The values $R_1 = 2\,492$ Å, $R_2 = 3\,524$ Å and $R_3 = 4\,316$ Å obtained for the coordination radius of the first three shells are in accordance with the known crystal structure of Ni when the phase shift is taken into accont

Table 1

The computational time of FT using classical, Filon and Cooley-Tukey algorithms for trial function.

n	$N = 2^n$	Theory T(class) / T (C−T)	Experimental T(class) / T(C−T)	Time required to FELIX C−256 T(Filon) (sec)	T(C−T) (sec)
4	16	2 7	2 4	0,005	0.005
5	32	4.3	4 1	0.154	0 015
6	64	7 1	6 4	0.347	0.027
7	128	12 2	11 8	0 668	0.051
8	256	21 3	20 7	1.122	0 119
9	512	38 0	32.1	3 341	0.328
10	1024	68 2	59 5	13.521	0.450

In conclusion we remark that the Fourier transform of the EXAFS data permits a determination of the local structure about an X-ray absorbing atom which, in principle, can be located in crystalline or disordered phases. For a great number of experimental data (e g greater than 200) and when the coordination shells are distinctly separated it is better to use a Cooley-Tukey algorithm; else we sugest to use the Filon algorithm for the Fourier transform

REFERENCES

1. A Papoulis, "The Fourier Integral and Its Applications,,, Mc Graw-Hill, New York, 1962
2 J W Cooley and J W Tukey, *Math Comput*, **19**,297 (1965)
3 I J Good, J Roi, *Statist Soc Ser B*, **20**,361 (1958)
4 M Abramowitz and I A Stegun, ,,Handbook of Mathematical Functions", Dover, New York, 1965
5 R. J. Bell, "Introductory Fourier Transform Spectroscopy", Academic Press, New York and London, 1972
6 E A Stern, *Phys Rev* **B 10**, 3027 (1974)
7. G. H Via, J H Sinfelt and F W Lytle, *J Chem Phys*, **71**, 690 (1979)
8 *E* Indrea and N Aldea, *Comput Phys Commun*, **21**, 91 (1980)

STUDIA UNIV BABEŞ—BOLYAI, PHYSICA, XXXI, 1, 1986

THE MAGNETIC BEHAVIOUR OF THE DIAMAGNETIC IONS IN A WEAK CRYSTALLINE FIELD

I. GH. POP*, I. POP**

Received September 24, 1986; accepted September 25, 1986

ABSTRACT. — The effective, radial and orbital magnetization coefficients were introduced. They are connected with the ionic distorsion in the framework of orbital overlapping deformable ions model in a weak crystaline field Concret k_{eff}, k_r, k_0 values in a graphical representation versus magnetic susceptibility and versus repulsion energy E_R are given The importance of the second neighbour interaction beween ions is revealed too.

Introduction. The knowledge of the behaviour of ionic diamagnetic crystaline compounds in the magnetic field supposes a lot of difficulties because of the ions diamagnetic free state. In the crystaline field, the Langevin susceptibility $\chi_{d,l}$ of the free ions is modified, and, at the same time, a paramagnetic Van Vleck susceptibility arises. Thus, such a system involves a measured diamagnetic susceptibility $\chi = \chi_d + \chi_p$ [1] · χ_d and χ_p being thermally and magnetically independent, their separate determination by experiment is quite impossible. Their calculation implies many complications for they are not separately gauge origin invariant.

In the present paper we are introducing the magnetization coefficients of diamagnetic ions by passing from free state to crystal, in the presence of a magnetic field. They are suggestively expressing the change of the charge density for free ions, when they are turning in to crystaline state

Diamagnetic coeficients of magnetization. In presence of the magnetic field the magnetic susceptibility of diamagnetic free ions is given by

$$\chi_{d,l}^{[A^+][B^-]} = \chi_{d,l}^{[A^+]} + \chi_{d,l}^{[B^-]} \tag{1}$$

and the magnetic susceptibility of the crystaline ionic compounds A^+B^- is

$$\chi_{cr}^{[A^+B^-]} = \chi_{d,cr}^{[A^+,B^-]} + \chi_p^{[A^+B^-]} \tag{2}$$

$\chi_{cr}^{[A^+B^-]}$ represents the measured magnetic susceptibility χ.

The Langevin diamagnetic susceptibility of the ions in a weak crystaline field is [2]

$$\chi_{d,cr}^{[A^+,B^-]} = k\,;\ \chi_{d,l}^{[A^+][B^-]} \tag{3}$$

k being the effective radial correction function, obtained using the anionic and cationic radial correction function in the framework of the deformable ion model [3].

* *Polythenical Institute of Cluj-Napoca, 3400 Cluj-Napoca, Romania*
** *University of Cluj-Napoca, Department of Physics, 3400 Cluj-Napoca, Romania*

The radial deformation of the ions A^+ and B^- in a weak crystalline field implies a charge redistribution, in a localized charge and in a non-localized charge The latter is correlated with paramagnetic Van Vleck susceptibility

$$\chi_p^{[A+B-]} = a_p\, k_i^2 \{\chi_{d,l}^{[A+]\,[B-]}\}^2 \tag{4}$$

determined by the orbital overlapping model of the radial deformable ions in a weak crystalline field [4]. The bonding parameter a_p of the ions in crystal [5] is depending on the lattice energy E_c and on the overlaping parameter η_r [6], as follows

$$a_p = \frac{2m}{\hbar^2}\,[-E_c]\,\eta_r \cdot \frac{a_B^2}{\chi_0} \tag{5}$$

where a_B is the Bohr radius, and $\chi_0 = \dfrac{Ne^2\mu_0\, a_B^3}{6m}$.

The effective magnetization coefficient is defined by the ratio

$$k_{eff} = \frac{\Delta\chi}{\chi_l} = \frac{\chi - \chi_{d,l}}{\chi_{d,l}} = k_r + k_o \tag{6}$$

where

$$k_r = \frac{\chi_{d,cr}^{[A+,\,B-]} - \chi_p^{[A+B-]}}{\chi_{d,l}^{[A+][B-]}} = k_s - 1 \tag{1}$$

is radial magnetization coefficient, and

$$k_o = \frac{\chi_p^{[A+B-]}}{\chi_{d,l}^{[A+][B-]}} = a_p \quad k_i^2\, \chi_{d,l}^{[A+][B-]} \tag{8}$$

represents the orbital magnetization coefficient, connected to the nonlocalized charge density of diamagnetic deformable ions system

Results and discussions. Using the magnetic susceptibility experiemntal data χ [7], the calculated values χ_d [8], and the effective radial correction function k_i, we have obtained the magnetization coefficients k_{eff}, k_r and k_0 as defined for alkali bromides As seen on Figs 1 and 2, we can make some remarks on these coefficients introduced by us Thus, the ionic distorsion largely differs from anion to cation The anions are tightening and the cations are loosening in crystal relative to free state When the positive ion size largely differs from there negative partner in crystal (LiBr, NaBr), the ionic distorsion of the cation is negligible, reletive to that of the anion, and the second neighbour repulsion becomes predominant. Thus, the orbital overlapping is determined only by negative ions, the big part from k_{eff} being given by the negative ion. The effect of second neighbour repulsion is important in those crystals where the size of ions largely differs from one another. On the other hand, in crystals composed by ions in comparable sizes, the effect of second neighbour repulsion is not high. In this case both the anion and the

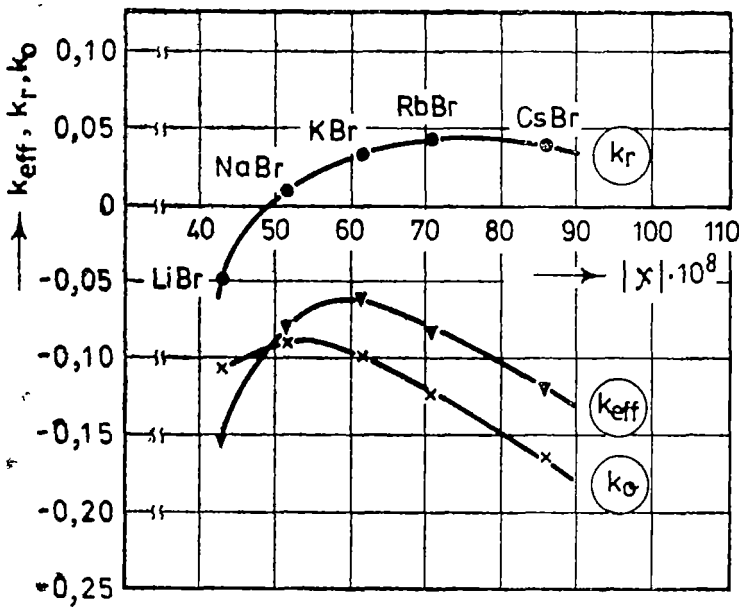

Fig. 1. Magnetization coefficients k_{eff}, k_r, k_0 vs. magnetic susceptibility for alkali bromides.

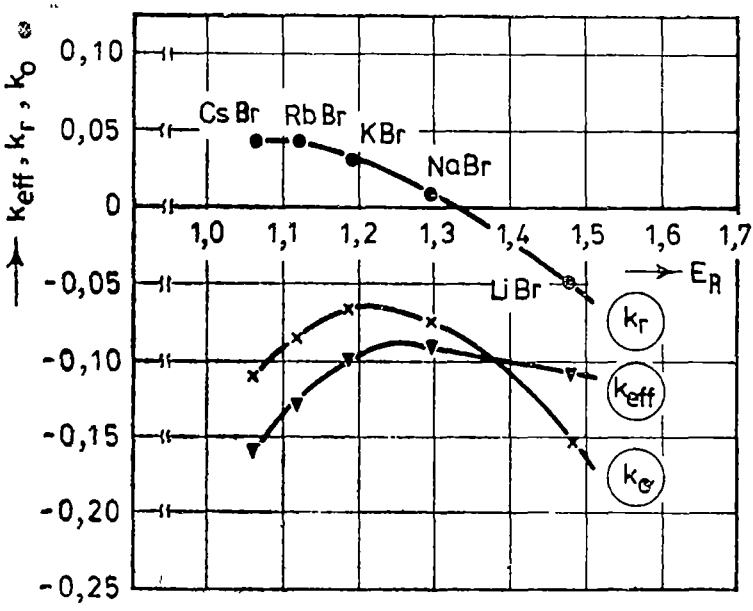

Fig 2. Magnetization coefficients k_{eff}, k_r, k_0 vs. repulsion energy E_R for alkali bromides.

cation are responsable for radial and orbital deformation in crystal The effect of second neighbour repulsion is expected to be smaller in crystals composed of isoelectronic ions than in the others

The chemical bonding in crystal is determined by the non-localized charge in the valence region, corresponding to orbital overlapping of the external ionic deformable orbitals in crystalline field A very small value of the effective magnetization coefficient k_{eff} cannot be supposed due to a radial deformation absence of the ions in crystal, but a compensation of the diamagnetic and paramagnetic moments in the bonding region is present The increase of radial deformation of ions in alkali bromides exhibits an increased value of the orbital magnetization coefficient k_0

Conclusions. The magnetic coefficients, effective k_{eff}, radial k_r and orbital k_0, introduced by us in this paper, in the framework of the orbital overlapping model, allows to connect the magnetic response of the alkali bromides (and other halides) crystaline systems with the charge distribution in crystal An increased value of the orbital magnetization coefficient assumes an important non-localized charge.

REFERENCES

1. J H Van Vleck, „The theory of Electric and Magnetic Susceptibilities", Oxford University Press, Oxford, 1932
2. I. Gh Pop, I Pop, V Toşa, „Progrese în fizică", *A 7-a sesiune anuală ICEFIZ*, Iaşi, 1985.
3. V P Gupta, *Indian J Phys*, **55A**, 459 (1981)
4. I Gh Pop, I Pop, Al M Imbroane, *Studia UBB, Physica*, **XXX**, 60 (1985)
5. I. Pop, I Gh Pop, *(to be published)*
6. I Gh Pop, I Pop, „Progrese în fizică", *A 8-a sesiune anuală ICEFIZ*, Galaţi, 1986
7. Ya G. Dorfman, „Diamagnetizm i himičeskaja svjaz", *Gos izd fiz mat lit*, Moskva, 1961
8. I Gh. Pop, I Pop, R I Cămpeanu, „Progrese în fizică", *A 7-a sesiune anuală ICEZIZ*, Iaşi, 1985

STUDIA UNIV BABEŞ—BOLYAI, PHYSICA, XXXI, 1, 1986

PARAMETRIC EXCITATION OF AN INHOMOGENEOUS MAGNETIZED PLASMA

C. BĂLEANU*, S. COLDEA* and J. KARACSONY*

Received September 25, 1986, accepted September 25, 1986

ABSTRACT. — The parametric instabilities of a magnetized inhomogeneous plasma with density gradient perpendicular to the external magnetic field is studied, by applying the method of [4] based on multitime scale perturbation It is found that three new cases of excitations of parametric modes appear due to inhomogeneity, and the two cases that appear in the homogeneous case are not affected

The parametric instabilities were intensively studied [9] because of their applications in devices proposed for thermonuclear fusion, astrophysics and electronics It is of interest for the study of this problem to use a perturbation method of multiple-time scale [3—8], [11] The purpose of this paper is to gegeralize the method in [4], applied to homogeneous plasma in the case of the inhomogenous one Parametric instabilities in an inhomogenous plasma were studied [5] by using multitime scale and by us [2] with the method already used in [1] and [10]

In the present paper we investigate the effect of the combination of the applied oscillating electric field and a constant magnetic field perpendicular to the former, on parametric excitation of electromagnetic waves propagating along the constant magnetic field As in [4] we choose the coordinates so that $\vec{E}_a = E_a \cos w_t t$ (1, 0, 0), or $\vec{K} = K(0, 0, 1)$ and $\vec{B}_a = B_a$ (0, 0, 1), where $\vec{E}_a$ and $\vec{B}_a$ are pump field and the constant magnetic field, respectively The plasma inhomogeneity is taken into account through the density gradient at the point r_0.

$$\vec{\eta} = N_0^{-1} \quad \nabla n \mid \vec{r} = \vec{r}_0 \tag{1}$$

where we have taken $\eta_t = 0$

By applying the perturbation method of multitime scales to systems formed from Vlasov and Maxwell equations, when the small parameter is the ratio of the electron excursion in the applied fields to the wavelength of the parametrically excited wave and eliminationg the secularities, we have obtained the following results

1 When $w_0 = w_1 + w_r$, $K_1 = K_r$, where w_1, K_1, w_r, K_r satisfy the dispersion relarions for longitudinal and right hand circularly polarized waves, respectivelly

$$w_1^2 - c^2K_1^2 - w_p^2\left(1 + \frac{K_1^2\alpha^2}{w_1^2}\right) = 0 \tag{2}$$

$$w_r^4 - w_r^2(w_p^2 + \Omega^2) - c^2K^2(w^2 - \Omega^2) + |w| \quad \Omega \quad w_p^2 = 0 \tag{3}$$

* *University of Cluj-Napoca, Department of Physics, 3400 Cluj-Napoca, Romania*

with the well known expressions for plasma and cyclotron frequencies

$$w_p^2 = \frac{4\pi N_0 e^2}{m} \tag{4}$$

and

$$\Omega = \frac{\overline{eBa}}{mc} \tag{5}$$

α being the thermal velocity. In this case the possibility of excitation of a transverse right polarized wave and a Langmuir wave appears, which propagate in the same direction The growth rate is given by the root (the positive real part) of the equation:

$$\lambda_{w_1+w_r} = \pm \sqrt{i\frac{b_1 b_3}{b_2 b_4}} \tag{6}$$

where

$$b_1 = w_r w_p^2 2\pi^2 \frac{a'}{A} K_1 \left\{ \frac{w_0^2 - w_p^2 - w_0\Omega}{(w_r - \Omega)^2} + [w_0(w_p^2 - w_0^2 + \Omega^2) + w_p^2\Omega] \cdot \right.$$

$$\cdot \left[-\frac{1}{w_1^2(w_r + \Omega)} + \frac{1}{w_1(w_r + \Omega)^2} \right] + 3K_1^2\alpha^2 \left\{ \left[\frac{1}{(w_r - \Omega)^4} + \right. \right.$$

$$\left. + \frac{w_r^4 + 6w_r^2\Omega^2 + \Omega^4}{(w_r^2 - \Omega^2)^4} \right] [(w_0^2 - w_p^2 - w_0 \cdot \Omega) + w_0(w_p^2 - w_0^2 + \Omega^2) + \Omega w_p^2] \cdot$$

$$\left. \left. \cdot \left[\frac{1}{w_1^4(w_r + \Omega)^4} - \frac{1}{w_1^3(w_r + \Omega)^3} + \frac{1}{w_1^3(w_r + \Omega)^2} - \frac{1}{w_1^4(w_r + \Omega)} \right] \right\} \right\} \tag{7a}$$

$$b_2 = 8\pi^2 \left[-w_r - \frac{c^2K_r^2}{w_r} + \frac{2w_r w_p^2}{(w_r + \Omega)^2} \left(1 + \frac{3K_1^2\Omega^2}{(w_r + \Omega)^2} \right) \right] \tag{7b}$$

$$b_3 = w_1 w_p^2 2\pi^2 K_r \left(\frac{1}{w_1^2} + \frac{1}{w_1 w_r} \right) \left(1 + \frac{3K_1^2\alpha^2}{w_1^2} \right) \cdot \frac{w_0^2 - w_p^2 - w_0 \cdot \Omega}{A} \tag{7c}$$

$$b_4 = 4\pi^2 \left[-w_1 + \frac{w_p^2}{w_1} \left(1 + \frac{9K_1^2\alpha^2}{w_1^2} \right) \right] \tag{7d}$$

$$a' = \frac{eE_a w_0^3 (\Omega^2 - w_0^2)}{m w_0 [w_0^2\Omega^2 - (w_p^2 - w_0^2)^2]} \tag{7e}$$

cu $A = \Omega^2 - w_0^2$

2. For the case $w_0 = w_1 + w_e$, $K_1 = K_e$, where w_e is the frequency of the left handed circularly polarized wave:

$$w_e^4 - w_e^2(w_p^2 + \Omega^2) + c^2K^2(w_e^2 - \Omega^2) - |w_e| \cdot \Omega w_p^2 = 0 \tag{8}$$

the result can be written by doing the replacements $w_r \to w_e$ and $\Omega \to -\Omega$ in the preceding equations (7a)—(7e).

3 For the case $w_0 = w_r + w_e$ there are two growth rates for each of the right and left hand circularly polarized modes

$$\lambda^{w_r}_{w_r+w_e} = \sqrt{-\frac{(-\imath\beta_2 + c_2)(-\imath\beta_4 - c_4)}{4a_1a_3}} \tag{9}$$

$$\lambda^{w_r}_{w_r+w_e} = \sqrt{-\frac{(c_4 - \imath b_5)(c_4 - \imath b_7)}{c_1a_1a_3}} \tag{10}$$

$$\lambda^{w_e}_{w_r+w_e} = \sqrt{-\frac{(\imath\beta_2 + c_2)(-\imath\beta_4 - c_4)}{4a_1a_3}} \tag{11}$$

$$\lambda^{w_e}_{w_r+w_e} = \sqrt{-\frac{(c_4 - \imath b_5)(c_6 + \imath b_7)}{4a_1a_3}} \tag{12}$$

with

$$a_1 = -w_r w_p^2\left(\frac{1}{(w_r+\Omega)^2} + \frac{3K_r^2\alpha^2}{(w_r+\Omega)^4}\right) - w_r - \frac{c^2K_r^2}{w_r}$$

$$\beta_2 = -w_r w_p^2 \eta_y \frac{a'}{2A}\left[2\left(\frac{1}{w_r+\Omega} + \frac{3K_r^2\alpha^2}{(w_r+\Omega)^3}\right) + \frac{1}{w_r-\Omega} + \frac{3K_r^2\alpha^2}{(w_r-\Omega)^3}\right]$$

$$c_2 = -w_r w_p^2 \eta_x \cdot \frac{a'(w_0^2 - w_p^2)}{2Aw_0}\left[\left(\frac{1}{w_r+\Omega} + \frac{3K_r^2\cdot\alpha^2}{(w_r+\Omega)^3}\right) + \frac{1}{w_r-\Omega} + \frac{3K_r^2\alpha^2}{(w_r-\Omega)^3}\right]$$

$$c_6 = -w_r w_p^2 \eta_x \frac{a'(w_0^2 - w_p^2)}{2Aw_0}\left(\frac{1}{w_r+\Omega} + \frac{3K_r^2\alpha^2}{(w_r+\Omega)^3}\right) \tag{13}$$

$$b_7 = w_r w_p^2 \eta_y \frac{a'}{2A}\left(\frac{1}{w_r+\Omega} + \frac{3K_r^2\alpha^2}{(w_r+\Omega)^3}\right)$$

where a_3, β_4, b_5' are obtained from a_1, β_2, b_7 and c_6 by replacement $w_r \to -w_e$ with a minus sign in front of β_4

4. When $w_0 = 2w_r$ the growth rates are obtained as:

$$\lambda^{w_r}_{2w_r} = \sqrt{-\frac{(c_7 + \imath b_8)(c_8 - \imath b_9)}{4a_1a_3}} \tag{14}$$

$$\lambda^{w_e}_{2w_r} = \sqrt{-\frac{(c_8 + \imath b_9)(c_7 - \imath b_8)}{4a_1a_3}} \tag{15}$$

where c_8 is obtained from c_7 with replacement of $w_r \to -w_e$ and c_7 from c_6 with $\Omega \to -\Omega$; b_9 is obtained from b_8 with $w_r \to -w_e$ and b_8 from b_7 with $\Omega \to -\Omega$.

5. When $w_0 = 2w_e$, the growth rate is

$$\lambda^{w_r}_{2w_e} = \lambda^{w_e}_{2w_e} = \sqrt{\frac{(c_6 - \imath b_8)(c_9 - \imath b_{10})}{4a_1a_3}} \tag{16}$$

where b_{10} is obtained from $-\beta_2$ by replacing $\Omega \to -\Omega$.

The last three cases of excitations of parametric instabilities appear as a result for plasma inhomogeneity, whereas the first two cases are identical with the homogeneous one. For these cases the excited waves propagate in the opposite directions. By applying the method of multitime scale perturbation the parametric instabilities of a inhomogeneous magnetized plasma were found, with density gradient perpendicular to the external magnetic field. Due to the inhomogeneity of plasma in the system, three new cases of excitations appear.

REFERENCES

1. T. Amano, M Okamato, *J. Phys Soc Japan*, **26**, 529 (1969).
2. C. Băleanu, S Coldea, J Karacsony, *Studia Univ Babeş-Bolyai, ser Physica* (1986)
3. C Baleanu, *Studia Univ Babeş-Bolyai, ser Physica*, 3 (1985).
4. C S Chen, G J Lewak, *J Plasma Phys*, **4**, 357 (1970)
5. C. S Chen, *J Plasma Phys*, **5**, 107 (1971).
6. K F. Lee, *J Plasma Phys*, **11**, 99 (1974).
7. K F Lee, *J Plasma Phys.*, **13**, 317 (1975).
8. K. F Lee, *J Plasma Phys*, **14**, 245 (1975)
9. M Porkolab, *Nuclear Fusion*, **18**, 367 (1978).
10. M. Prasad, *Phys Fluids*, **13**, 1310 (1970).
11. R Prasad, *J Plasma Phys*, **5**, 291 (1971).

STUDIA UNIV BABEŞ—BOLYAI, PHYSICA, XXXI, 1, 1986

MODULATION GENERATOR FOR DIFFERENTIAL RECORDINGS

E. TĂTARU*, V. IONCU*, GH. CRISTEA*, I. ARDELEAN*, and GH. ILONCA*

Received September 9, 1986, accepted September 25, 1986

ABSTRACT. — A sinusoidal signal generator for differential recording of NMR and QNR spectra, synchronized with a quartz generator, ensuring a high frequency and amplitude stability is presented The working frequency range of the generator is between 100 Hz — 10 kHz and relative frequency stability is better than $2\ 10^{-5}$

Introduction. One of the essential problems in observing Quadrupolar Nuclear Resonance (QNR) phenomon and Nuclear Magnetic Resonance (NMR) in general, is the improvement of the signal/noise ratio The decrease of the ,,passing band" of the processing circuits of the QNR signals brings with it an increase in signal/noise ratio. For this reason the technique of differential processing of these signals is used In this case, the working principle assumes the modulation of the radiofrequency field with a low frequency signal of ω_j frequency After detection only the fundamental frequency (or one of its harmonics) is selectively amplified, up to a level suitable for phase detection In such experiments the first derivative of the absorbtion or dispersion curve is recorded By this procedure the ,,passing band" of the circuit can be preferencially narrowed It is worth pointing out that in this case the ,,passing band" is positioned around ω_j frequency, and not around zero frequency, where the spectral density of the noise has its maximum (due to instability, faiding and so on)

The use of selective narrow band amplification requires for the low frequency generator, by which the support signals in QNR are modulated, a good frequency and amplitude stability, as well as a low distortion quotient In this paper we are proposing a modulation generator for the differential recording of QNR signals

The Amplitude and Frequency Stability Features of the Modulation Generator. For the setting up of a low frequency generator, of high frequency and amplitude stability, the common practice is to make use of operational amplifiers Our oscillator incorporates such operational amplifiers conected in bridge, to which the double feed back principle is applied The block diagram shown in Figure 1 contains the active element (AE) and the group which ensures the feed backs (FBG) consisting of filter F, which represents the phasorial element (PE), and the automatic amplitude control (AAC), as a frequence independent element

The operational amplifier, which plays the role of the AE, is meant to have a transfer function, represented by a real number In such cases the generator works on the quasiresonant frequency ω_r, imposed by the transfer characteristic of the filter F (ω_r is the frequency for which the filter F has a real transfer)

* *University of Cluj-Napoca, Department of Physics, 3400 Cluj-Napoca, Romania*

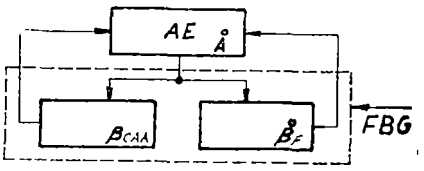

Fig 1

The frequency instability of the generator is due to the variation of ω_r and of transfer A of the active element The ω_r frequency variations are due to temperature changes, to time etc , which affects the components of the filter F, while the variation of A is due to the power supply voltage changes as well as to the temperature changes The effect of A variation on the oscillation frequency stability is much greater compared with that caused by ω_r variations, as it results from the tolowing analysis

The F filter is a classic ,,band passing'' filter, realised with passive RC components In the same way as for the LC circuites, we may define an analogue quality factor Q but its value is smaller in this case [1] Nevertheless, the Q-value could be easily increased, by several orders of magnitude, using a bridge circuit (Fig 1) Such an increase of Q-factor implies the increase of the amplification A of the active element, which entails an increase of its instability On the other hand, the active element used in bridge generators must have both ,,inversing'' and ,,noninversing'' inputs For this reason we have used monolitic operational amplifiers, which for the frequency range of interest (100 Hz $\div$ 10 kHz) have the phase difference input-output corrected to the value of abou $-\pi/2$

In order to ensure a stable behaviour of the generator the condition to be fulfilled is :

$$\mathring{\beta} \cdot \mathring{A} = 1 \tag{1}$$

where $\mathring{\beta}$, and $\mathring{A}$ are the complex transfer functions for the FBG and AE respectively If one rewrites explicitly these notations, by taking $\mathring{\beta} = \beta e^{j\theta}$ and $\mathring{A} = Ae^{j\theta}$ the relation (1) is equivalent to :

$$\theta + \theta_A = 0 \tag{2}$$

and

$$\beta \cdot A = 1 \tag{3}$$

Equation (2) is the phasorial oscillation condition while equation (3) is the amplitude condition.

Usually, for the setting up of bridge generators one cares that condition (3) is satisfied so that the AAC, characterized by the β_{AAC} transfer, should be obtained with nonlinear components, whose parameters are dependent on the signal amplitude (incandescent lamps, thersmistors, diodes, field effect transistors, analogue multipliers and so on) [3, 4]

The way in which one realizes the AAC is essential. In our case it is achived, as shown before, i. e by the automatic fitting of the β_{AAC} transfer, which leads to the change of the transfer A, of the active element. Then the corresponding deviation of the frequency characteristics of the FBG are shown in Figure 2. As one can see, the β_{AAC} values are shifted to the left or to the right relative to the initial value [2] If, for example, under the effect of temperature the phase angle of the transfer characteristic of the active element is modified by $\Delta\theta_A$ (the

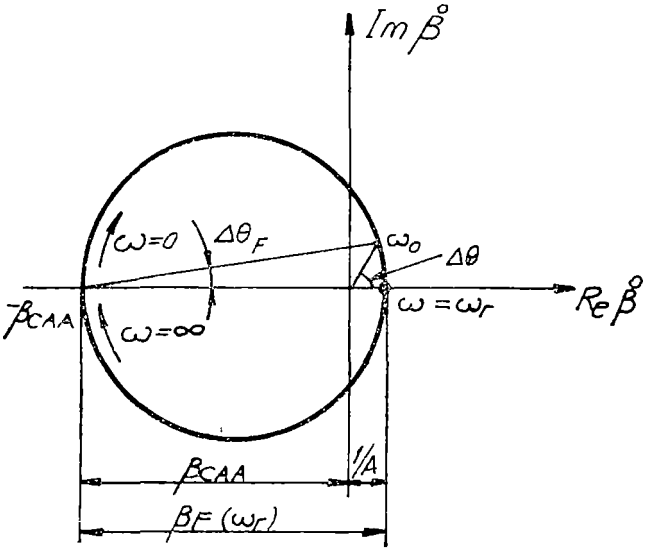

Fig 2

transfer function modulus remains unchanged), then we must also modify the β_{AAC} modulus, so that in the new state the (2) and (3) conditions are satisfied again (see Figure 3)

According to (2), the phase angle of FBG must be changed by $\Delta\theta = -\Delta\theta_A$. In addition, according to (3) te modulus $\beta(\omega_0)$, ω_0 beeing the new oscillation fre-

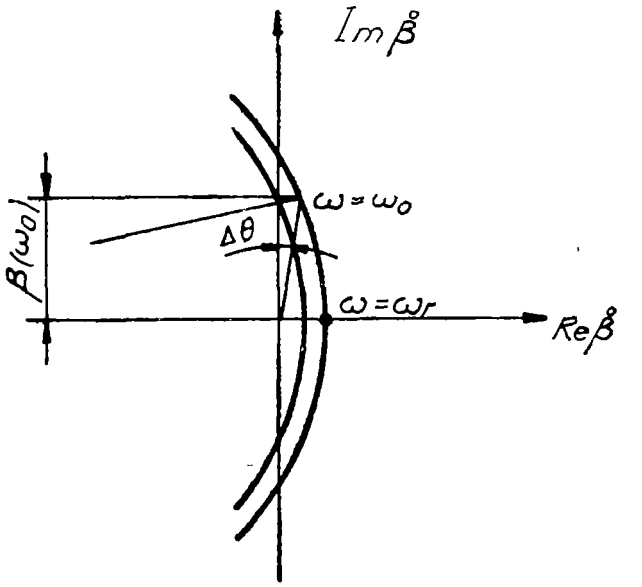

Fig. 3

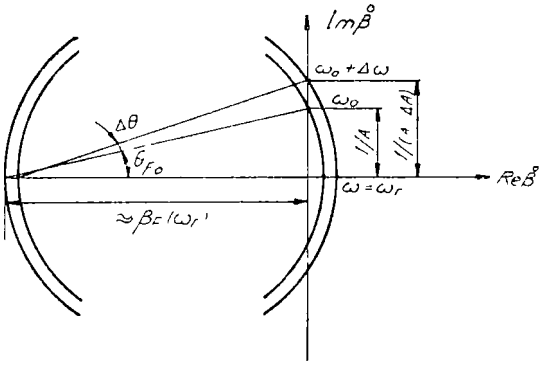

Fig 4

quency, must remain unchanged and equal to $1/A$ Figure 3 shows that the only result is the displace to the right of the FBC characteristic, without any change in oscillation frequency

The modification of the transfer function modulus of the active element has an important influence on the oscillation frequency stability (Fig 4) The frequency characteristic of the FBG element, for the initial value of the amplification, is indicated by the left circle and the modified phase 0_{F_0} value of the filter, shown in Figure 4, corresponds to ω_0 frequency A change by ΔA of the amplification produces such a change in β_{AAC}, that the amplitude condition (3) remains valid

The oscillation frequency determines the phase characteristic of the filter According to Figure 4 one can write the approximate relation

$$\Delta\theta_F = \frac{\dfrac{1}{(A-\Delta A)} - \dfrac{1}{A}}{\beta_F(\omega_r)} \simeq \frac{A}{A^2\,\beta_F(\omega_r)} \tag{4}$$

But $\Delta\theta = \theta(\omega_r + \Delta\omega) - \theta(\omega_r) = \theta'(\omega_r)\Delta\omega_r$ hence $\Delta\omega_r = \Delta\theta/\theta'(\omega_r)$ By dividing both sides of the last equalit with ω_r one obtaines

$$\frac{\Delta\omega_r}{\omega_r} = \frac{\Delta\theta}{\omega_r\,\theta'(\omega_r)} \tag{5}$$

By introducing the quality factor Q of the FBG, as usual

$$Q = \frac{1}{2}\,|\,\omega_r \cdot\ \theta'(\omega_r)\,| \tag{6}$$

from (5) and (6) we have

$$\left|\frac{\Delta\omega_r}{\omega_r}\right| = \left|\frac{\Delta\theta}{2Q}\right| \tag{7}$$

with Q dependent only on qualities of the FBG circuit Now, taking into account the expression (4) for $\Delta\theta$, we have

$$\left|\frac{\Delta\omega_r}{\omega_r}\right| = \frac{\Delta\theta_F}{2\theta_F} = \frac{1}{2Q_F\,\beta_F(\omega_r)}\left|\frac{1}{A}\quad\frac{\Delta A}{A}\right| \tag{8}$$

We note $Q_M = Q_F\ \ \beta_F(\omega_r)$ — the Q-factor of the arm of the bridge which contains the filter Here Q_F is the Q-factor of the filter at frequency ω_r, and $\beta_F(\omega_r)$ is the modulus of transfer function of the filter at cuasiresonance frequency ω_r.

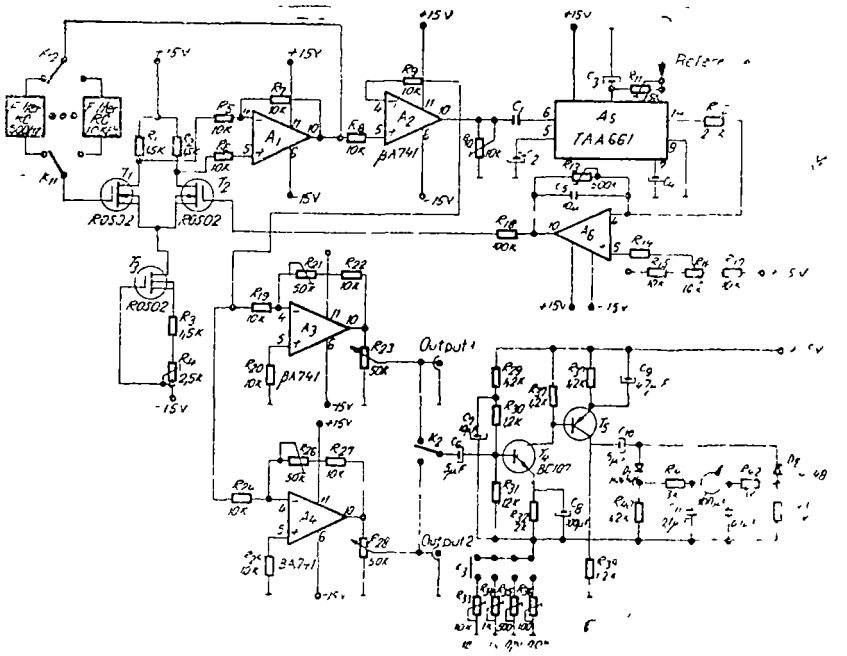

Fig. 5

The relation (8) allows us to drow the following conclusions

— The frequency stability of the generator does not depend on the stability of the phase deviation of the amplifier, around the $\theta(= -\pi/2)$ value,

— The frequency stability of the generator depends strongly on stability and on the value of modulus of the amplification of the active element

The Construction of Modulation Generator The principle diagram of the modulation generator which we have built is shown in Figure 5 The filter circuit, which determines the frequency of the oscillation, can be followed in Figure 6 By using the T_1 (ROS02) MOSFET, which rotates the phase by 180°, this circuit ensures the inverse reaction between the output of the active element and its noninversal input The attenuation of ths scheme is slightly compensated by the R_5 and R_7 resistors

The amplitude condition (3) and the automatic amplitude control are ensured by the phase detector built on a TAA661 (A_5) integrated circuit, and by A_6 integrated circuit The phase detector compares the phases of two signals of the same frequency, one supplied by the generator itself, represented in Figure 5 and the second selected from a numeric freguency meter (not shown in figure) by a commutator By means of the R_{11} potentiometer one can control the phase of signal selected from the frequency meter

The voltage on the gate transistor T_2 is established for the best working regime, by means of R_{16} potentiometer. The phase (frequency) deviation of the sinusoidal generator, due mainly to the changes in signal amplitude, generates

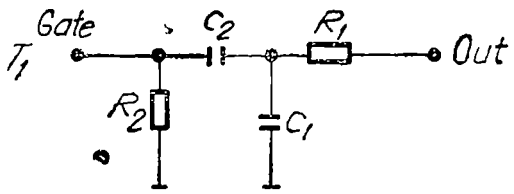

Fig. 6

a reaction voltage across the phase detector A_6 and integrator A_5. This voltage acts correspondingly upon the gate of T_2, reestablishing the preselected frequency by an indirect, but very efficient, action on the signal amplitude.

The oscillation frequency of the generator, for the RC filter type which we are using (Fig. 6), can by determined from the relation given in [1]:

$$\omega_r = \frac{1}{RC\sqrt{\rho\gamma}} \tag{9}$$

and the Q-factor can be determined from the relation

$$Q_M = \frac{\sqrt{\rho\gamma}}{(1+\rho+\rho\gamma)^2} \tag{10}$$

For $\rho \to 0$ and $\gamma \to \infty$, in such a way that $\rho\gamma = 1/3$, the Q-factor receives its maximum value. This maximum value of Q_M for our circuit is 0,325 and is greater than the maximum value for the Q-factor of a clasic oscillator with Wien bridge [2], for which $Q_{M\,max} = 0{,}125$.

From the expression (10) it is clearly seen that for approaching the maximum value of Q-factor it is necessary to select the filter components in such a way that the input resistence is low, while the output resitence be large enough. The output resitence of the active element will not have a significant influence on the frequency stability. This is because its effect can be included whithin the amplification magnitude We cannot say the same thing about the imput resistence of the active element of the amplifier, nor about its eventual variations. Though, in order to avoide this influence, two MOSFET's have been connected to the input of the amplifier

The operational circuit, connected as noninverting follower, has the role to prevent the influence exerted by the charge variation upon the generated frequency. The generated signal is delivered out on two ways, by means of the operational amplifiers A_3 and A_4. The necessity of a double output was determined by the double differential detection offered by the selective detection and amplification system and by the QNR detection device for an automatic tuning on the quadrupolar resonance frequency.

The measuring of the output voltage (the voltage used for frequency modulation, for a differential detection of the QNR oscilator-detectors) is done by simple electronic voltmeter, having a vary good scale linearity for the frequency range of interest. This voltmeter is built up on the T_4 and T_5 group of transistors.

This amplifier has quite good performances: a broad passing band and sufficient resources for amplification. In order to reduce its nonlinearity we made use of the negative feed-back, from the output to the input of the amplifier. The detector group current generates a voltge drop on the R_{33} resistor ($R_{34} \div R_{36}$), which is the fed-back signal that linearizes the ratio input voltage/output current.

The magnitude of the negative feed-back and of sensitivity can be controlled by commuting the resistors $R_{33} \div R_{36}$ with the k_3 commutator.

The main characteristics of the generator are:

— The maximum output voltage 10V, ~ ;
— The frequency stability: $(\Delta f/f) < 2 \cdot 10^{-5}$;
— The distortion quotient: $< 0\ 1\%$;
— The generated frequencies · 100 Hz, 500 Hz, 1 kHz, 2 kHz, 5 kHz, 10 kHz.

REFERENCES

1 V. Vachela, I Kristan, „Oscilatory a Generatory", Praha, 1974.
2. J Kolouch, *Sdelovaci tehnika*, **4**, 135 (1977)
3 V. D. Korovin, S M Vork, *PTE*, **2**, 161 (1981)
4. *J.* Lautier, *Tout l'electronique*, No **437**, 81 nov 1978

Ligıt Scattering in Solids (I), Second Edition, M Cardona (Editor), Springer-Verlag, Berlin, Heidelberg, New York, 1984, 363 pp

Two of the causes which impeded the studies on light scattering through semiconductors as to those on liquids and gases have lain in the need for excitation of the lasers of power and more sophisticated spectral equipment as double and triple monochromators, necessary for such studies

Once these difficulties have been overcome, the number of the scientific reports has increased dramatically — the here reviewed book being the first volume of the four meant to systematization in the field

Chapter I, after an account of generalities, dwells upon light scattering on one and two phonones, the Raman resonance scattering included

Chapter II deals with some essential aspects on light scattering in semiconductors and isolators such as the scattering cross-section, selection rules and an introduction to the microscope theory

Chapter III focuses on Raman resonance spectroscopy pointing to the contribution of the electron state participating in resonance to obtention of information on the scattering mechanism and the electron-photon interaction Models of interpretation of the resonance spectra are described

Aspects on light scattering with implication of a technological nature are presented in Chapter IV, which includes Raman scattering through a free-electron gas, bound electrons and holes In all cases the specific effects of the intricacies of constant-energy surfaces in semiconductors are considered

Chapter V is allotted to Raman scattering through amorphous semiconductors Some peculiarities of the spectra determined by short-range order and chemical bonding are discussed The Brillouin and the stimulated Raman scattering are dealt with in Chapters VI and VII

Althoug each chapter is contributed by different authors, the book poses presentation unity By both content and references the book turns essential for those involved in light scattering through solids

T. ILIESCU

M Young, **Optics and Laser,** Second Revised Edition, Springer-Verlag, Berlin, Heidelberg, New York, Tokyo, 1984, 269 pp

The book consists of the lectures delivered by the author at Rensselaer Polytechnic Institute, Department of Physics, University of Waterloo (Canada) The present (second) edition is revised in that most recent publications have been inserted in the references and also some new chapters have been included

We consider that one of the great merits of the book is that in a restricted number of pages (256) the author has been successful in presenting the most important aspects of the modern and classical optics Thus, Chapters I and II give a brief account on the basic notes of geometrical optics with application in the running of optical equipment.

After dealing, in Chapter III, with the main problemes of photometry, as well as the most oftenly used light sources and detectors, the author dwells upon interference and difraction of light in Chapters IV and V, while in Chapter VIII he approaches polarization of light.

Although the number of the pages of the book is relatively small, the author considered it useful to devote one chapter to the modern notions of hollography and the Fourier optics and another one to lasers (Chapters VI and VII) The last three chapters (IX, X and XI) focus on aspects relating to optical waveguides and integrated optics

The material is presented gradually, stress being laid on the physical meaning of the phenomena, the use of an intricate mathematical complex being thus avoided, yet without diminishing the scientific rigor The solution of each paraghaf-ending problems brings its share in inforcement of the exhibited ideas.

The book is fluently written and it is very useful for those eager to initiate themselves in the mistery of optics

T. ILIESCU

ÎNTREPRINDEREA POLIGRAFICĂ CLUJ,
Municipiul Cluj-Napoca, Cd nr. 445/1986.

Revista ştiinţifică a Universităţii din Cluj-Napoca, **STUDIA UNIVERSITATIS BABEŞ—BOLYAI**, apare începînd cu anul 1986 în următoarele condiţii:

matematică — trimestrial
fizică — semestrial
chimie — semestrial
geologie-geografie — semestrial pentru geologie şi anual pentru geografie
biologie — semestrial
filozofie — semestrial
ştiinţe economice — semestrial
ştiinţe juridice — semestrial
istorie — semestrial
filologie — semestrial

Studia Universitatis Babeş—Bolyai, the scientific journal of the University of Cluj-Napoca, starting with 1986 is issued as follows:

mathematics: quarterly
physics: biannually
chemistry: biannually
geology-geography: biannually on geology and yearly on geography
biology: biannually
philosophy: biannually
economic sciences: biannually
juridical sciences: biannually
history: biannually
philology: biannually

Abonamentele se fac la oficiile poştale, prin factorii poştali şi prin difuzorii de presă, iar pentru străinătate prin „ROMPRESFILATELIA", sectorul export-import presă, P. O. Box 12—201, telex. 10376 prsfir, Bucureşti, Calea Griviţei nr. 64—66